IOWA STATE UNIVERSITY
Digital Repository

Graduate Theses and Dissertations

Iowa State University Capstones, Theses and Dissertations

2009

Fate of fluid mixed at the boundaries of a lake

Danielle Julia Wain
Iowa State University

Follow this and additional works at: https://lib.dr.iastate.edu/etd

 Part of the Civil and Environmental Engineering Commons

Recommended Citation
Wain, Danielle Julia, "Fate of fluid mixed at the boundaries of a lake" (2009). *Graduate Theses and Dissertations*. 11048.
https://lib.dr.iastate.edu/etd/11048

This Dissertation is brought to you for free and open access by the Iowa State University Capstones, Theses and Dissertations at Iowa State University Digital Repository. It has been accepted for inclusion in Graduate Theses and Dissertations by an authorized administrator of Iowa State University Digital Repository. For more information, please contact digirep@iastate.edu.

Fate of fluid mixed at the boundaries of a lake

by

Danielle Julia Wain

A dissertation submitted to the graduate faculty

in partial fulfillment of the requirements for the degree of

DOCTOR OF PHILOSOPHY

Major: Civil Engineering (Environmental Engineering)

Program of Study Committee:
Chris Rehmann, Major Professor
Roy Gu
James Hill
Hui Hu
Say Kee Ong

Iowa State University

Ames, Iowa

2009

Copyright © Danielle Julia Wain, 2009. All rights reserved.

This dissertation is dedicated to my mom and dad, who have always supported me, even though I am sure they have always wondered if I was ever going to get out of school.

TABLE OF CONTENTS

ACKNOWLEDGMENTS

I would first like to thank the National Science Foundation Physical Oceanography Program for their financial support of this project. I would next like to acknowledge Meredith Carr and Ryan Jackson, my academic older siblings, for help with the logistical planning and execution of the 2005 experiments and for picking up the phone when I was calling for last minute advice or just to vent. For their dedication to this project and their willingness to drop everything whenever it got windy out, I am grateful to Mike Kohn and Josh Scanlon. I would also like to thank the undergraduates who have assisted in this field work: Adam Wright, Anton Boose, Christine Reinders, and Emily Libbey. If there were ever a four man marine battery hauling relay, they would win. For commiserating about grad student life and regularly making me laugh, I am ever appreciative to Lisa Neef and Jaymi LeBrun. For providing well needed distraction from grad school, my roommate Samantha Houston, my running/sushi buddy Kori Heuss and the rest of Team Vardo, and my partner-in-crime-for-scheming-crazy-ideas Joe Greenseid were invaluable. Without my daily writing date with Heath Sledge and Anita Hardeman, this dissertation would probably still be in shambles. I also appreciated the support and motivation I received from my LuAnne Thompson, Fiamma Straneo, and the rest of my MPOWIR mentoring group. I would also like to thank my committee Drs. Hui Hu, Jim Hill, Roy Gu, and Say Kee Ong for their comments on my work. . I also appreciate the encouragement I received as an undergraduate from Dr. Todd Cowen – I would never have chosen this path if I hadn't stumbled upon his classes and if he hadn't planted the idea of doing a PhD in my brain. Finally, I'd like to extend my gratitude to my advisor Dr. Chris Rehmann for his guidance and advice, his endless patience with me (despite all my efforts to try it), for continually cracking me up, and for making me a better scientist and writer. I'm not sure which one of us gave the other more gray hairs in the last seven years. I didn't expect grad school to be the adventure it was, but I have no regrets.

ABSTRACT

Three field studies were conducted in Ada Hayden Lake in Ames, Iowa to study generation of turbulence on the sloping boundary and to investigate boundary-interior communication in a lake with dye tracking experiments and measurements of meteorological conditions, internal wave response, and turbulence. The objectives of these studies were to (1) predict the occurrence and strength of turbulent mixing in terms of meteorological forcing and stratification by investigating the dependence of internal waves and turbulence on the slope on the Lake number, (2) investigate the fate of mixed fluid by tracking an intrusion generated at the boundary; and (3) evaluate offshore transport by basin scale seiches.

To predict the Lake number conditions under which turbulence will be generated at the slopes (objective 1), the rate of dissipation of turbulent kinetic energy was determine from near-bottom velocity measurements using the structure function method, and histograms of $\varepsilon/\nu N^2$ were analyzed for all the data and for five different Lake number regimes. Although a quantitative relationship between the Lake number and the turbulence intensity could not be determined, some relationships between the Lake number and $\varepsilon/\nu N^2$ for different Lake number regimes could be observed. For example, for high Lake number, most of the values of $\varepsilon/\nu N^2$ were low enough to suggest that transport was mainly caused by molecular diffusion, while for low Lake number, turbulence was energetic. For moderate Lake numbers, the value of $\varepsilon/\nu N^2$ at the peak in the histogram increased as the Lake number decreased from 30 to 1.

To investigate intrusion generation and propagation (objective 2), temperature microstructure measurements on the slope and horizontal and vertical dye mapping were used. Profiles of temperature microstructure measured soon after the injection both at the injection site and offshore showed large eddy diffusivity near the boundary. The propagation characteristics of the intrusion were predicted most closely by a formulation for an axisymmetric intrusion governed by a balance between buoyancy and inertia.

To evaluate offshore transport by basin scale seiches (objective 3), the horizontal variation in internal wave shear and strain, which can increase the lateral dispersion between the boundary and the interior, was analyzed. The strain can spread the mixed fluid far enough

from the boundary that vertical shear becomes an important dispersion process**.** These findings improve the understanding of the pathway from energy input from the wind to offshore transport.

CHAPTER 1. INTRODUCTION

1. Significance

Understanding the transport of dissolved substances such as oxygen, nutrients, microorganisms, and plankton is essential for managing water quality in lakes and reservoirs. The ability of stratification, which is caused by temperature, salinity, or sometimes chemical species, to restrict vertical mixing and control the spatial variability of nutrients and other substances affects the distribution of dissolved oxygen in the water column (e.g., Rao et al. 2008), the availability of nutrients to phytoplankton (e.g., MacIntyre et al. 1999) and transport of pollutants between the hypolimnion and epilimnion (e.g., Morillo et al. 2008). Most temperate lakes experience seasonal overturns twice a year, although some lakes remain stratified for years. As large scale mixing events do not dominate transport within a lake during the strong summer stratification, small-scale mixing plays an important role in distributing dissolved substances.

The current model in ocean and lake mixing is that turbulence created at the boundaries by internal waves and currents causes most of the mixing (e.g., Gregg 1998; Ledwell et al. 2000; Wunsch and Ferrari 2004). The turbulence created on the boundaries by internal waves or currents can suspend bottom sediments (Gloor et al.1994), possibly releasing nutrients stored in the sediment pore waters. Alternately, if nutrients are trapped in a particular portion of the water column, the vertical mixing at the boundaries can entrain the nutrient-rich water into the nutrient-poor water (MacIntyre et al. 1999). While much work has been done to investigate mixing at boundaries in lakes and the ocean, less attention has been paid to the fate of the mixed fluid.

2. Background

This section reviews the background and previous work on boundary mixing and the fate of mixed fluid. Part a reviews the background on lake stratification. Internal waves and seiches are discussed in part b. In part c, previous research on boundary mixing is

summarized. Two possible mechanisms for boundary-interior communication are discussed in parts d and e.

a. Stratification in Lakes

For most lakes, the dominant sources of energy are solar radiation and the wind. Solar radiation sets up a stable thermal stratification, with a well mixed surface layer (the epilimnion), a region of strong temperature gradient (the metalimnion or thermocline), and then another more weakly stratified bottom layer (the hypolimnion) as seen in Figure 1. For dimictic lakes (typically found between 40º and 60º latitude), this stratification is established early in the summer and persists until the fall overturn when the air temperature drops sufficiently to cool the surface water to the same temperature as the bottom water.

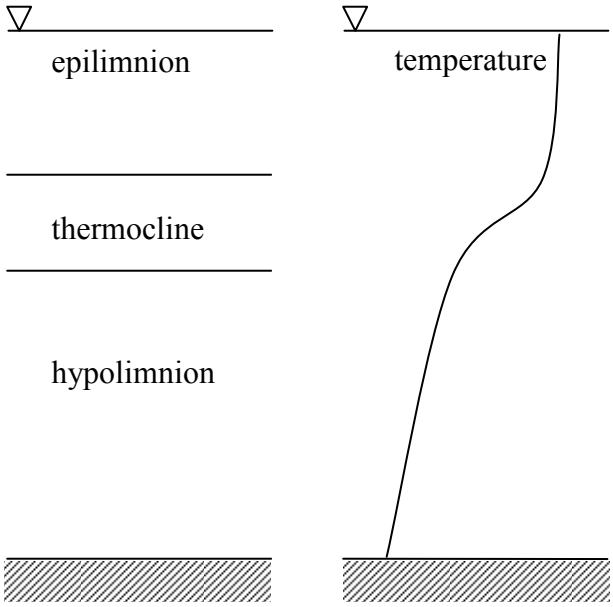

Figure 1. Typical vertical structure of lakes, with the warmer, less dense water at the surface.

The wind adds energy to the lake through several mechanisms that affect the stratification. Turbulent mixing generated by the wind keeps the epilimnion well-mixed. These turbulent motions in the epilimnion can also erode the thermocline, but the effect of

this direct wind stirring is confined to the surface layer. Wind stresses can also cause the surface to tilt. To reduce the horizontal pressure gradient that this tilt creates, the water below the epilimnion tilts as well. This wind set-up allows energy from the wind to be transferred to the entire water column, but wind set-up occurs only when the wind is sufficiently strong.

To determine if wind set-up will occur, the information about the lake stratification and the wind forcing can be combined through the dimensionless Lake number. The Lake number is a ratio between the strength of the stratification strength and the strength of the wind, which is acting to overturn the stable density structure (Imberger and Patterson 1989):

$$L_N = \frac{gS_t(1 - z_T / z_S)}{\rho_S u_*^2 A_S^{3/2}(1 - z_V / z_S)} \tag{1}$$

where g is the gravitational acceleration, z_T is the center of the metalimnion, z_S is the height of the surface, ρ_s is the density at the surface, u_* is the shear velocity of the wind, A_s is the area of the surface, z_v is the height of the center of volume, and S_t is the stability of the water body defined as

$$S_t = \int_0^{z_S} (z_v - z)\rho(z)A(z)dz. \tag{2}$$

The shear velocity of the wind is defined as

$$u_* = \sqrt{\rho_a C_{Dw} u_w^2 / \rho_S} \tag{3}$$

where ρ_a is the air density, C_{Dw} is the wind drag coefficient, and u_w is wind speed. The wind drag coefficient depends on the wind speed. For $u_w < 5$ m/s, Wüest and Lorke (2003) did a least squares fit of data from several studies to yield $C_{Dw} = 0.0044 u_w^{-1.15}$, where u_w is in m/s. For $u_w > 5$ m/s, $C_{Dw} = (1/\kappa \ln(10g/C_{Dw}/u_w^2) + 11.3)^{-2}$. Note that u_w is typically taken as the velocity 10 m above the water; if the velocity is measured at a different level, the measured

velocity has to be converted to a velocity at 10 m using the logarithmic law for velocity profiles over a rough surface.

b. Internal Waves and Seiches

When a horizontal density interface, such as that between air and water or between the epilimnion and hypolimnion of a lake, is disturbed, gravity restores the horizontal interface and waves are generated. Internal waves are generated within the water column, as opposed to on the surface. The interface on which the waves are generated need not be sharp, like the examples mentioned above; internal waves can exist wherever there is a stable density stratification.

When the amplitudes of the waves are considered to be small compared to the wavelength, then linear wave theory applies. For two-dimensional internal waves in a linearly stratified fluid, the frequency ω of the wave is related to the wavenumber vector $\boldsymbol{k}$ by the dispersion relation

$$\omega = N\left(\frac{k^2}{k^2 + m^2}\right)^{1/2} = N\cos\theta \tag{4}$$

where k and m are the horizontal and vertical components of the wavenumber respectively, θ is the angle that the wavenumber vector $\boldsymbol{k}$ makes with the horizontal plane and N is the buoyancy frequency defined as

$$N = \sqrt{-\frac{g}{\rho_0}\frac{\partial\overline{\rho}}{\partial z}} \tag{5}$$

where ρ_0 is a reference density and $\overline{\rho}$ is the background density (Turner 1973). This relation states that a wave with a given frequency in a fluid of a given stratification has a phase that propagates at a specific angle. This relation also shows that waves of frequencies higher than

the buoyancy frequency cannot be sustained. For surface waves, both the phase and energy propagate in the same direction. For internal waves, the energy propagates perpendicular to the phase (i.e., at an angle $\phi = \pi/2 - \theta$).

To conserve energy, internal wave energy must reflect from boundaries. Upon reflection, the angle ϕ with respect to the horizontal plane must be maintained. When the wave approaches a boundary with a slope α, three scenarios are possible (Figure 2). If $\phi < \alpha$, the wave energy is reflected back into the lake interior (subcritical reflection). If $\phi > \alpha$, the wave energy is reflected forward up the slope (supercritical reflection). When $\phi = \alpha$, critical reflection occurs and the energy propagates along the boundary. When critical reflection occurs, linear wave theory breaks down as the vertical wavenumber of the reflected wave approaches infinity (because of energy considerations).

This simplified reflection theory is limited in its application to real waves on real topography. In natural water bodies, more than one frequency of wave exists (Garrett and Munk 1979). Eriksen (1985) theoretically analyzed how this spectrum of internal waves changes upon reflection from a slope and observed the spectrum was most perturbed around the critical frequency, where there should be a singularity in the reflected spectrum. Gilbert and Garrett (1989) addressed the issue of irregular bottom topography and theoretically evaluated internal waves reflecting off convex and concave slopes, finding more energy enhancement over convex topography. Using oceanic observations, Eriksen (1998) investigated internal waves reflecting off a steep sloping boundary and found significant differences between the measurements and the behavior predicted by the linear theory. Because the amplitude of the reflected waves decayed with the wavenumber and the dominant mode critically reflecting resulted in a vanishing vertical wavenumber (as opposed to an infinite one), care must be taken when applying linear wave theory to field observations. Dauxois and Young (1999) theoretically addressed this case of non-linear near-critical internal waves interacting with a slope in a linearly stratified fluid and analyzed the conditions in which these near-critical waves can create turbulence and intrusive layers.

A seiche is a special case of internal wave. When the wind relaxes after wind set-up, a basin-scale standing wave, or seiche, is formed. For a rectangular basin of constant width, the first horizontal mode seiche has a wavelength that is twice the length of the lake with a single

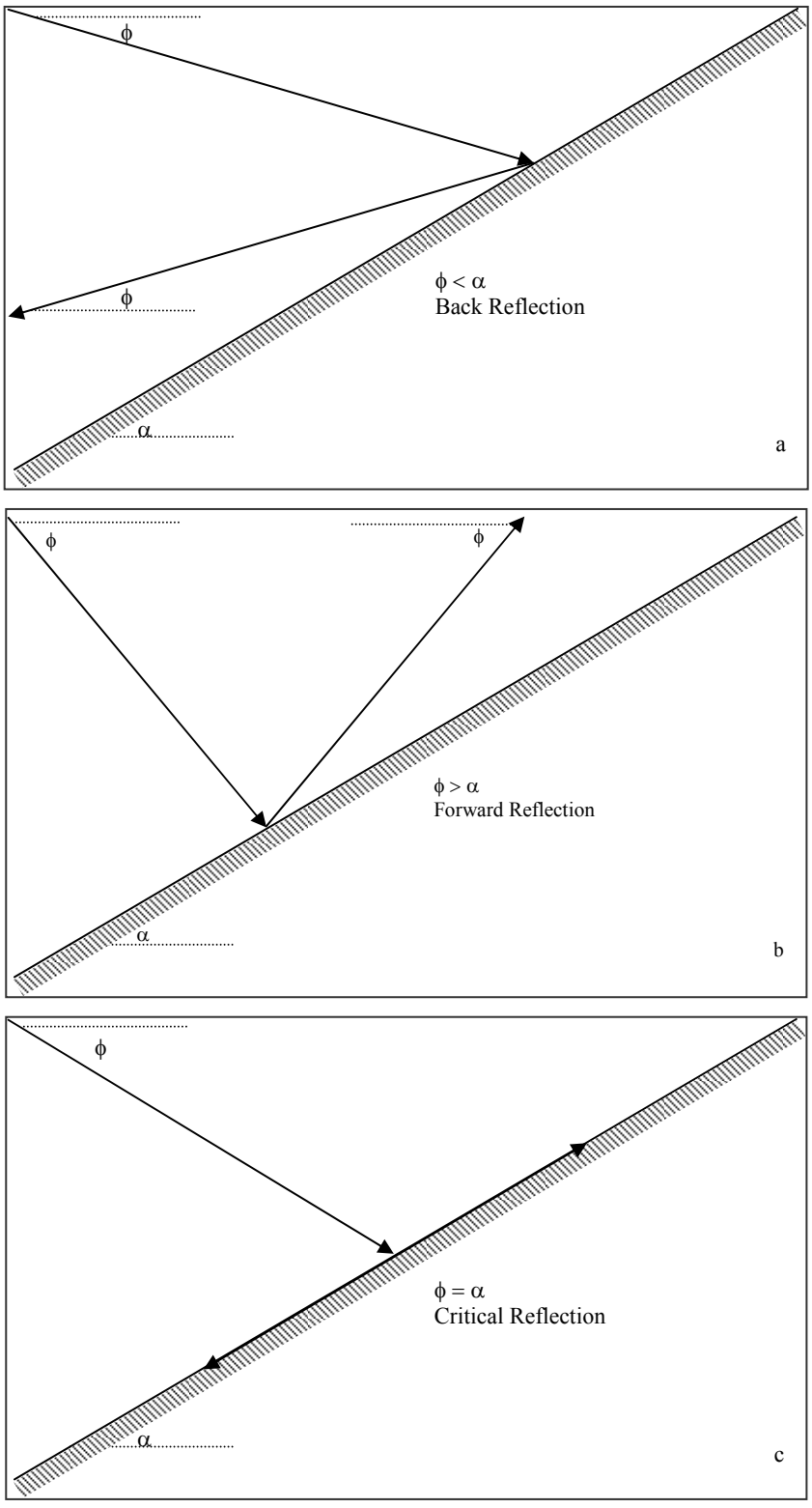

Figure 2. Internal waves reflecting off a sloping boundary: (a) subcritical reflection; (b) supercritical reflection; (c) critical reflection.

node in the middle; the complex geometry and bathymetry of real lakes change the modal structure (e.g., Fricker and Nepf 2000). Higher modes have more nodes (the second mode has two nodes, etc.). Under different conditions, the wind can alternatively create surges or solitary waves, which do not follow linear internal wave theory. Boegman et al. (2005) conducted laboratory experiments with a two-layer stratification to determine the energy distribution between standing seiches and these other wave forms. They found that if the inverse of the Wedderburn number (a simpler version of the Lake number derived for two layer stratification in a rectangular basin) $W^{-1} < 0.3$, seiches should form; otherwise, nonlinear surges and solitary waves should form. During these same experiments, Boegman et al. (2005) found that 98% of the energy was contained in the first horizontal mode seiche. In a two-layer stratification such as theirs, only the first vertical mode can exist; in lakes with a thermocline of finite thickness (i.e., a metalimnion), the second vertical mode can dominate the first mode and can cause large isotherm displacements (e.g., Wiegand and Chamberlain 1987, Münnich et al. 1992).

The seiches can generate observable currents in the water column. A first vertical mode seiche has peak velocities at the top and bottom of the water column with a minimum in the metalimnion. The compression of the metalimnion that is a signature of the second vertical mode results in a velocity maximum in the metalimnion. Higher modes have more peaks in the velocity profile. Current profiles have shown this velocity structure induced by higher mode seiches in several lakes (e.g. Antenucci et al. 2000, Vidal et al. 2005, Boehrer et al. 2000).

Once seiching motions have been initiated, they will continue until they are damped by the lake boundary, but field observations (e.g., Stevens et al. 1996) have shown that the energy in the seiches sometimes is dissipated faster than would be expected by viscous damping because other mechanisms transfer energy from the seiches. Using laboratory experiments with a two-layer fluid, Horn et al. (2001) classified how seiches degenerate in a lake based on the Wedderburn number and the ratio between the depth of the thermocline and the total depth (Figure 3). The response was classified into five regimes indicating the dominant mechanism for energy loss from the seiches: damped linear waves, solitons, supercritical flow, Kelvin-Helmholtz billows, and bores and billows. For all depth ratios, $W >$

5 falls into the first regime of damped linear waves, as the time scale for damping is less than the time scale for nonlinear steepening of the waves, which produces solitons. Outside of the first regime, linear wave theory would no longer apply.

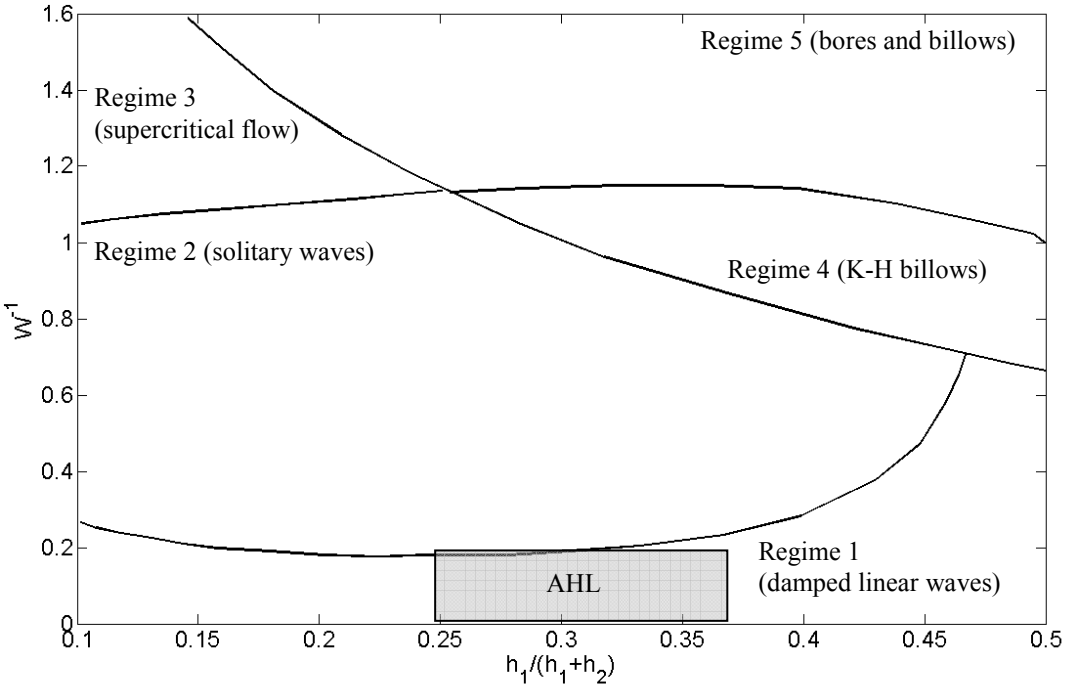

Figure 3. Regimes from Horn et al. (2001) predicting wave behavior given the Wedderburn number and the depth of the thermocline. The parameter range for Ada Hayden Lake during typical summer stratification is shaded.

c. Boundary Mixing

Using a balance between a downward turbulent heat flux and upwelling of cold bottom water in the ocean, Munk (1966) estimated that a vertical eddy diffusivity *K*, which is a measure of the mixing on the order of 10^{-4} m^2/s, a value 1000 times greater than the molecular diffusivity of heat, was required to maintain the observed stratification. While microstructure measurements in the open ocean have yielded estimates ranging from only 10^{-6} to 10^{-5} m^2/s (Polzin et al. 1997), measurements near topography, using both microstructure (see Gregg (1998) for a review) and dye dispersion (Ledwell et al. 2000), show *K* ranging

from 10^{-5} to 10^{-2} m^2/s. This elevated mixing at topography is important for closing the global oceanic heat budget (e.g., Wunsch and Ferrari 2004).

Similarly to the ocean, boundary mixing has been shown to be an integral mechanism for vertical fluxes in lakes. Goudsmit et al. (1997) performed a tracer release experiment in a lake to investigate the importance of boundary mixing to vertical transport. They observed that the vertical diffusivity was small in the interior of the lake and increased by an order of magnitude at the boundaries. This enhanced mixing over the boundary is often attributed to critical internal wave reflection or currents passing over the bottom.

When wind acts on the surface of a stratified lake, it can set up seiches, which generate currents along the boundaries. The friction with the bottom generates turbulence that mixes the water locally to create a turbulent bottom boundary layer (e.g., Gloor et al. 2000, Hondzo and Haider 2004). The seiching motions can also degenerate into higher frequency waves. Some of these waves propagate towards the boundary with a critical frequency set by the stratification and the slope of the boundary. When the critical waves approach the boundary, their energy reflects along the slope and energizes a turbulent bottom boundary layer (e.g., Eriksen 1998, MacIntyre et al. 1999).

Boundary mixing due to breaking internal waves in lakes has been observed in several lakes. MacIntyre et al. (1999) measured temperature microstructure profiles in a lake at offshore and onshore sites to determine the presence of boundary mixing and its effect on nutrient fluxes. Measurements at the onshore site (on a sloping boundary) showed enhanced mixing at the bottom that they attributed to the presence of critical internal waves breaking on the sloping bottom onshore. Hondzo and Haider (2004) measured turbulence in the benthic boundary layer on the sloping boundary of a lake using an acoustic Doppler velocimeter and temperature microstructure and attributed the high dissipation levels to energy from the internal wave field. With detailed measurements of temperature and velocity in the bottom boundary layer, Lorke (2007) observed periodic enhanced turbulence on the slope, coinciding with the period of high-frequency internal waves seen at a mooring in the deepest part of the lake. This oscillation in the turbulence in the bottom boundary layer was also observed in numerical simulations of mixing from internal wave reflection on a slope (Slinn and Riley 1996).

Fewer researchers have looked at the turbulence generated by seiching currents, although several have proposed that large amplitude internal seiches may create significant mixing (e.g., Patterson et al. 1984). Lorke and Wüest (2005) estimated the dissipation rate of turbulent kinetic energy over the lake bottom and observed oscillations in the dissipation with the same period as the dominant seiching currents. The currents elevated the dissipation rate by over two orders of magnitude compared to measurements in the interior. Lorke et al. (2005) observed convective turbulence in the bottom boundary resulting from the periodic seiching currents. Because of friction with the boundary the fluid near the boundary moves slower than the fluid at the top of the boundary layer. As a result, when the direction of the seiching currents is up the slope, denser water is advected over less dense water, causing convection. When the seiche moves downslope, the stratification in the boundary layer becomes even stronger. As the velocity magnitude (and hence the shear) is the same regardless of the direction of the seiching movements, shear induced mixing will necessarily be smaller during this period of stronger stratification than during the upslope seiching phase. Lorke et al. (2008) confirmed that this behavior by observing differences in mixing on the slope when the seiche was moving upslope and downslope.

Low mode waves that have associated observable currents (such as seiches) can be critical with respect to the boundary as well. One question that has not been addressed is if such waves cause enhanced turbulence on the boundary or if turbulence due to breaking or friction dominates. In the ocean, the closest analogy would be the behavior of the semi-diurnal M2 tide; oceanographers typically attribute the enhanced mixing they observe on the continental slope to internal tides reflecting critically (e.g., Nash et al. 2004, Rudnick et al. 2003), not to the currents generated by such a tide.

Once the turbulence has been generated (whether by breaking internal waves or currents), it is important to determine if the turbulence can overcome the stable stratification to irreversibly mix the fluid and create a turbulent bottom boundary layer. To describe the turbulence generated at a slope, a Reynolds number (Re_T) and a Froude number (Fr_T) can be defined using three standard length scales in stratified turbulence: the centered displacement scale L_C (a measure of the size of the overturns in a density profile, attributed to large scale turbulent eddies), the Ozmidov scale $L_O = (\varepsilon/N^3)^{1/2}$, and the Kolmogorov scale $L_K = (\nu^3/\varepsilon)^{1/4}$

(Ivey and Imberger 1991). The last two are derived from dimensional analysis using scaling arguments. The Ozmidov scale is the length scale at which the buoyancy force are of the same order of magnitude as the inertial forces of the overturning motions. The Kolmogorov scale is the smallest turbulent length scale that can exist before viscosity resists the inertial forces. Using these scales, $Re_T = (L_C/L_K)^{4/3}$ and $Fr_T = (L_O/L_C)^{2/3}$. The remaining combination of length scales can be used to define the turbulence intensity parameter $\varepsilon/\nu N^2 = (L_O/L_K)^{4/3}$ (Ivey et al. 2008).

The eddy diffusivity K has been shown to depend on $\varepsilon/\nu N^2$. With measurements of the dissipation rate, the eddy diffusivity in lakes and the ocean is often estimated using the Osborn (1980) model. In this method, Osborn (1980) used the turbulent kinetic energy equation:

$$\frac{\partial k}{\partial t} + U_j \frac{\partial k}{\partial x_j} = -\frac{\partial J_j}{\partial x_j} - \overline{u_i' u_j'} \frac{dU_i}{dx_j} - b - \varepsilon \qquad (6)$$

where J_j is a flux of turbulent kinetic energy, $b = g\overline{\rho' w'}/\rho_0$ is the buoyancy flux, and ρ_0 is a reference density. For oceanic flows, Osborn (1980) argued that the last three terms balance. For more general flows, Ivey and Imberger (1991) wrote (6) as $m = b + \varepsilon$. Using the generalized flux Richardson number $R_f = b/m$ and the flux-gradient relationship $\overline{\rho' w'} = -K_\rho \partial\overline{\rho}/\partial z$ gives

$$K_\rho = \frac{R_f}{1 - R_f} \frac{\varepsilon}{N^2} = \Gamma \frac{\varepsilon}{N^2} \qquad (7)$$

where Γ is the dissipation coefficient.

Some uncertainty in estimating the eddy diffusivity K_ρ computed with the Osborn method comes from uncertainty in the value used for the dissipation coefficient Γ. The dissipation coefficient Γ is commonly assumed to be 0.2, although it can vary with stratification strength and the process generating the turbulence (e.g., Ivey and Imberger

1991). Laboratory measurements show that Γ decreases when $\varepsilon/\nu N^2 > O(10^3)$ (Itsweire et al. 1986, Barry et al. 2001, Rehmann and Koseff 2004), although measurements from the upper ocean show the opposite trend (Ruddick et al. 1997). Using the results from direct numerical simulations and laboratory experiments, Shih et al. (2005) defined three regimes of stratified turbulence based on $\varepsilon/\nu N^2$. For $\varepsilon/\nu N^2 < 7$, the diffusivity is molecular; Ivey and Imberger (1991) found cutoff values for turbulence generation at about twice this value ($\varepsilon/\nu N^2 = 15$, for $Re_T > 15$). For $7 < \varepsilon/\nu N^2 < 100$, $\Gamma = 0.2$ approximated the results well. But Shih et al. (2005) found that as $\varepsilon/\nu N^2$increases above 100, the mixing efficiency decreases because the turbulence is more energetic than necessary to break down the stratification; thus, the turbulence acts on fluid that has already been mixed. In the field this can occur after a bottom boundary layer is formed and the turbulence continues to act upon already mixed fluid in the boundary layer (Garrett 1979).

d. Fate of Mixed Fluid: Intrusions

The mixed bottom boundary layer that develops due to boundary mixing is hydrodynamically unstable with respect to the stratified interior. Gravitational adjustment of this mixed fluid leads to collapse into an intrusion that propagates horizontally along an isopycnal (level of constant density) into the interior. These intrusions can transport the mixed fluid from the boundaries into the lake interior to a distance from the slope on the order of the internal Rossby radius of deformation (the length scale at which Coriolis forces begin to dominate the buoyant forces driving the flow), but there is a lack of knowledge of how efficiently intrusions transport material from the boundaries into the interior of lakes (Thorpe 1998). Figure 4 shows a schematic of the mechanisms for creating turbulence at the boundary layer and the process of intrusion generation that may result.

Neglecting this horizontal transport may lead to an underestimate of the nutrients available for biological production offshore. Also, the vertical boundaries of intrusions are characterized by sharp density gradients where there is very little vertical mixing, creating thin layers where biological matter gets trapped. Knowledge of the properties of these

intrusions and when they occur is essential for understanding how mixing in a very limited spatial domain (i.e., the boundary region) affects the ecology of the larger water body.

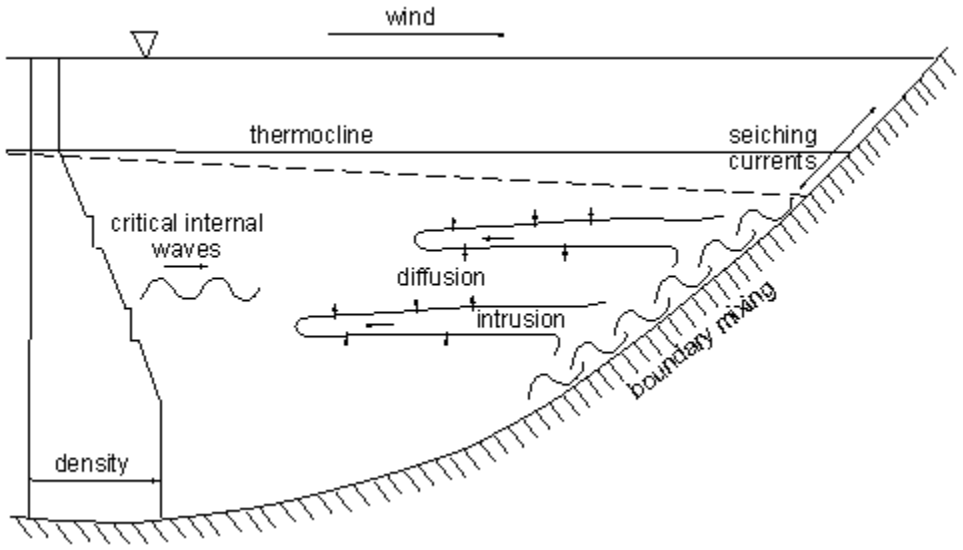

Figure 4. Schematic of physical processes leading to boundary mixing and intrusions in a lake. Wind on a stratified lake can create internal seiching currents and critical internal waves.

Several studies provide evidence for intrusions from boundary processes. Caldwell et al. (1978) observed stepped profiles near sloping boundaries in a lake that they attributed to intrusions generated by boundary mixing. Gloor et al. (2000) observed mixed water masses extending up to 200 m into the lake interior and ascribed them to intrusions, which reduce the boundary layer thickness by discharging mixed fluid into the interior. Intrusions can also explain turbid layers observed in the interior of a water body. Dickson and McCave (1986) and Thorpe and White (1988) proposed that nepheloid layers along a continental slope resulted from boundary mixing due to the semi-diurnal M2 tide reflecting critically. Dye injected into the water column above a slope in a fjord was eventually entrained into a turbulent boundary layer generated by the semidiurnal tide moving over rough topography, and then it entered the interior as intrusions (Inall 2009).

While several field experiments have provided evidence of intrusions from boundary mixing, intrusions resulting from the collapse of turbulent regions have been tracked from the

boundary into the interior mostly in laboratory experiments. Some laboratory work focuses on intrusive gravity currents traveling along the interface between two fluids (e.g., Lowe et al. 2002, Sutherland et al. 2004), a scenario that might mimic behavior of an intrusion along the thermocline in a lake. While these intrusions are generally not created by boundary mixing processes, these experiments relate intrusion properties, such as the velocity, to the depth and density of the ambient fluids. Phillips et al. (1986) conducted laboratory experiments in a two layer fluid where a turbulent boundary layer was generated on a slope by an oscillating bed. Gravitational adjustment of the turbulent boundary layer created intrusions. From their observations and a theoretical analysis, they proposed a model for the intrusion velocity that is based on a viscous-buoyant balance.

Other laboratory experiments investigate intrusions in a linearly stratified fluid, which is typical of the hypolimnion of many lakes or the ocean thermocline. In some earlier studies, the turbulence was generated by an oscillating grid that created a uniform vertical turbulent patch that gravitationally collapsed into several intrusions (e.g., Ivey and Corcos 1982, Thorpe 1982). Hopfinger (1987) summarized previous stratified turbulence experiments and found that collapse appears to occur when $Fr_T \sim 1$. Browand et al. (1987) showed that the vertical scale of the intrusions was limited by the Ozmidov scale. The intrusions that make up the front propagated at a rate that was related to a local Froude number that decreased as the intrusion advanced.

Several experiments have investigated the vertical mixing from breaking internal waves and observed intrusions (e.g., Cacchione and Wunsch 1974, Ivey and Nokes 1989), but fewer have quantified the intrusion properties. De Silva et al. (1997) and McPhee-Shaw and Kunze (2002) measured propagation of intrusions resulting from breaking internal waves on a slope and related the intrusion speed to the energy of the incident internal waves. The former observed no change in the background density stratification due to the intrusion, whereas the latter observed persistent steps; however, as De Silva et al. (1997) noted, even if the intrusion does not change the thermal structure of a lake, dissolved substances can still be transported offshore. The experiments of Wells and Helfrich (2004) provide information on the three-dimensional behavior of an intrusion generated at the boundary; in those, effects of rotation limited the propagation of the intrusion.

e. Fate of Mixed Fluid: Internal Wave Driven Transport

While intrusions are an outcome of the internal waves interacting with the boundary, the internal waves themselves may drive transport between the boundary and the interior. As described above, the mechanisms by which internal waves may contribute to horizontal mixing in a lake are through lateral advection by the mean velocity field of the internal waves in the metalimnion, shear dispersion by the vertical variation of internal wave induced velocities, and strain due to the horizontal variation in the internal wave velocity field, and

In a lake, the first potential mechanism for this offshore transport is the water column currents generated by the internal seiches. Marti and Imberger (2008) observed a well-defined turbid layer in a large lake and used numerical modeling with field measurements of turbulence and the internal wave field to predict exchange between the boundary and the lake interior. They associated the change in the turbid layer with the changes in the bottom boundary layer as the seiches passed over the slope. Given the basin-scale internal waves in the lake, they concluded that the turbid layer was advected offshore by a jet in the metalimnion that resulted from a second vertical mode wave. Their numerical model showed residual velocities in the metalimnion after such a seiching event and these residual velocities can explain some aspects of the observed distribution of the turbid layer.

Due to the oscillatory nature of seiching motions, significant movement due to mean advection as observed in Marti and Imberger (2008) is expected to be rare as any transport into the interior will be reversed when the seiche moves in the other direction. But the velocities in a lake vary significantly both horizontally and vertically. The vertical variations in velocity can lead to lateral shear dispersion, while the horizontal velocity variations causes straining of the water mass.

Young et al. (1982) studied dispersion in an infinite fluid with an oscillating velocity profile and a horizontal velocity component given by

$$u = U \cos mz \cos \omega t \tag{8}$$

and found

$$K_{eff} = K_x + \frac{1}{4}\frac{U^2}{\omega}\frac{d}{1+d^2}. \quad (9)$$

where $d = K_z m^2 / \omega$, U is the maximum velocity, m is the vertical wavenumber, K_x is the horizontal diffusivity without the presence of internal wave shear, and K_z is the vertical eddy diffusivity. Sundermeyer and Ledwell (2001) used the Young et al. (1982) results with the results of Smith (1982) to estimate this enhanced horizontal diffusivity and compare the estimates to the observed spreading from four dye release experiments in the coastal ocean. They found that this shear dispersion was not sufficient to explain their dye distributions and oftentimes was an order of magnitude too low. There appear to be no similar tracer experiments in lakes; tracer experiments carried out in the metalimnion of the lake focused on mean shear, not internal wave induced shear (Peeters et al. 1996).

The horizontal variations in velocity can cause the cloud to spread laterally. Unlike shear dispersion, this spreading mechanism is reversible (Sundermeyer and Ledwell 2001). Because there can be no flow into a boundary, the horizontal velocity normal to the wall of the lake must be zero. For basin scale seiches, a first horizontal mode wave has a sinusoidal form with the horizontal velocity maximum in the middle of the lake. Thus all velocity fields induced by seiches have horizontal gradients. While the internal wave strain parameterizations have been used to estimate vertical mixing in lakes (e.g. MacIntyre et al. 2009), internal wave strain as a mechanism for spreading mixed fluid away from the boundaries has not been investigated. As the straining is at a maximum at the boundary for first horizontal modes, this process may be important for moving mixed fluid into the interior where other dispersive forces may act on it.

f. Summary

Boundary mixing has been shown to be an integral mechanism for vertical fluxes in lakes, and boundary mixing due to breaking internal waves in lakes has been observed in several lakes. However, fewer researchers have studied the turbulence generated by seiching

currents, although several have proposed that large amplitude internal seiches may create significant mixing. Once the turbulence has been generated (whether by breaking internal waves or currents), it is important to determine if the turbulence can overcome the stable stratification to irreversibly mix the fluid. While observational evidence exists that connects the forcing conditions to internal wave generation and then to boundary mixing, there have been no systematic studies to determine if the forcing conditions can be used to predict boundary mixing in a lake, information which would be useful for water quality management in lakes and reservoirs.

The mixed bottom boundary layer that develops due to boundary mixing is hydrodynamically unstable with respect to the stratified interior. As a result, the mixed layer can collapse and form and intrusion of mixed fluid into the interior. From a water quality perspective, intrusions can transport nutrients offshore, making them more readily available to phytoplankton in the pelagic zone. While several field experiments have provided evidence of intrusions from boundary mixing, intrusions resulting from the collapse of turbulent regions have been tracked from the boundary into the interior mostly in laboratory experiments.

While intrusions are an outcome of the internal waves interacting with the boundary, the internal waves themselves may drive transport between the boundary and the interior. In a lake, the potential mechanism for this offshore transport is the water column currents generated by the internal seiches. Due to the oscillatory nature of seiching motions, significant net movement due to mean advection is expected to be rare as any transport into the interior will be reversed when the seiche moves in the other direction. While the net advection might be minimal, the vertical shear generated by these currents can lead to lateral shear dispersion. Additionally, the horizontal variations in velocity can cause the cloud to spread laterally by internal wave straining. While there have been tracer studies in the open ocean that address these transport mechanisms, this process has not been well-studied in boundary regions where it may enhance boundary-interior communication.

3. Objectives

In the present work, field experiments were used to study transport by turbulence generation at a sloping boundary and the fate of this boundary mixed fluid. The objectives of this study were to

1. Predict the occurrence and strength of turbulent mixing in terms of meteorological forcing and stratification by investigating the dependence of internal waves and turbulence on the slope on the Lake number, which compares the stabilizing tendency of stratification to the destabilizing tendency of the wind.
2. Investigate the fate of mixed fluid in a lake by using a tracer to track an intrusion generated at the boundary and conducting simultaneous turbulence measurements.
3. Evaluate offshore transport by basin scale seiches by tracking tracer as it spread from the boundary region into the interior

These objectives were achieved through measurements and observations throughout three summers at Ada Hayden Lake in Ames, Iowa. Measurements included bathymetry, currents, velocity profiles, turbidity, temperature profiles, wind direction and speed, internal wave spectra and temperature microstructure in addition to dye tracking experiments. These results will aid in predicting when boundary mixing will occur and enable us to estimate lateral transport from the boundaries, which can have serious implications for the spatial distribution of dissolved substances such as oxygen, nutrients, microorganisms, and plankton. Understanding the extent to which boundary mixing and the fate of the mixed fluid might control these distributions is essential for maintaining the water quality of a stratified water body.

4. Dissertation Organization

In this dissertation, the pathway from wind forcing to boundary mixing and possible outcomes of boundary mixing are examined. In Chapter 1, the background on lake

stratification, internal waves, boundary mixing, and possible fates of mixed fluid were examined. In Chapter 2, prediction of boundary mixing in a lake from basic measurements of stratification, wind forcing, and bathymetry is addressed. In Chapters 3 and 4, some mechanisms by which internal waves may lead to lateral transport in lakes are investigated. These mechanisms of boundary-interior communication include intrusions of mixed fluid from the turbulent boundary layer into the interior, lateral advection by the velocity field of the internal waves, shear dispersion by the vertical variation of internal wave induced velocities, and strain due to the horizontal variation in the internal wave velocity field.

CHAPTER 2. LAKE NUMBER AS A PREDICTOR OF TURBULENCE GENERATION ON A SLOPE

A paper to be submitted to *Journal of Geophysical Research - Oceans*

Danielle Wain and Chris Rehmann

Abstract

A crucial unanswered question in lake and reservoir management is whether the Lake number can be used to predict mixing in a lake. To address this question, three field campaigns with measurements of meteorological conditions, internal wave response by three thermistor chains, and dissipation of turbulent kinetic energy were conducted to study generation of turbulence on the sloping boundary of a small lake for Lake numbers between 0.1 and 1000. We measured the velocities in the bottom boundary layer with a high resolution acoustic current profiler and then computed the dissipation using the structure function method, which uses the spatial correlations of velocity along a beam to estimate the dissipation. During the low Lake number events, the dissipation of turbulent kinetic energy increased by up to four orders of magnitude above the default background level of 10^{-10} m^2/s^3, except during the fall turnover when the wind energy was used in thermocline deepening. To evaluate the Lake number conditions under which turbulence will be generated at the slopes, histograms of $\varepsilon/\nu N^2$ were analyzed for all the data and for five different Lake number regimes. While the spread of the measurements defied developing a quantitative relationship between the Lake number and $\varepsilon/\nu N^2$, several patterns were observed. In general, the typical value of $\varepsilon/\nu N^2$ increased as the Lake number decreased below 30. A larger jump within the energetic regime was observed when the Lake number dropped below 1.

1. Introduction

Stratification in lakes restricts vertical mixing and often controls the spatial variability of nutrients and other substances, affecting the distribution of dissolved oxygen in the water column (e.g., Rao et al. 2008), the availability of nutrients to phytoplankton (e.g., MacIntyre et al. 1999), and transport of pollutants between the hypolimnion and epilimnion (e.g., Morillo et al. 2008). The current model in ocean and lake mixing is that turbulence created at the boundaries by internal waves and currents causes most of the mixing (e.g., Gregg 1998, Ledwell et al. 2000, Wunsch and Ferrari 2004). In the ocean, much of this mixing is driven by regular tidal motions; in most lakes, this mixing is the result of wind-induced internal waves. Both the strength of the wind forcing required to generate these waves and the ability of these waves to mix fluid at the boundary depend on the stratification and the bathymetry. Because turbulence is difficult to measure, we seek to determine whether turbulence at the boundary can be predicted from standard measurements of meteorological conditions, stratification, and bathymetry.

Wind acting on the surface of a stratified lake can set up seiches, which generate currents along the boundaries. The friction with the bottom generates turbulence that mixes the water locally to create a turbulent bottom boundary layer (e.g., Gloor et al. 2000, Hondzo and Haider 2004). The seiching motions can also degenerate into higher frequency waves. Some of these waves propagate towards the boundary with a critical frequency set by the stratification and the slope of the boundary. When the critical waves approach the boundary, their energy reflects along the slope and energizes a turbulent bottom boundary layer (e.g., Eriksen 1998, MacIntyre et al. 1999).

Boundary mixing due to breaking internal waves in lakes has been observed in several lakes. MacIntyre et al. (1999) measured temperature microstructure profiles in a lake at offshore and onshore sites to determine the presence of boundary mixing and its effect on nutrient fluxes. Measurements at the onshore site (on a sloping boundary) showed enhanced mixing at the bottom which they attribute to the presence of critical internal waves breaking on the sloping bottom onshore. Hondzo and Haider (2004) measured turbulence in the benthic boundary layer on the sloping boundary of a lake using temperature microstructure

measurements and an acoustic Doppler velocimeter; they attributed the high dissipation levels to energy from the internal wave field. With detailed measurements of temperature and velocity in the bottom boundary layer, Lorke (2007) observed periodic enhanced turbulence on the slope, coinciding with the period of high-frequency internal waves seen at a mooring in the deepest part of the lake. This oscillation in the turbulence in the bottom boundary layer was also observed in numerical simulations of mixing from internal wave reflection on a slope (Slinn and Riley 1996).

Fewer researchers have looked at the turbulence generated by seiching currents, although several have proposed that large amplitude internal seiches may create significant mixing (e.g., Patterson et al. 1984). Lorke and Wüest (2005) estimated the dissipation rate of turbulent kinetic energy over the lake bottom and observed oscillations in the dissipation with the same period as the dominant seiching currents. The currents elevated the dissipation rate by over two orders of magnitude compared to measurements in the interior. Lorke et al. (2005) observed convective turbulence in the bottom boundary resulting from the periodic seiching currents. Because of friction with the boundary the fluid near the boundary moves slower than the fluid at the top of the boundary layer. As a result, when the direction of the seiching currents is up the slope, denser water is advected over less dense water, causing convection. When the seiche moves downslope, the stratification in the boundary layer becomes even stronger. As the velocity magnitude (and hence the shear) is the same regardless of the direction of the seiching movements, shear induced mixing will necessarily be smaller during this period of stronger stratification than during the upslope seiching phase. Lorke et al. (2008) confirmed that this behavior by observing differences in mixing on the slope when the seiche was moving upslope and downslope.

Once the turbulence has been generated (whether by breaking internal waves or currents), it is important to determine if the turbulence can overcome the stable stratification to irreversibly mix the fluid and create a turbulent bottom boundary layer. Using the results from direct numerical simulations and laboratory experiments, Shih et al. (2005) defined diffusive, transitional and energetic regimes of stratified turbulence based on $\varepsilon/\nu N^2$. They determined a threshold for turbulent mixing and found that as $\varepsilon/\nu N^2$ continued to increase above 100, the mixing efficiency decreases because the turbulence is more energetic than

necessary to break down the stratification; thus, the turbulence acts on fluid that has already been mixed. In the field this can occur after a bottom boundary layer is formed and the turbulence continues to act upon already mixed fluid in the boundary layer (Garrett 1979). Based on reported values of eddy diffusivity in lakes, typical values of $\varepsilon/\nu N^2$ in lakes range between 5 and 5000.

To predict the occurrence and strength of turbulent mixing in terms of meteorological forcing and stratification, we investigated the dependence of internal waves and turbulence on the slope on the Lake number, which compares the stabilizing tendency of stratification to the destabilizing tendency of the wind. Section 2 describes the lake, the measurements, and the analysis. In Section 3, we discuss the analysis of the data to extract Lake number and dissipation of turbulent kinetic energy. In Section 4, we present details of the Lake number, internal wave field and turbulence for each of the three field studies. Lastly, in Section 5, we describe the patterns of turbulence generation as a function of Lake number.

2. Experiment

Two thermistor chains and a Lake Diagnostic System (LDS) manufactured by Precision Measurements Engineering were deployed in the south basin of Ada Hayden Lake in Ames, IA, and a Nortek HR Aquadopp, a high resolution pulse coherent acoustic Doppler current profiler, was placed on a slope in the metalimnion of the lake for three deployments of 13, 15, and 8 days in July, September, and October 2008 respectively.

Ada Hayden Lake (Figure 1) is an abandoned rock quarry that is used as a secondary water supply for Ames. It consists of two basins, and the experiment was performed in the larger, deeper south basin, which has a surface area of about 0.3 km^2 and a maximum depth of about 17 m. Water enters the lake from groundwater and surface water runoff, which is filtered through wetlands. The two basins are separated by a 3-m deep sill. Because the sill is shallower than the summer thermocline, exchange between the two basins most likely consists only of epilimnetic waters. Stirring from boat traffic is small because motorized boats are prohibited on the lake. The lake has steep sides except for a few areas; the southern

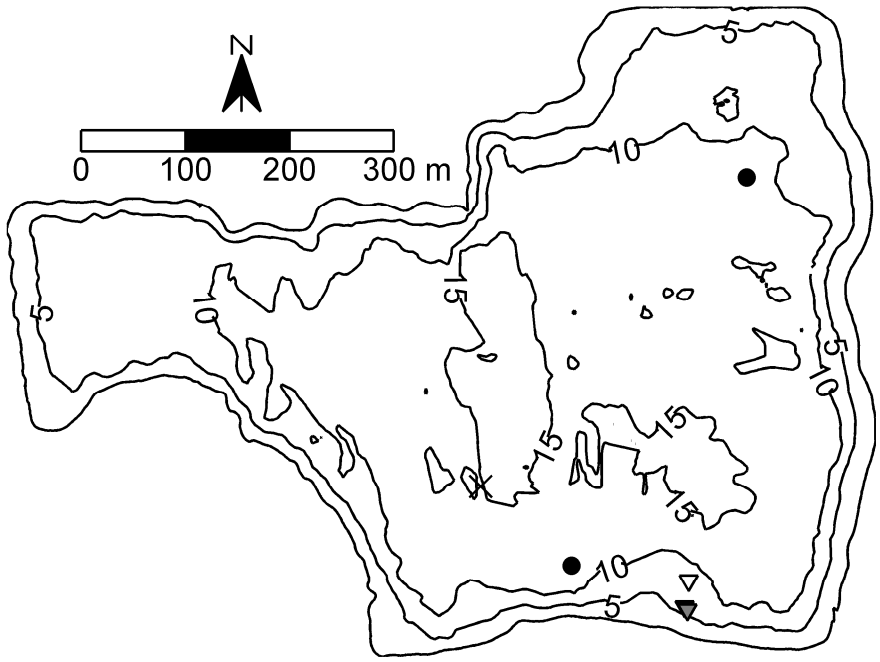

Figure 1. Bathymetric map of Ada Hayden Lake with contour intervals in meters. The locations of the LDS (×), the T-chains (●), and the Aquadopp (▼). The black, gray, and white indicate the location of the Aquadopp during the July, September, and October deployments, respectively. The Aquadopp was almost in an identical position in July and September. Two other thermistor chains manufactured by Precision Measurements Engineering were deployed in the lake.

slope, where the Aquadopp was placed, has a more moderate slope ranging between 5 and 10%

The LDS is a meteorological station with an attached thermistor chain (described below) that was moored in the lake for the entire summer. The LDS measures wind speed and direction, solar radiation, net radiation, relative humidity, and air temperature. To determine the wind forcing on the lake, the wind speed and direction were measured approximately 2.5 m above the water surface by a propeller anemometer and a wind vane,

respectively, both by Met One Instruments, Inc. All the sensors on the LDS were sampled every 15 s.

Two other thermistor chains manufactured by Precision Measurements Engineering were deployed in the lake. Our thermistor chains each have 29 nodes starting approximately 1 m below the surface and were speaced approximately every half meter. The thermistors were sampled at 15 s intervals and stored in a submersible data logger. The temperature time series that result from these measurements were used to examine the internal wave field in the lake.

The high resolution 2-MHz Aquadopp Profiler manufactured by Nortek AS has three beams; each acoustic beam is slanted at 25 degrees from the vertical. The instrument was configured to measure and report beam velocity measurements. The Aquadopp has an internal tilt and compass sensor to measure the current direction within 0.2° and 2° respectively. The high resolution system allows greater accuracy of measurements at smaller cell sizes and greater sampling rates (over a short range). The Aquadopp was set to sample in burst mode, in which 512 samples were collected at 8 Hz every five minutes.

The Aquadopp measured velocity profiles in the bottom boundary layer of Ada Hayden Lake. The Aquadopp measured in uplooking mode and was mounted on a weighted PVC frame that was designed to have a low profile (7.5 cm) and lie flat on the lake bottom. The frame may have sunk into the bottom sediments, but the strong amplitude of the Aquadopp signal suggested that the instrument sensors were not buried. Because preliminary work indicated that the boundary layer is on the order of 1 m thick, the Aquadopp was configured to measure up to 1.5 m above the bottom. To study turbulence generated on the sloping boundary, the Aquadopp was placed on the slope indicated in Figure 1. The Aquadopp also has a temperature sensor on it, which can show the temperature oscillations right at the boundary.

3. Processing

The Lake number L_N can indicate whether boundary mixing from seiching and breaking internal waves should be present in Ada Hayden Lake. The Lake number compares

the strengths of the stratification and the wind, which can cause the stable density structure to overturn. The Lake number extends the concept of the Wedderburn number to account for arbitrary stratification and bathymetry (Imberger and Patterson 1990):

$$L_N = \frac{g S_t (1 - z_T / z_S)}{\rho_s u_*^2 A_s^{3/2} (1 - z_v / z_s)} \tag{1}$$

where g is the acceleration of gravity, z_T is the center of the metalimnion, z_S is the height of the water surface, ρ_s is the density at the surface, u_* is the wind shear velocity, A_s is the area of the surface, z_v is the height of the center of volume, and S_t is the stability of the water body defined as

$$S_t = \int_0^{z_s} (z_v - z) \rho(z) A(z) dz \,, \tag{2}$$

where $A(z)$ is the surface area as a function of depth. The shear velocity of the wind is defined as

$$u_* = \left(C_{Dw} \frac{\rho_a}{\rho_1} \right)^{1/2} u_w \tag{3}$$

where ρ_a is the air density, C_{Dw} is the wind drag coefficient, and u_w is wind speed. The drag coefficient was computed with the formulas from Wüest and Lorke (2003). The wind speed is typically taken as the velocity 10 m above the water. A Lake number of 1 implies upwelling conditions. Low Lake numbers ($L_N < 10$) indicate that the wind stress is sufficient to generate wind setup throughout the water column (Imberger and Patterson 1990).

A 15-minute moving average of the meteorological and thermistor chain data from the LDS were used to compute the Lake number. The temperature profile was interpolated onto a 1-m grid to match the hypsograph. Given the thick metalimnion with a non-constant buoyancy frequency, finding the depth of the thermocline to use in the Lake number formulation is not obvious. The region of highest temperature gradient is directly below the

well-mixed surface layer; computing the Lake number using this depth will most likely underestimate the Lake number. Instead, the depth of the thermocline was determined by finding the depth of the maximum amplitude of the first vertical mode seiche. as this would be the depth around which the lake will oscillate.

To estimate the internal wave energy in the lake, we use the depth integrated potential energy defined as

$$PE(t) = \int_0^{z_s} \rho(z,t)\, g dz \tag{4}$$

(Antenucci et al. 2000). As discussed in Antenucci et al. (2000), the primary advantage of this approach is that it does not rely on the selection of a single isotherm to represent the entire time series. The disadvantage is that it is most sensitive to first vertical mode waves and can mask higher vertical modes. One concern not addressed by Antenucci et al. (2000) is how to remove the effects of daily heating from solar radiation, which creates diurnal oscillations in the integrated potential energy. To emphasize the contribution of internal waves to potential energy changes, the upper portion of the water column that appeared to be most affected by surface heating was removed from the analysis. For the July deployment, this was the top 3 m and for the September and October deployments, the top 5 m were removed. We are primarily concerned with *changes* in the potential energy, not absolute values; as the surface layer is well mixed and cannot support internal waves, it does not contribute to internal wave generated changes in PE.

To compute the integrated potential energy, each temperature profile measured by the LDS and two thermistor chains was mapped onto a vertical grid of 25 cm intervals from 3 or 5 m to 15 m (the depth of the lake at the LDS position) and then integrated numerically. The PE was then divided by a reference density to yield a potential energy per unit mass.

The time series of the rate of dissipation of turbulent kinetic energy was computed using the structure function method developed by Wiles et al. (2006). This method uses the spatial correlations of velocity along a beam to estimate the dissipation as

$$\varepsilon(z) = \frac{(D(z,r) - N(z))^{3/2}}{C_v^3 r} \tag{5}$$

where $D(z,r) = \overline{(v'(z) - v'(z+r))^2}$ where the overbar denotes a temporal average, z is the normal distance from the boundary, r is the separation between the two points in the turbulent field, $N = 2\sigma_n^2$ where σ_n^2 is the noise variance, C_v is a constant approximately equal to 2.1, and v' is the turbulent velocity fluctuation. Two other methods were initially investigated: fitting a logarithmic velocity profile to the measurements to estimate dissipation and using the inertial subrange of the spectrum of the turbulent velocity fluctuations. A clear logarithmic boundary layer was not apparent in many of the profiles, so that method proved to be unsound. The weakness of the inertial subrange fitting method is that using the beam velocities for spectral analysis is limited because no direction is defined as streamwise and the theoretical turbulent spectrum has a different constant for the streamwise direction. As Lorke and Wüest (2005) noted, the directional uncertainty leads to uncertainty of up to a factor of 0.65 in their estimates of the dissipation rate, but Lorke (2007) compared the inertial subrange fitting method and the structure function method and found good agreement between the two. As the structure function method has successfully been used in the oscillatory bottom boundary of a lake (Lorke 2007, Lorke et al. 2008), we use that method here.

As in Wiles et al. (2006), *D* was computed from a central difference over three bins; thus with 5 cm bins, along the beam $r \approx 11$cm. The values of *D* in a bin were squared and averaged over each burst for each beam. Because the noise variance has been shown to be a function of depth (Gordon et al. 1999), the noise variance for each bin in each beam for each data set was determined. Following Gordon et al. (1999), the noise level was determined by visual inspection of the spectra of the fluctuating velocity. Given the large number of individual spectra (~100,000), each spectrum was not evaluated. Instead five arbitrary bursts from each data set were chosen, and the noise level in each bin of each beam was chosen manually. The log of the five noise estimates for each bin were then averaged and a mean noise level of 10 raised to this mean was determined. The noise level was then multiplied by

the bandwidth of the spectra (4 Hz) to determine the noise variance. Then a profile of the dissipation was computed using (5). If D was below the noise (thus yielding an imaginary estimate of the dissipation), then it was assumed that the turbulence was negligible and a background dissipation estimate of 10^{-10} m^2/s^3 was substituted (see Table 1 for a summary by dataset of the occurrence of measurements below the noise). The three estimates of dissipation for each bin (one for each beam) were logarithmically averaged to yield a single dissipation profile. Then the estimates from all the bin were logarithmically averaged to yield a single depth averaged dissipation rate for each measurement burst. The noise level in the velocity measurements increased with the distance from the transducer and was different between datasets. The noise variance ranged between 10^{-7} m^2/s^2 and 10^{-4} m^2/s^2. The measurements that were below the noise were not discarded but set to background levels because otherwise this averaging of the three beams and over the depth is biased high.

Table 1. Summary of the percentage of bins that were below the noise by dataset and the percentage of the dataset where the Lake number is greater than 100.

	July	September	October
$D <$ noise	70%	86%	52%
$L_N < 100$	62%	55%	4%

4. Results

Between the study periods, the lake stratification changed significantly (Figure 2). As is typical of a dimictic lake, the thermocline deepened, and the stratification weakened from summer to fall. The depth of maximum buoyancy frequency increased from ~5 m in July, to ~7 m in September, and then to ~9 m in October. Because of the increasing mixed layer depth, the Aquadopp was placed deeper on the slope during the October deployment (Figure 1).

During the July/August deployment, low Lake numbers were caused by isolated storms (Figure 3a). Only twice did the Lake number drop below 10. On seven other occasions, the Lake number dropped to between 10 and 30. The temperature recorded at the

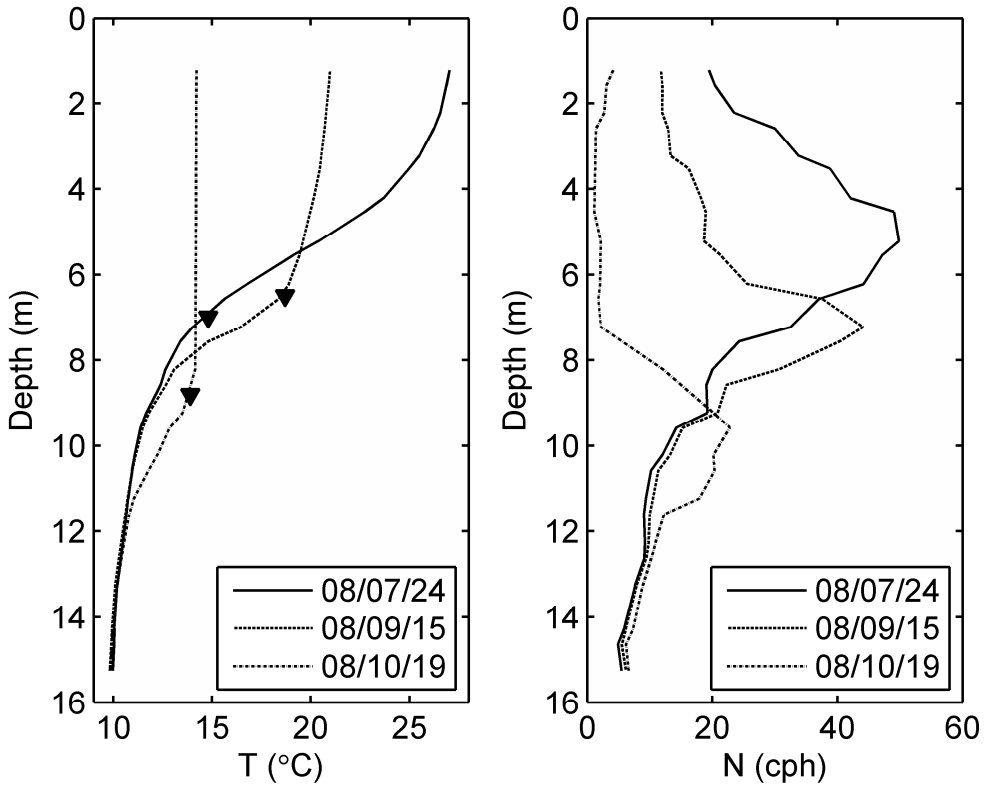

Figure 2. Mean temperature and buoyancy frequency profiles for the three Aquadopp deployments. Temperature measurements come from the Lake Diagnostic System. The depth of the Aquadopp during each deployment is indicated (▼).

Aquadopp at 7.0 m depth (Figure 3b) suggests that some internal wave activity may even occur for $L_N < 40$. For example, on 7/31 temperature oscillations measured in the bottom boundary layer were of the same magnitude as those during $L_N < 10$ events. Of note is that the integrated potential energy, which is a measure of the interal wave activity, (Figure 3c) shows very little change on this day. Visual inspection of the temperature record during on 7/31 shows potential metalimnetic compression and expansion, implying that a second vertical mode wave was excited (Figure 4); the expansion of the metalimnion at 12:00, contraction at 14:00, and expansion at 16:00 yield a period of about 4 hours, which falls within the range of 3-4.5 hours (depending on the fetch) predicted for the V2H1 seiche from a normal mode analysis. The thick metalimnion during the deployment is conducive to the generation of higher vertical modes, and as noted above, the integrated potential energy

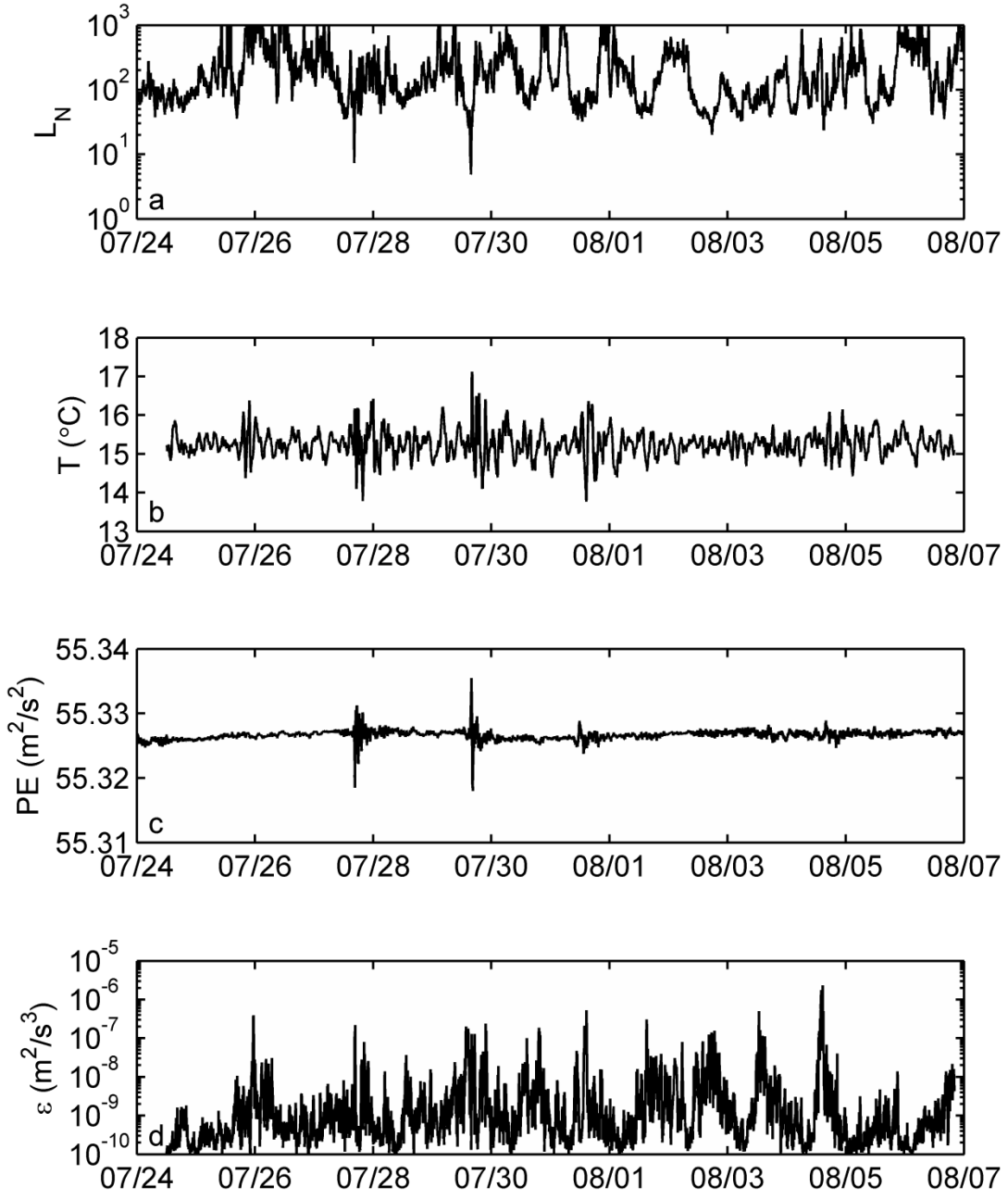

Figure 3. LDS and Aqaudopp data for the Aquadopp deployment beginning 24 July 2008. (a) Lake number measured at the LDS. (b) Temperature recorded by the Aquadopp on the slope. (c) The depth-averaged potential energy computed from the LDS thermistor chain. (d) Dissipation measured by the Aquadopp.

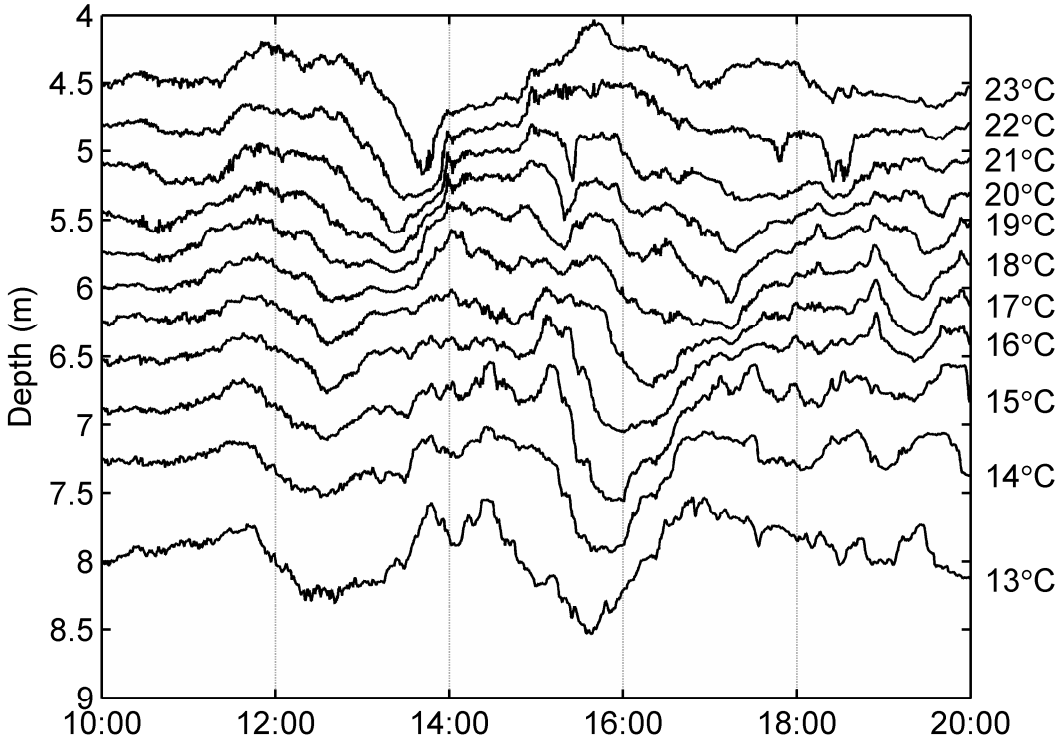

Figure 4. Metalimnetic expansion and compression on 31 July 2008.

masks these modes. The integrated potential energy from the two thermistor chains is not shown, but both have similar patterns as the LDS, although in the case of the northern thermistor chain, the oscillations are in the opposite direction as the LDS thermistor chain, which is consistent with a first horizontal mode wave.

During the low Lake number events, the dissipation of turbulent kinetic energy increased by up to four orders of magnitude above the default background level of 10^{-10} m^2/s^3 (Figure 3d). During this deployment, the peaks in the dissipation coincided with the drops in the Lake number, a pattern confirmed in the power spectra (Figure 5). The large peak at approximately 1 cpd indicates a diurnal component to the wind forcing that causes a daily pattern in the dissipation to emerge. At this frequency, the phase shift between the two signals, determined from the cross spectrum, indicates that the dissipation lags behind the Lake number by approximately three hours. While at lower frequencies the dissipation is correlated with the Lake number, at higher frequencies the spectral density of the dissipation

is slightly elevated near the frequencies of the V2H1 and V1H1 seiches. For the stratification during this period and the method of normal modes, the V2H1 frequency is between 5 and 8 cpd and the V1H1 frequency is between 16 and 23 cpd; the range is due to uncertainty in the fetch as this changes with wind direction. Also of note is that a moderate Lake number event that persists for a longer time (e.g., the event on 7/31) can have the same effect on turbulence at the slope as the impulsive winds that produced the values of $L_N < 10$ (e.g., the event on 7/29).

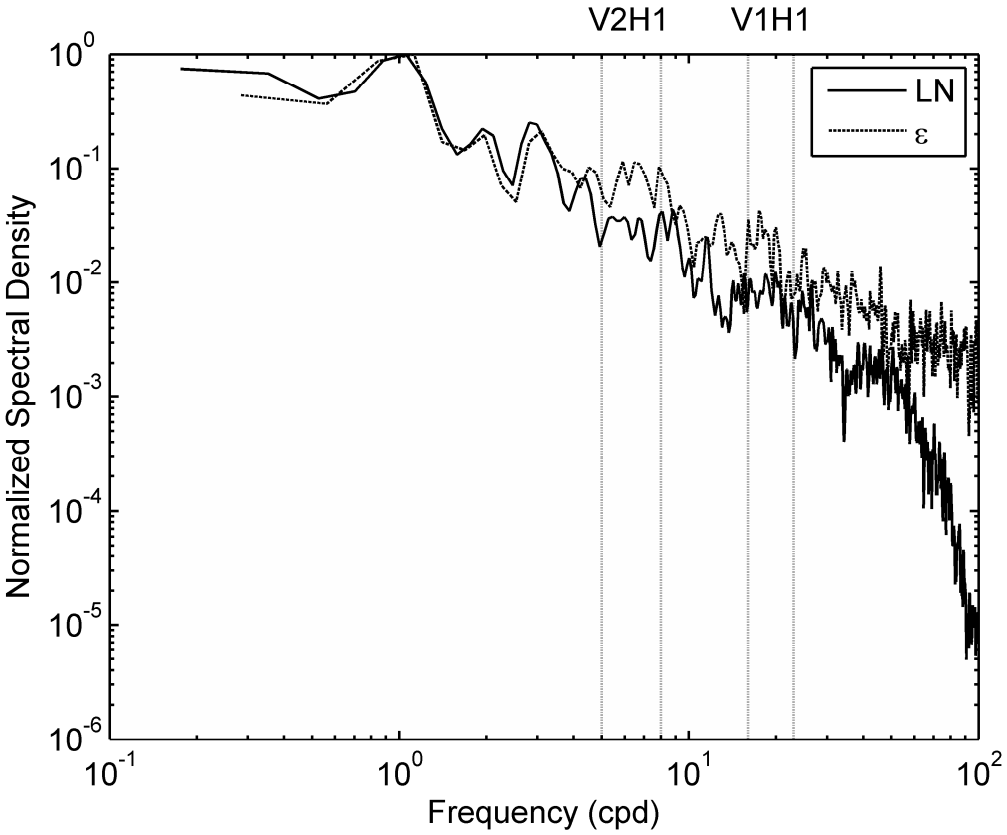

Figure 5. Frequency spectra of Lake number and dissipation rate for the July/August 2008 deployment. Following Lorke et al. (2008), the spectra were computed from the logs of the variables, and the spectral density was normalized by the maximum value.

During the September deployment, the Lake number dropped each day due to seasonal wind patterns (Figure 6a). The Lake number dropped below 10 in seven events and dropped below 30 on 67 occasions. An event is defined as starting when the Lake number drops below 30 and ending when the Lake number rises above 30 again. Despite the more

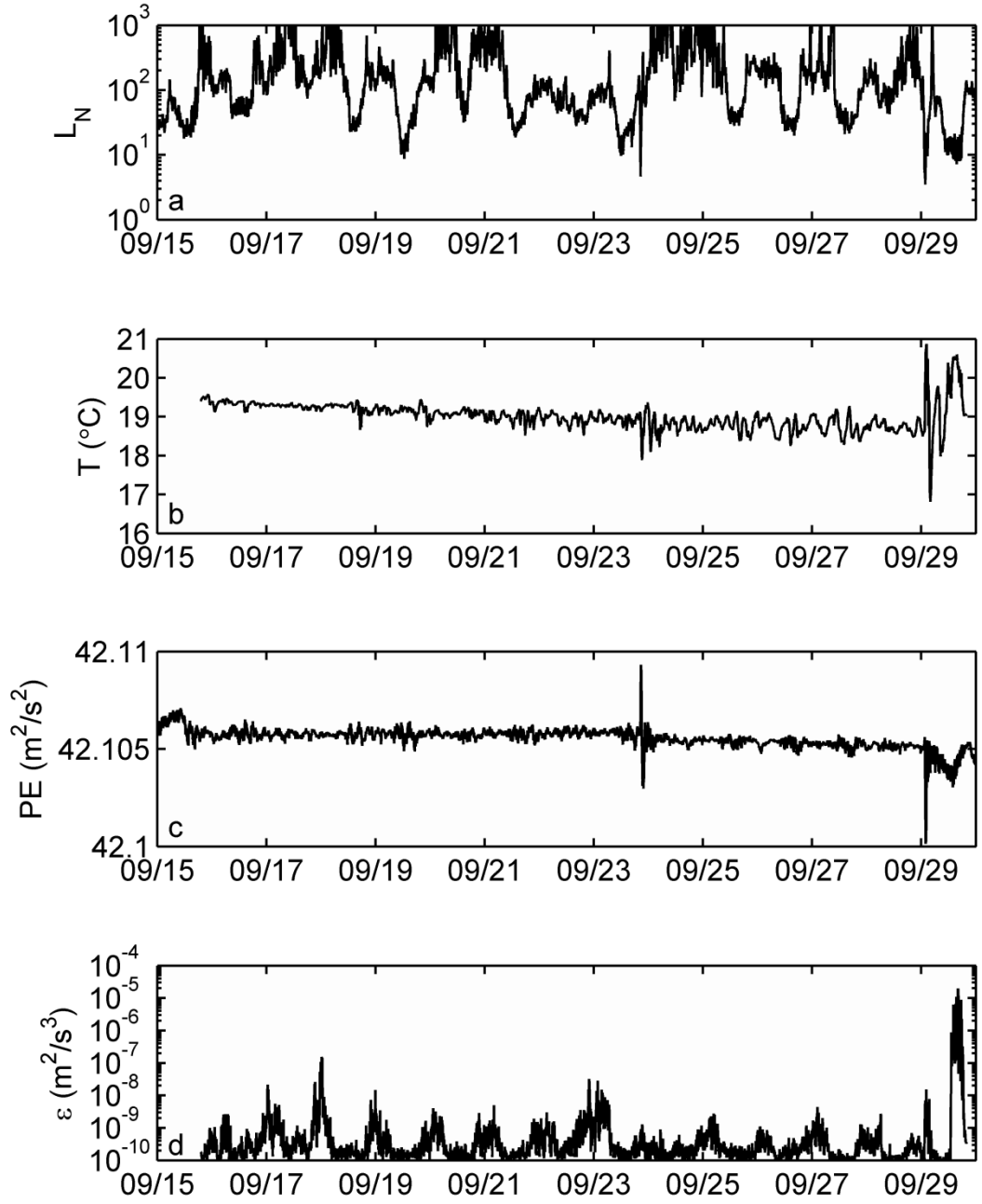

Figure 6. Same as Figure 3 for the Aquadopp deployment beginning 15 September 2008.

frequent drops in Lake number, the temperature oscillated less in the bottom boundary layer (Figure 6b), probably because of the position of the Aquadopp on the slope. The Aquadopp was at 6.5 m deep, which is right at the base of the surface mixed layer for the stratification

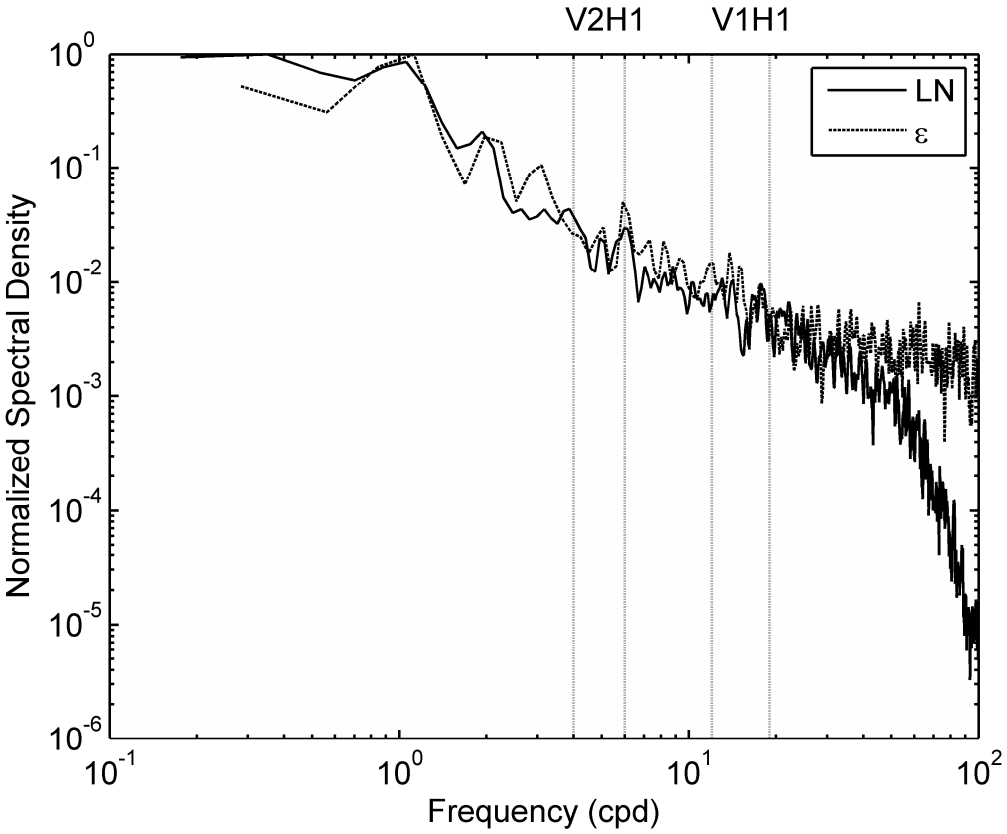

Figure 7. Frequency spectra of Lake number and dissipation rate for the September 2008 deployment. The spectra were computed from the logs of the variables and the spectral density was normalized by the maximum value.

in September. Thus, only large oscillations will generate a signal in the temperature measurements. As in the July/August deployment, the integrated potential energy (Figure 6c) increased only with more impulsive wind events.

The time record of dissipation (Figure 6d) also showed daily increases in dissipation, following the dips in Lake number. Unlike the July/August deployment, the signal was dominated by regular patterns instead of impulse events. Again, a pronounced peak at a frequency of 1 cpd appears in spectra of the Lake number and dissipation (Figure 7). Unlike the July/August deployment, the spectral density was not enhanced at the V2H1 and V1H1 frequencies (4-6 cpd and 12-19 cpd, respectively, for this stratification). The dissipation lagged the Lake number (Figure 6d) by 10 hours during this deployment instead of 3 hours as in the July/August dataset. The low Lake number events during this period were longer, and

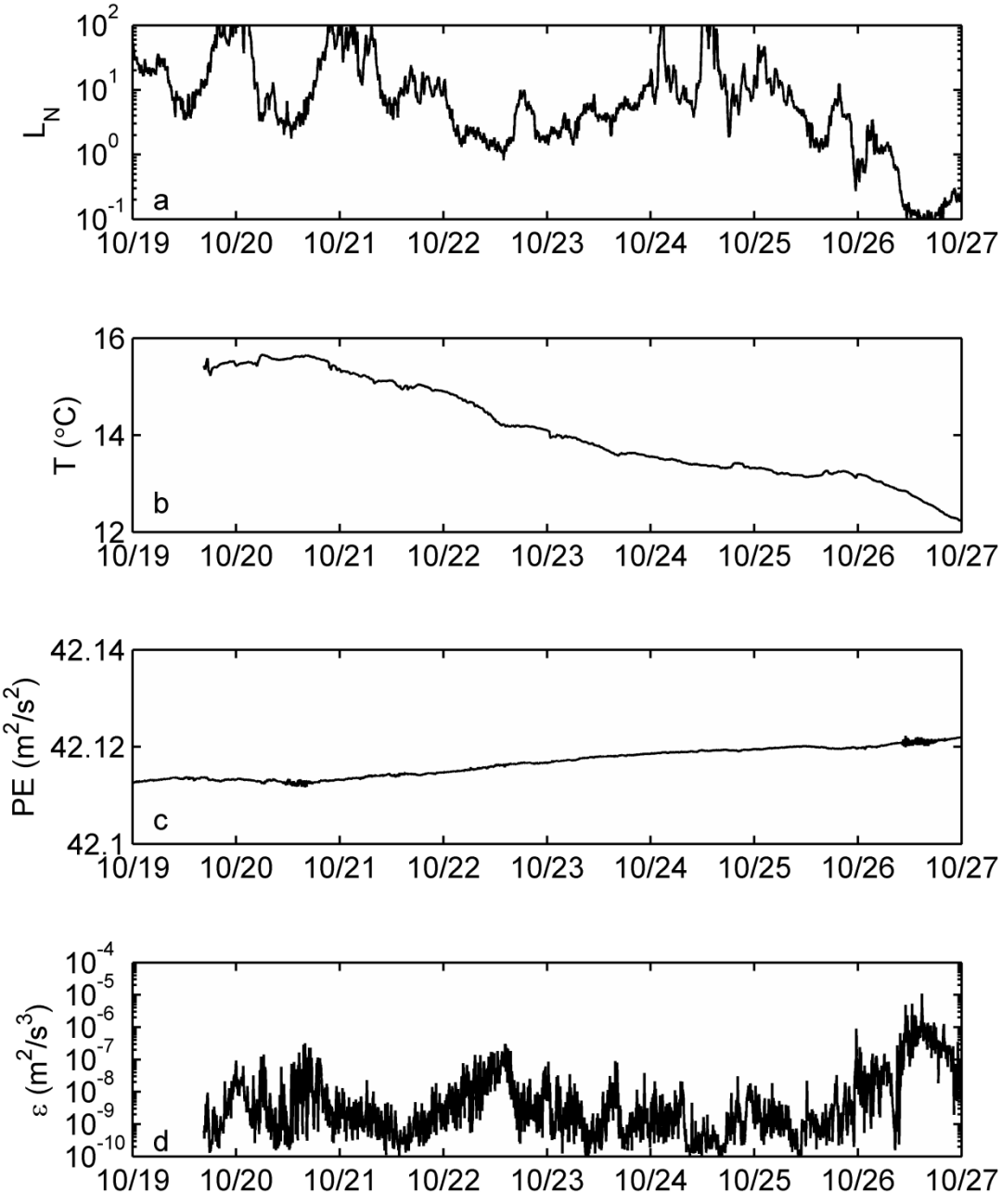

Figure 8. Same as Figure 3 for the Aquadopp deployment beginning 19 October 2008.

the lag time encompasses the time until the wind relaxes, when internal wave motions should theoretically begin. Thus, the lag between the Lake number and the dissipation is consistent with internal waves being damped on a slope after a wind event. However, if the turbulence is then generated by these motions after the wind relaxes, then spectra should be enhanced at

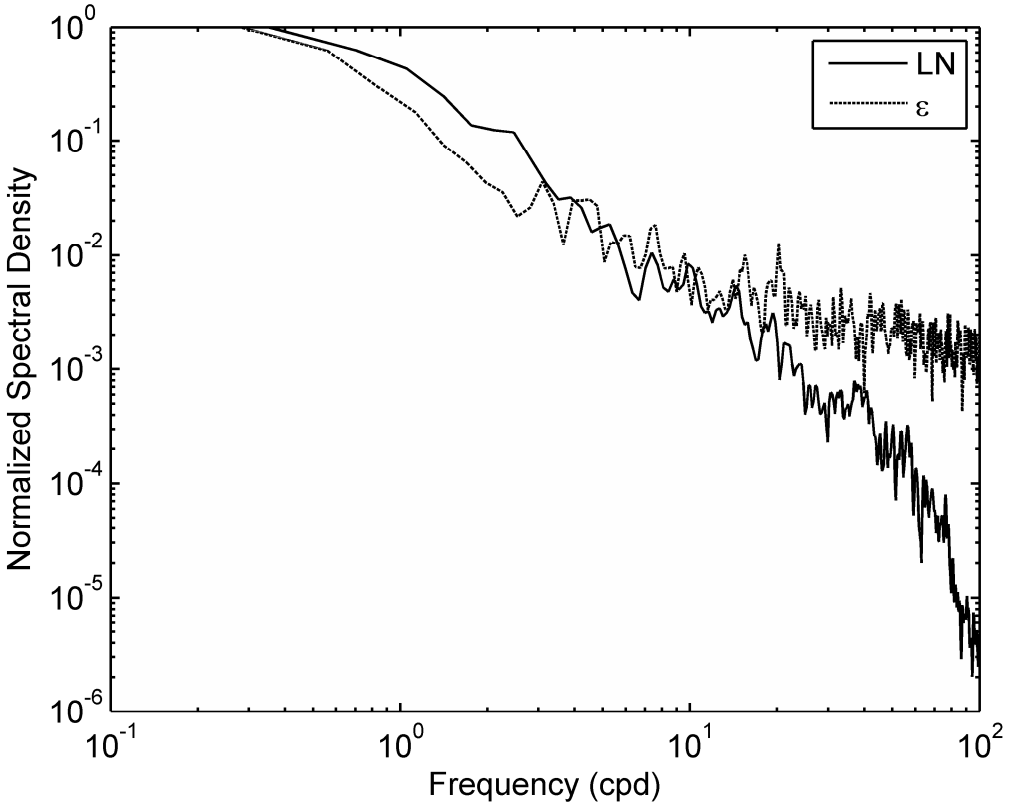

Figure 9. Frequency spectra of Lake number and dissipation rate for the October 2008 deployment. The spectra were computed from the logs of the variables and the spectral density was normalized by the maximum value.

the seiche frequencies. One potential explanation for a lack of enhancement is the position of the current profiler in the water column. With each oscillation of the seiche, the amplitude is damped by friction with the boundaries. Because the Aquadopp was relatively high in the metalimnion, it may have measured the initial turbulence generated by the first oscillation, but the subsequent oscillations were too damped to generate turbulence that far up the slope.

During the deployment of October 2008, the lake experienced strong winds that eroded the thermocline and led to the fall turnover. The Lake number dropped below the upwelling value of 1 four times and on 21 occasions, it dropped below 3 (Figure 8a). The Lake number dropped between 3 and 10 in only one isolated event. The Lake number never decreased below 30 without continuing to decrease below 10; in fact for 85% of the record, the Lake number was below 30. As in September, the Aquadopp was located at the base of

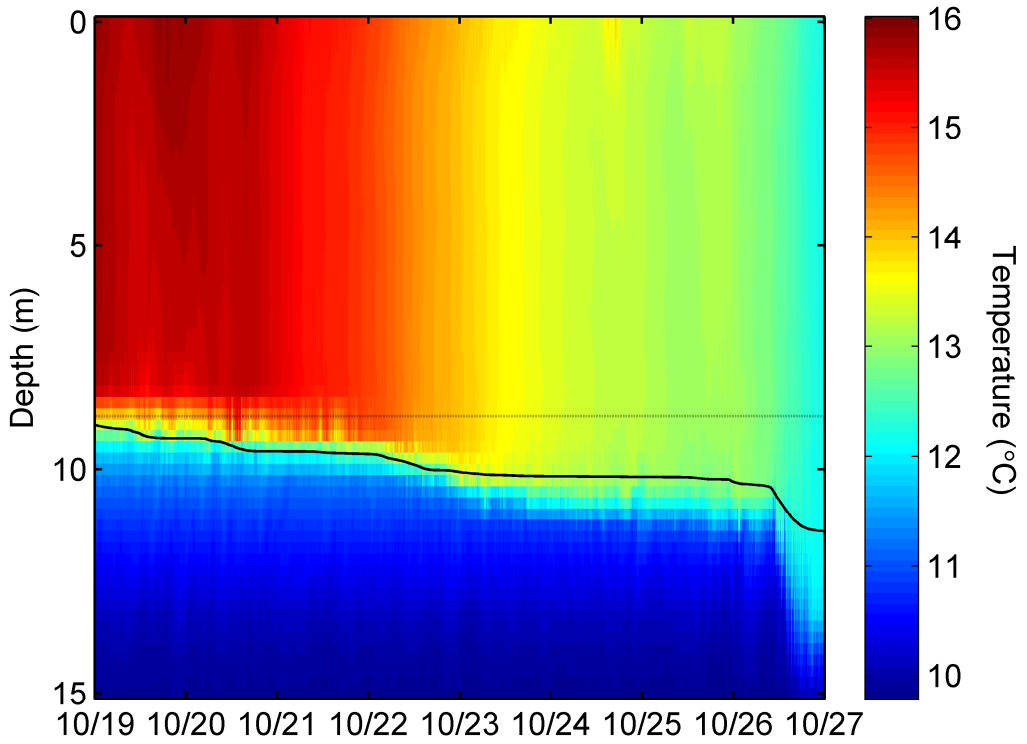

Figure 10. Thermocline deepening during the October Aquadopp deployment. The solid line indicated the theoretical thermocline depth from wind mixing. The depth of the Aquadopp is indicated by the gray horizontal line.

the surface mixed layer (at 8.8 m). Thus the temperature signal at the instrument was dominated by the wind mixing that eroded the thermocline (Figure 8b). The change in integrated potential energy in the lake was also dominated by the thermocline deepening (Figure 8c).

The time series of dissipation shows surprisingly low values, given the low Lake numbers during this period (Figure 8d). Over 40% of the dissipation estimates were below 10^{-9} m^2/s^3, while only 5% were above 10^{-7} m^2/s^3. The spectra of the Lake number and dissipation show no dominant frequencies (Figure 9). It is likely that the wind energy input into the lake was used to permanently change the thermal structure instead of to generate internal waves that are damped at the boundaries. , we can estimate The thermocline deepening due to wind mixing can be estimated by using a simple surface layer model

(Fischer et al. 1979, p.177) and assuming, from the LDS data, that the lake starts with a 9 m thick mixed layer with a mean temperature of 15.7°C, overlying a 1.5 m linearly stratified metalimnion with a temperature gradient equal to the average gradient in that region. The theoretical thermocline depth follows the data quite closely. After 10/23, the model does not account for some of the thermocline deepening. Horn et al. (2001) found that for a deep thermocline and Wedderburn number (a simplified form of the Lake number) < 1.5, that Kelvin-Helmholtz billows were more likely to form than damped internal waves, in which case the mixing is occurring in the interior as opposed to the boundary. The high values of dissipation at the end of the record coincide with Lake numbers of 0.1; because the Aquadopp was in the surface layer at this point, the dissipation rates measured by the Aquadopp may be from surface layer turbulence and not particular to the boundary region.

5. Discussion

We now address the issue of whether the Lake number can be used to predict mixing in a lake, a question of relevance for management of water quality in lakes and reservoirs. Turbulence measurements in the field are difficult and require specialized knowledge and equipment. The Lake number can be computed from commonly measured variables on a monitored lake or reservoir. Thus it would be valuable to be able to predict mixing from the Lake number.

Dissipation rates of turbulent kinetic energy are just one element that determines whether mixing will occur. In less stratified environments, less turbulent production is needed to generate the same amount of mixing. The three study periods each had different stratification, so to compare the Lake number to turbulence generation and mixing, we use the dimensionless parameter $\varepsilon/\nu N^2$. Shih et al. (2005) classified the turbulence as diffusive, transitional or energetic based on $\varepsilon/\nu N^2$. For $\varepsilon/\nu N^2 < 7$ (the diffusive regime), the diffusivity is molecular; Ivey and Imberger (1991) found cutoff values for turbulence generation at about twice this value ($\varepsilon/\nu N^2 = 15$). For $7 < \varepsilon/\nu N^2 < 100$ (the transitional regime), the mixing efficiency was constant and coincided well with the typical value used in eddy diffusivity

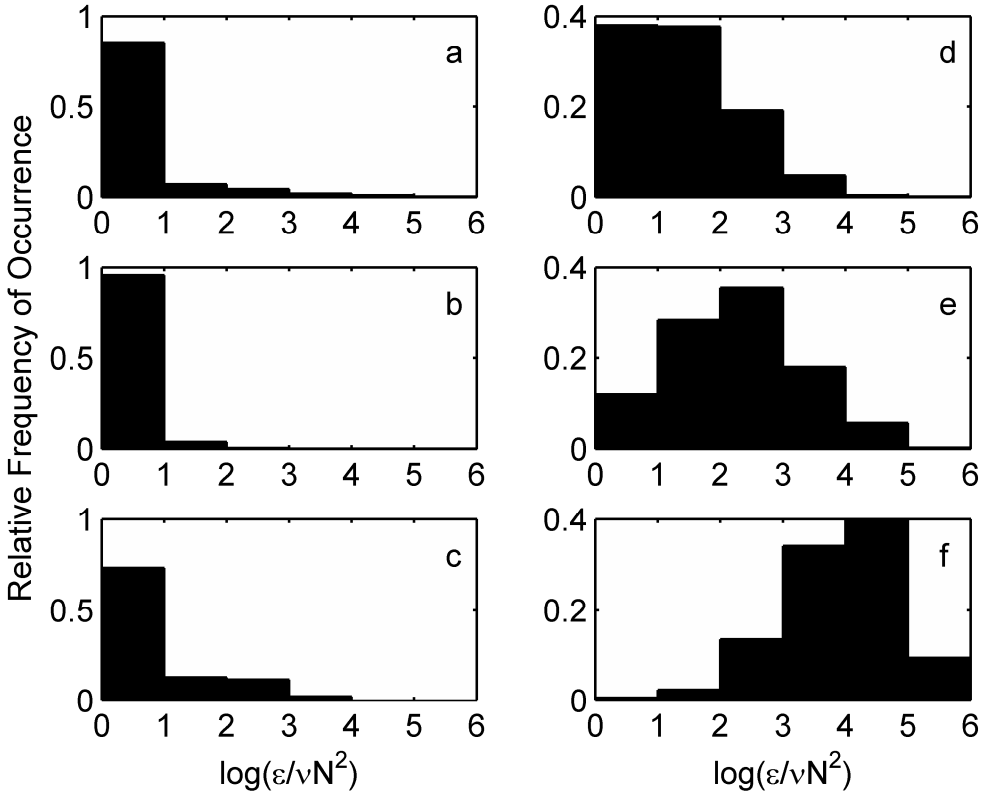

Figure 11. Relative frequency of occurrence for $\varepsilon/\nu N^2$ for different Lake number regimes: (a) all the data (n = 11857), (b) $30 \leq L_N < 100$ (n = 2989), (c) $10 \leq L_N < 30$ (n = 769), (d) $3 \leq L_N < 10$ (n = 811), (e) $1 \leq L_N < 3$ (n = 451), and (f) $L_N < 1$ (n = 2001).

parameterizations in lakes and the ocean; the mixing efficiency decreased as $\varepsilon/\nu N^2$ grows above 100 (the energetic regime).

For each measurement of dissipation, the Lake number at the closest measurement time was used for comparison. In Figure 11, we show histograms of the relative frequency of occurrence of each decade of $\varepsilon/\nu N^2$ for all the data (Figure 11a) and five different Lake number regimes (Figure 11b-f). The histogram for all of the data (Figure 11a) is dominated by values of $\varepsilon/\nu N^2$ below 10, although a small tail extends to 10^6. As the data is analyzed by order of magnitude, in the following we define $\varepsilon/\nu N^2 = 10$ as the turbulence threshold, which is the same order of magnitude as the thresholds defined by Shih et al. (2005) and Ivey and Imberger (1991). Most of the dataset is in the diffusive regime, below the threshold for

turbulent mixing. In a lake interior, values of dissipation as low as 10^{-10} m^2/s^3 are not rare (Wüest and Lorke 2003). When the Lake number is between 30 and 100 (Figure 11b), while there are a few instances of elevated $\varepsilon/\nu N^2$ (> 10), for the most part the measurements remain in the diffusive regime. As the Lake number drops further to between 10 and 30 (Figure 11c), higher values of $\varepsilon/\nu N^2$ occur more frequently, although most values still fall within the diffusive regime. When the Lake number drops below 10 (Figure 11d), most of the estimates of elevated $\varepsilon/\nu N^2$ are above the turbulence threshold, although transitional turbulence (between 10 and 100) dominates. When the Lake number drops below 3 (Figure 11e), dramatically fewer measurements fall in the diffusive regime, and the peak in the $\varepsilon/\nu N^2$ histogram moved to the energetic turbulence regime between 10^2 and 10^3. Finally, when the Lake number drops below 1 (Figure 11f), almost all the measurements of $\varepsilon/\nu N^2$ are elevated and the location of the peak is between 10^4 and 10^5.

While the spread of the measurements defies developing a functional relationship between the two variables, several observations can be made. First, Lake numbers between 30 and 100 very rarely will produce turbulence that surpasses the threshold for mixing, although it is not impossible. Second, the threshold of Lake number = 10 (Imberger and Patterson 1990) may be too low for mixing considerations; during the current deployments, 27% of estimates of $\varepsilon/\nu N^2$ were above in the transitional and energetic turbulence regimes when the Lake number was between 10 and 30. Third, the changes in $\varepsilon/\nu N^2$ with Lake number may have a continuous functional relationship, but the spread in the measurements makes it difficult to quantify. The peak in $\varepsilon/\nu N^2$ increased by an order of magnitude with each regime of decreasing Lake number below 30. When the Lake number dropped below 1, however, $\varepsilon/\nu N^2$ increased by two orders of magnitude. This data spans three very different sets of background conditions. If other factors that may affect the spread of the measurements can be constrained, there is potential for predicting boundary mixing within an order of magnitude with commonly measured lake parameters.

5. Summary

Three field campaigns with measurements of meteorological conditions, internal wave response, and dissipation of turbulent kinetic energy were conducted to study generation of turbulence on the sloping boundary of a small lake. The temperature time series from three thermistor chains were used to examine the internal wave field in the lake. The Aquadopp also had a temperature sensor on it, which can show the temperature oscillations right at the boundary. The dissipation rate was estimated from the Aquadopp using the structure function method.

During the July/August 2008 deployment, the integrated potential energies from the two thermistor chains on opposite ends of the lake were out of phase with each other following wind events, which is consistent with the generation of first horizontal mode seiches. The highest dissipation rate was recorded during an event that had a Lake number of approximately 30; a moderate Lake number event that persisted for a longer time appeared to have the same effect on turbulence at the slope as the impulsive winds that produced the values of $L_N < 10$. During the September 2008 deployment, the dissipation lagged behind the Lake number, consistent with the wind setting up internal seiches which then dissipate by friction with the boundary.

During the October 2008 deployment, the lake was entering the fall overturn; thus the change in integrated potential energy in the lake was dominated by the thermocline deepening. The high values of dissipation at the end of the record coincided with Lake numbers of 0.1; because the Aquadopp was in the surface layer at this point, the dissipation rates measured by the Aquadopp may be from wind mixing and not particular to the boundary region.

To evaluate the Lake number conditions under which turbulence will be generated at the slopes, histograms of $\varepsilon/\nu N^2$ were analyzed for all the data and for five different Lake number regimes. While the spread of the measurements was restrictively large for determining a quantitative relationship between the Lake number and the turbulence intensity, some relationships between the Lake number and $\varepsilon/\nu N^2$ for different Lake number regimes could be observed. In general, the typical value of $\varepsilon/\nu N^2$ increased as the Lake

number decreased below 30. A larger jump within the energetic regime was observed when the Lake number dropped below 1. Further work to understand the spread of $\varepsilon/\nu N^2$ in each Lake number regime would assist in helping to define a functional relationship between Lake number and mixing that could be used by those responsible for lake and reservoir management.

Acknowledgements

The authors thank Mike Kohn, Josh Scanlon, Adam Wright, and Emily Libbey for help with the experiments and acknowledge support from the National Science Foundation under Grant OCE 06-47253. Any opinions, findings, and conclusions or recommendations expressed in this material are those of the authors and do not necessarily reflect the views of the National Science Foundation.

CHAPTER 3. TRANSPORT BY AN INTRUSION GENERATED BY BOUNDARY MIXING IN A LAKE

A paper in revision for *Water Resources Research*

Danielle Wain and Chris Rehmann

Abstract

A dye study was conducted to track an intrusion generated at the boundary of a small lake. Persistent turbid layers offshore presented evidence of possible intrusions from boundary mixing. After high winds, a streak of Rhodamine WT was injected at the boundary of the lake where the slope was between 5 and 10%. Both vertical profiles and horizontal transects of the dye concentration were measured. The three dimensional dye mapping showed a distinct dye intrusion, ranging between 0.5 and 1 m thick, over 200 m in horizontal extent offshore, one day after the injection. Profiles of temperature microstructure measured soon after the injection both at the injection site and offshore showed an elevated eddy diffusivity near the boundary where the dye was injected, indicating that the intrusion results from boundary mixing. Because the dominant internal waves are subcritical, the mixing is most likely due to seiching currents interacting with the boundary. The propagation characteristics of the intrusion were predicted most closely by a formulation for an axisymmetric intrusion governed by a balance between buoyancy and inertia. These results show that intrusion generation and propagation may be a significant process for mass transport in stratified lakes and reservoirs.

1. Introduction

Understanding the transport of dissolved substances such as oxygen, nutrients, microorganisms, and plankton is essential for managing water quality in lakes and reservoirs. The ability of stratification, which is caused by temperature, salinity, or sometimes chemical species, to restrict vertical mixing and control the spatial variability of nutrients and other

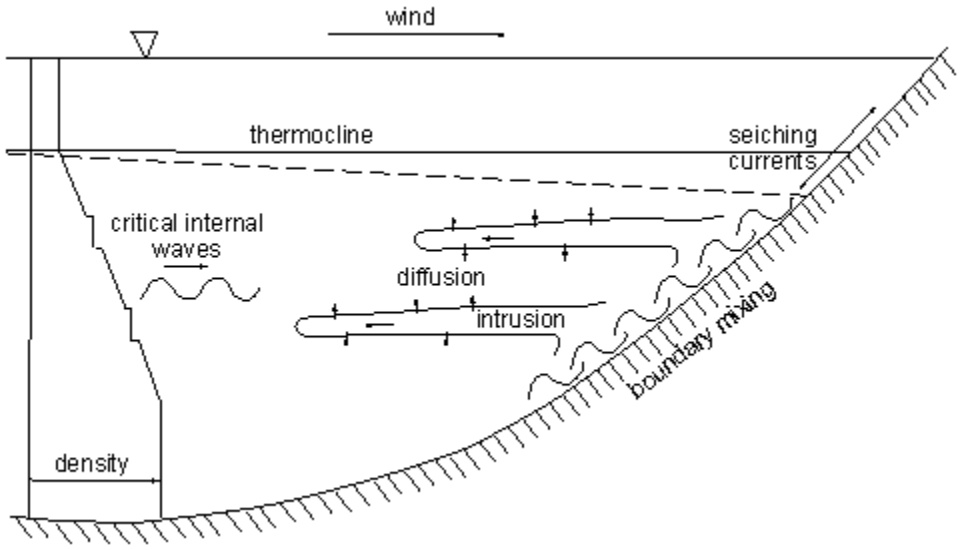

Figure 1. Schematic of physical processes leading to boundary mixing and intrusions in a lake. Wind on a stratified lake can create internal seiching currents and critical internal waves.

substances affects the distribution of dissolved oxygen in the water column [e.g., *Rao et al.*, 2008], the availability of nutrients to phytoplankton [e.g., *MacIntyre et al.*, 1999], and transport of pollutants between the hypolimnion and epilimnion [e.g., *Morillo et al.*, 2008]. The current model in ocean and lake mixing is that turbulence created at the boundaries by internal waves and currents causes most of the mixing [e.g., *Gregg*, 1998; *Ledwell et al.*, 2000; *Wunsch and Ferrari*, 2004]. While much work has been done to investigate mixing at boundaries in lakes and the ocean, less attention has been paid to the fate of the mixed fluid. One possible outcome, investigated in this study, is that intrusions transport mixed fluid into the interior.

Two main mechanisms generate turbulence at a boundary that can lead to intrusions (Figure 1). Wind acting on the surface of a stratified lake can set up seiches, which generate currents along the boundaries. The friction with the bottom generates turbulence that mixes the water locally to create a turbulent bottom boundary layer [e.g., *Gloor et al*., 2000]. The seiching motions can also degenerate into higher frequency waves. Some of these waves propagate towards the boundary with a critical frequency set by the stratification and the

slope of the boundary. When the critical waves approach the boundary, their energy reflects along the slope and energizes a turbulent bottom boundary layer [e.g. *Eriksen*, 1998; *MacIntyre et al*., 1999]. Once a turbulent boundary layer is created on the slope, the mixed boundary layer fluid becomes gravitationally unstable with respect to the stratified water adjacent to it, and the mixed patch collapses and redistributes laterally.

Several studies provide evidence for intrusions from boundary processes. *Caldwell et al.* [1978] observed stepped profiles near sloping boundaries in a lake that they attributed to intrusions generated by boundary mixing. *Gloor et al*. [2000] observed mixed water masses extending up to 200 m into the lake interior and ascribed them to intrusions, which reduce the boundary layer thickness by discharging mixed fluid into the interior. Intrusions can also explain turbid layers observed in the interior of a water body. *Dickson and McCave* [1986] and *Thorpe and White* [1988] proposed that nepheloid layers along a continental slope resulted from boundary mixing due to the semi-diurnal M2 tide reflecting critically. Dye injected into the water column above a slope in a fjord was eventually entrained into a turbulent boundary layer generated by the semidiurnal tide moving over rough topography, and then it entered the interior as intrusions [*Inall*, 2009]. Such observations in lakes are rare: *Marti and Imberger* [2008] observed a well-defined turbid layer whose thickness was associated with the thickness of the seiche generated bottom boundary layer; they concluded that the turbid layer was advected offshore by a jet in the metalimnion that resulted from a second vertical mode seiche.

While several field experiments have provided evidence of intrusions from boundary mixing, intrusions resulting from the collapse of turbulent regions have been tracked from the boundary into the interior mostly in laboratory experiments. Several experiments have investigated the vertical mixing from breaking internal waves and observed intrusions [e.g., *Cacchione and Wunsch*, 1974; *Ivey and Nokes*, 1989], but fewer have quantified the intrusion properties. *De Silva et al.* [1997] and *McPhee-Shaw and Kunze* [2002] measured propagation of intrusions resulting from breaking internal waves on a slope and related the intrusion speed to the energy of the incident internal waves. The former observed no change in the background density stratification due to the intrusion, whereas the latter observed persistent steps; however, as *De Silva et al*. [1997] noted, even if the intrusion does not change the

thermal structure of a lake, dissolved substances can still be transported offshore. The experiments of *Wells and Helfrich* [2004] provide information on the three-dimensional behavior of an intrusion generated at the boundary; in those, effects of rotation limited the propagation of the intrusion.

To investigate the fate of mixed fluid in a lake, we used a tracer to track an intrusion generated at the boundary and conducted simultaneous turbulence measurements. Section 2 describes the lake, the measurements, and the analysis. In Section 3, we present measurements of the wind, eddy diffusivity, and dye concentrations. In Section 4 we compare our measurements to previous work on intrusions, discuss the source of the intrusion, the force balance that drives its propagation, and the implications for water quality.

2. Experiment

An experiment that combined microstructure measurements with a dye release was conducted at Ada Hayden Lake in Ames, Iowa, USA (Figure 2). The combined tracer/microstructure study took place one hour after a storm front passed on July 21, 2005. An atmospheric gravity wave produced strong winds that reversed direction by 180 degrees as the wave passed. We measured the temperature microstructure six hours after the dye injection and mapped the dye cloud one day after the injection. Another atmospheric gravity wave passed over the lake 17 hours after the injection but before the mapping.

Ada Hayden Lake is an abandoned rock quarry that is used as a secondary water supply for Ames. It consists of two basins, and the experiment was performed in the larger, deeper south basin, which has a surface area of about 0.3 km^2 and a maximum depth of about 17 m. The fetch in the primary wind direction is approximately 700 m. The lake is strongly stratified in the summer with a well-mixed epilimnion lying over a strongly stratified metalimnion and a weakly stratified hypolimnion (Figure 3a). Water enters the lake from groundwater and surface water runoff, which is filtered through wetlands. The two basins are separated by a 3-m deep sill. Because the sill is shallower than the summer thermocline, exchange between the two basins most likely consists only of epilimnetic waters. Stirring from boat traffic is small because motorized boats are prohibited on the lake. The lake has

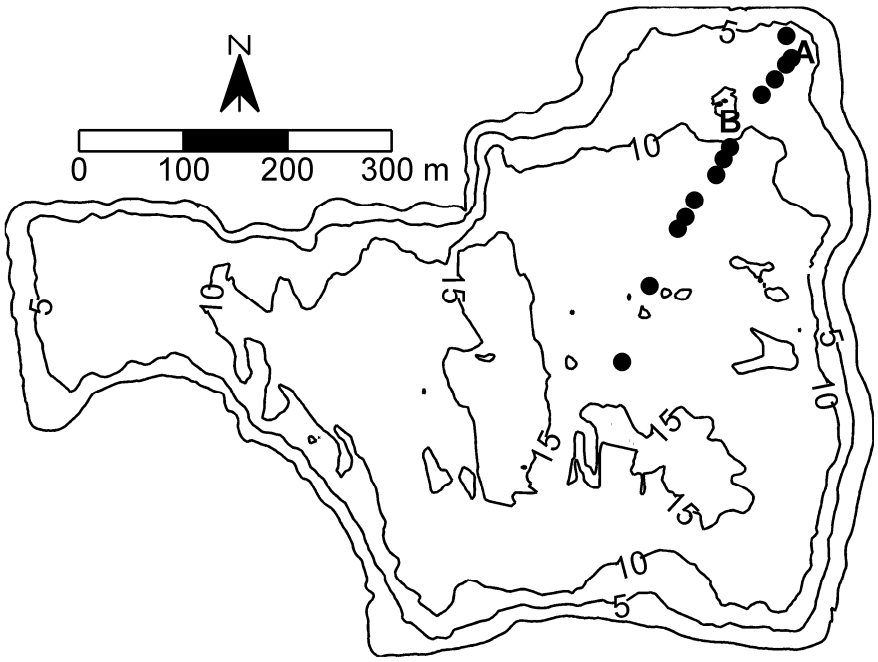

Figure 2. Map of the south basin of Ada Hayden Lake. Depth contours are marked in meters. Dye was injected at Station A, and microstructure was measured near Stations A and B. Closed circles (•) indicate where dye profiles were measured for the transect series in Figure 7.

steep sides except for a few areas; the northeast corner, where dye was injected, has a more moderate slope ranging between 5 and 10%.

During July, the mean winds at Ada Hayden Lake are 2-3 m/s SSE. Stronger winds (>5 m/s) are typically associated with storms, most often from the south. Wind measurements come from the Ames Municipal Airport, approximately 8 km south of the lake. Comparing these measurements to those from several meteorological stations in communities surrounding the lake suggests that wind speeds measured at the airport represent the conditions at the lake. The wind was measured every minute at the airport, and then a moving average over a 15 minute interval was computed. The strength of the wind, which can cause

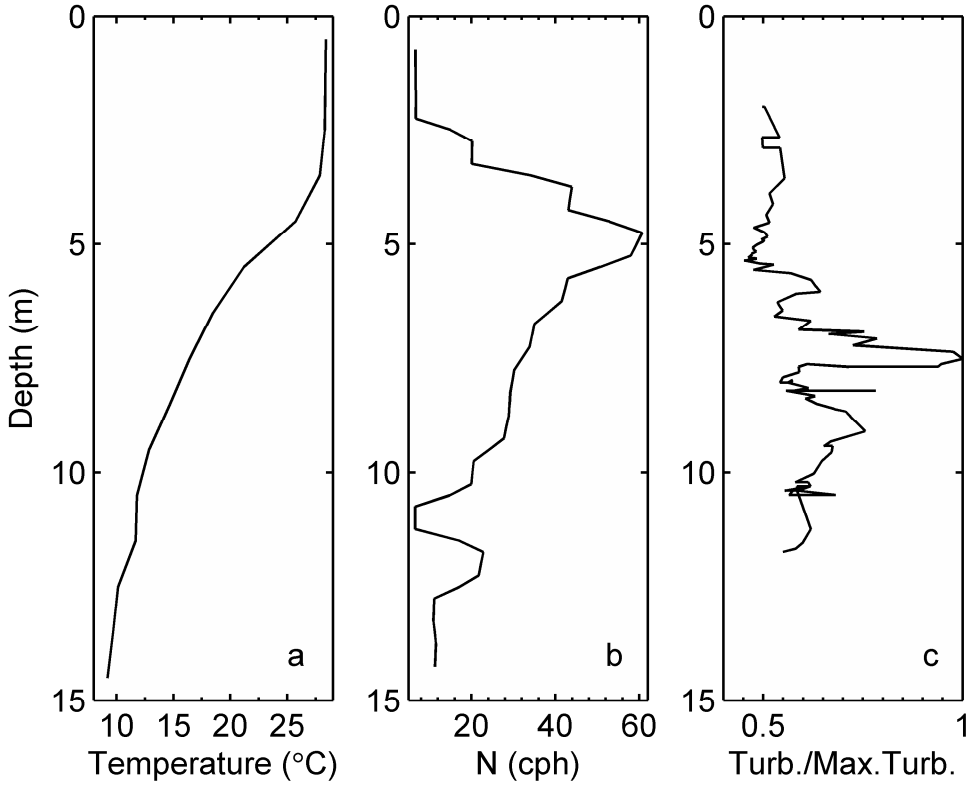

Figure 3. Conditions during the experiment: (a) Average temperature profile, (b) buoyancy frequency *N*, and (c) turbidity profile before the dye injection. The turbidity profile as a function of temperature was mapped onto the mean temperature profile to remove internal wave effects.

the stable density structure to overturn, was compared to the strength of the stratification, which resists overturning, with the Lake number [*Imberger and Patterson*, 1990]:

$$L_N = \frac{gS_t(1 - z_T / z_S)}{\rho_s u_*^2 A_s^{3/2}(1 - z_v / z_s)} \qquad (1)$$

where g is the acceleration of gravity, z_T is the center of the metalimnion, z_S is the height of the water surface, ρ_s is the density at the surface, u_* is the shear velocity of the wind, A_s is the

area of the surface, z_v is the height of the center of volume, and S_t is the stability of the water body defined as

$$S_t = \int_0^{z_s} (z_v - z)\rho(z)A(z)dz\,, \tag{2}$$

where $A(z)$ is the surface area as a function of depth. The shear velocity of the wind is defined as

$$u_* = \left(C_{Dw} \frac{\rho_a}{\rho_1} \right)^{1/2} u_w \tag{3}$$

where ρ_a is the air density, C_{Dw} is the wind drag coefficient, and u_w is wind speed, typically taken as the velocity 10 m above the water. The drag coefficient was computed with the formulas from *Wüest and Lorke* [2003]. A Lake number of 1 implies upwelling conditions. Low Lake numbers ($L_N < 10$) indicate that the wind stress is sufficient to generate wind setup throughout the water column [*Imberger and Patterson*, 1990]. When the wind relaxes after wind setup occurs, seiching motions are generally observed in other lakes [e.g., *MacIntyre et al.,* 2009; *Romero et al.*, 1998; *Stevens and Lawrence*, 1997], so we expect the same outcome here.

Temperature profiles were measured with the temperature sensor on a Self-Contained Underwater Fluorescence Apparatus (SCUFA) from Turner Designs, which was sampled simultaneously at 1 Hz with an SBE 50 Digital Oceanographic Pressure Sensor from Sea-Bird Electronics. The instruments were lowered by hand at approximately 0.25 m/s, and 76 vertical profiles were measured. The water column was divided into 1-m bins, and all the measurements in the depth bin were averaged to produce a mean temperature profile for the experiment, with the mean value associated with the center of the bin. The equation of state of *Chen and Millero* [1977] was used to compute the density profile from the mean temperature profile. This density profile was mapped onto a 0.25 m grid, and the buoyancy

frequency was computed using a centered difference (Figure 3b). Background turbidity was also measured with the SCUFA.

Temperature microstructure was measured with a Self Contained Autonomous MicroProfiler (SCAMP) manufactured by Precision Measurement Engineering. The SCAMP measures small-scale temperature fluctuations with Thermometrics FP07 thermistors, which have a nominal response time of 7 ms, though the actual response depends on probe speed and sensor construction [*Gregg*, 1999]. The fall rate of the SCAMP was approximately 0.1 m/s, and temperatures were recorded at 100 Hz. Analog signal processors in the SCAMP computed the time derivative of the voltage signals from the thermistors before the signals were digitized, and profiles of temperature gradient were computed with Taylor's hypothesis.

The temperature gradients were then used to compute the dissipation of temperature variance χ_T and eddy diffusivity K_T. As in *Soga and Rehmann* [2004], χ_T was computed by assuming isotropy and integrating the difference of the observed spectrum S_{obs}, computed in segments of 256 points or about 0.25 m, and the noise spectrum S_n over the wavenumber k_1:

$$\chi_T = 6D_T \int_0^\infty [S_{obs}(k_1) - S_n(k_1)]dk_1 , \tag{4}$$

where D_T is the molecular diffusivity of heat. The eddy diffusivity was computed with the relation from *Osborn and Cox* [1972]:

$$K_T = \frac{\chi_T}{2\left(\partial \overline{T} / \partial z\right)^2} . \tag{5}$$

The mean temperature gradient $d\overline{T}/dz$ was determined by fitting a line to the temperature in each segment. Values of $d\overline{T}/dz$ and χ_T were assigned to 0.25 m intervals in the vertical, and profiles of the ensemble averages and their 95% confidence limits were computed for each sampling site from 200 bootstrap resampled populations. Data from segments with unstable temperature gradients (i.e., $d\overline{T}/dz < 0$) were discarded before averaging because the

Osborn-Cox method was developed for stably stratified flows. The statistics for χ_T and the temperature gradient were used to compute profiles of K_T and their 95% confidence limits using equation (5). *Wain and Rehmann* [2005] addressed the uncertainty in the eddy diffusivity K_T computed with the Osborn-Cox method, which comes from the assumption of isotropy, the fit of the mean temperature gradient for each segment, the resolution of χ_T, and the validity of the Osborn-Cox balance.

Rhodamine WT was used to track mixed fluid from the slope into the interior. The presence of a turbid layer (Figure 3c) and steps in the individual temperature profiles, which indicate mixed layers that may result from intrusions, were used to determine the target depth of 6 m for injection. The dye was mixed with surface water to match the density on the target isotherm. The dye was injected in a 10 m streak by pumping from the shore through a hose connected to a diffuser that spread the dye and reduced the turbulence generated by the injection. The injection device included the SCUFA and SBE 50 so that the diffuser could be set to the target depth. Once the dye mixture was emptied from the vessel in which it was mixed, the remaining dye was flushed out the hoses with surface water.

After the dye was injected, it was tracked using the SCUFA. The SCUFA compensates for the effect of temperature on fluorescence, and it responds linearly to concentrations up to 200 ppb [*Turner Designs*, pers. comm.]. The SCUFA was calibrated using a 50 ppb Rhodamine WT standard. Profiles of concentration were measured throughout the northeast portion of the lake to capture the major characteristics and the edges of the dye cloud. All the measurements were combined to yield a map of the dye cloud. Following *Ledwell et al*. [2004], a column integral of the concentration was computed for each profile. The column integral represents the mass of dye in each box of the grid in the dye mapping. The column integral allows neglect of the effect of internal waves and seiches on the depth of the dye cloud because it essentially yields a depth-averaged value. Each profile's position was determined using a hand held global positioning system. The column integral calculated for each profile yielded a two-dimensional map of the dye cloud. To bound the cloud, the column integral was set to zero at the 4-m depth contour, the depth of the epilimnion, because no dye was observed in the epilimnion during the study. The column integrals were

then mapped onto a regular grid, and a contour plot was generated to delineate the edges of the cloud.

3. Results

The wind measurements indicate the passage of atmospheric gravity waves before the injection and on the second day of the experiment (Figure 4a). The peaks in wind speed were accompanied by 180 degree changes in wind direction (Figure 4b). The Lake number varied between 4 and 600 (Figure 4c). The low values of L_N suggest that seiches and internal waves were generated. Data from a meteorological station with a thermistor chain that was placed on the lake in 2007 and 2008 confirmed that wind speeds greater than approximately 7 m/s (corresponding to a Lake number of approximately 14) are sufficient to generate internal waves during summer stratification.

Mixing was enhanced where the thermocline intersected the sloping boundary (Figure 5a). The eddy diffusivity was more than an order of magnitude greater on the slope (site A) than in the interior (site B). At the bottom of the water column at site A, mixing was enhanced relative to that at both site B and in the upper portion of the water column below the epilimnion. There was another peak in the eddy diffusivity profile at 8.25 m; however, the 95% confidence intervals at this depth span two orders of magnitude. The enhanced turbulence at site A generated a mixed layer on the slope between 6 and 7 m depth (Figure 5b). This layer is not present on the lake bottom at site B, where the stratified water column reaches the bottom at about 9 m. However, the temperature step bounding the mixed layer generated at the slope is seen in the water column at site B at about 6.8 m depth, indicating possible intrusion formation due to the elevated mixing on the slope. The dye profiles from sites A and B confirm the connection between the mixed fluid at the boundary and the mixed layer in the interior (Figure 5c). The difference in the depths of the peaks is due to seiching motions between measurements; the peaks coincide when concentration is plotted as a function of temperature.

The dye cloud propagated approximately 260 m into the interior of the lake one day after the injection (Figures 6 and 7). A small amount of dye appeared to have separated from

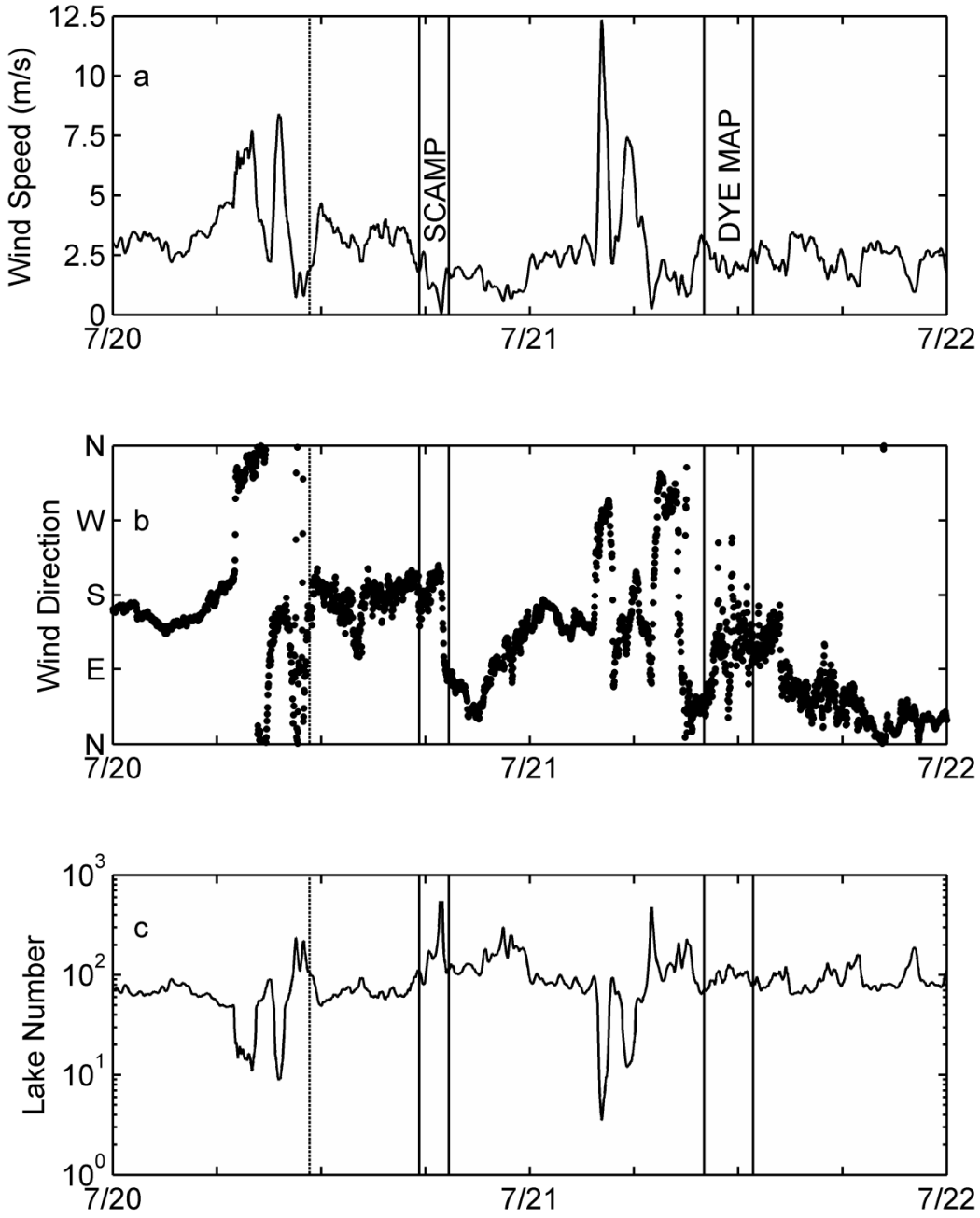

Figure 4. Wind at Ames Municipal Airport: (a) Wind speed, (b) wind direction, and (c) Lake number. The time of dye injection is marked with a dashed line, and the times of the SCAMP measurements and dye cloud mapping are also indicated

the main cloud and was observed at the circled point in Figure 6. Because the main cloud contained 91% of the mass of dye injected, this point was removed to make the analysis

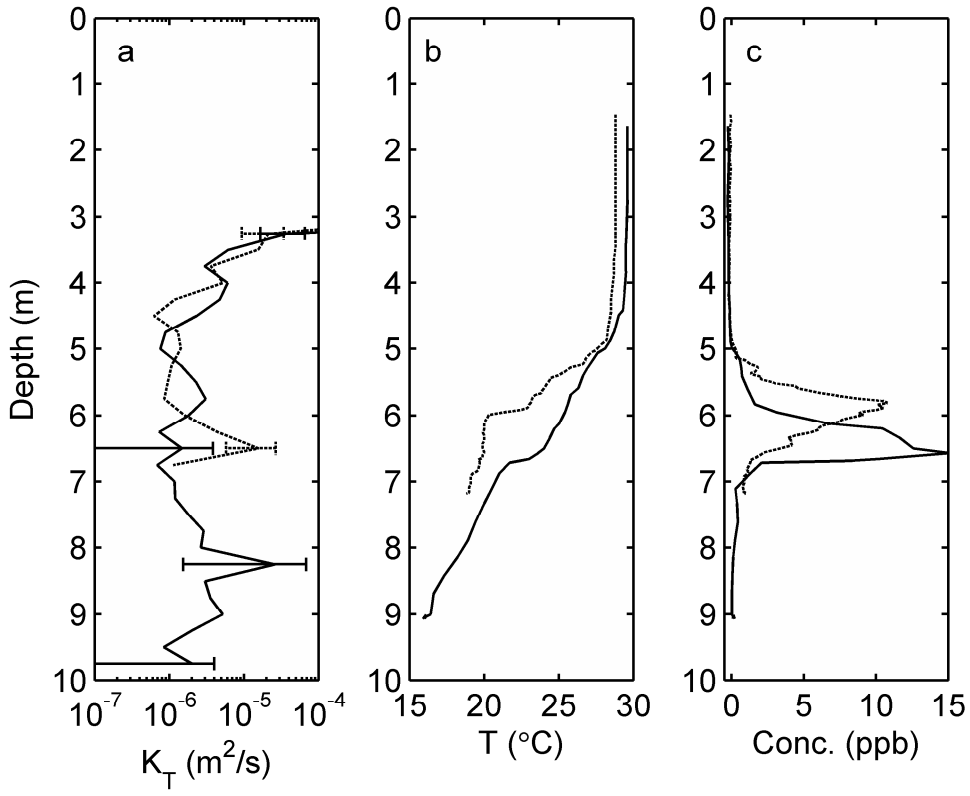

Figure 5. Comparison of profiles on the slope (site A, dashed line) and in the interior (site B, solid line): (a) Vertical eddy diffusivity with 95% confidence intervals, (b) temperature, and (c) dye concentration.

clearer. Within one day, over 58% of the dye injected moved off the slope region, defined by the 10 m isobath, with a front velocity of 0.3 cm/s. On average, the intrusion was 1 m thick over an area of approximately 50,000 m^2.

The propagation distance was determined from the transect in Figure 7; the edge of the dye cloud was considered to be where the dye concentration dropped to 5% of the maximum concentration in the transect. The maximum dye concentration was located in the middle of the cloud, indicating that diffusion alone cannot be responsible for the dye distribution. While we expect that some background horizontal diffusion processes may occur in the lake, some of the assumptions behind standard tracer moment analysis are invalid when the tracer interacts with the boundary, so we cannot compute a dispersion coefficient from the current tracer study. Additionally, laboratory experiments that have

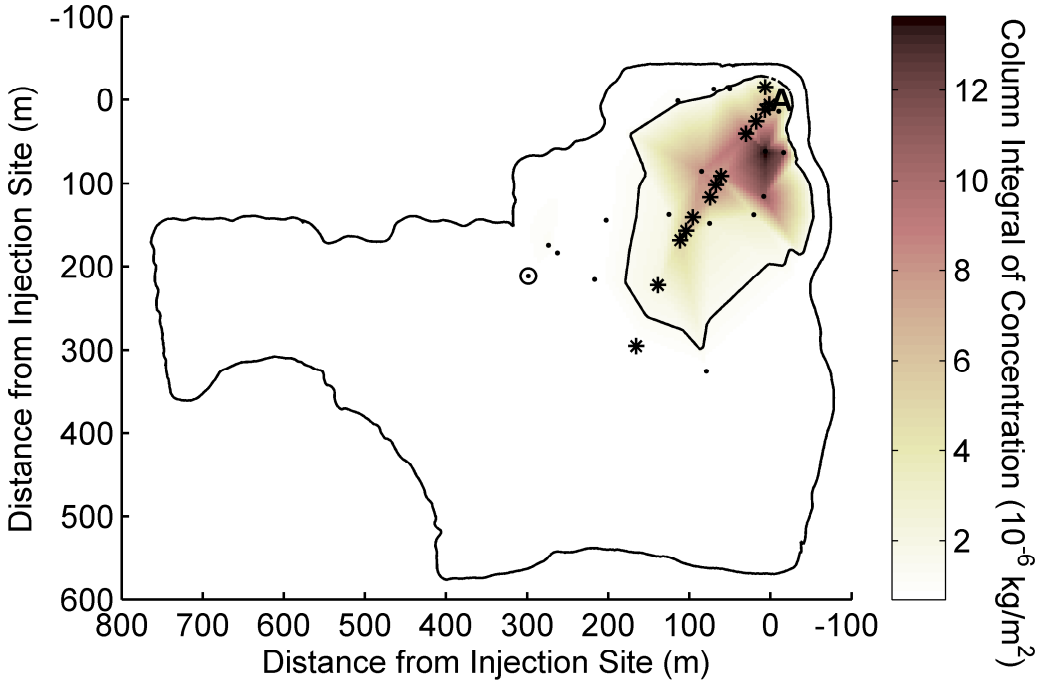

Figure 6. Spread of the dye cloud 24 hours after injection. The contour indicates where the column integral is below 5% of the maximum. Dots indicate dye profile locations, and stars (*) indicate the profiles shown in the transect series below. Site A is the injection site. At the circled dye profiling location, a small amount of dye was detected. This point was removed from the analysis as described in the text.

tracked dye from boundary mixing processes (*De Silva et al.* [1997], *McPhee-Shaw and Kunze* [2002], and *Wells and Helfrich* [2004]) describe dye injected at the boundary propagating as a front, as opposed to the distribution being controlled by diffusive processes.

4. Discussion

In this section, we, discuss the source of the turbulence that generates the intrusion, compare the intrusion propagation distance to results derived from a force balance, compare our results to the field measurements of *Inall* [2009], and investigate the mass transport

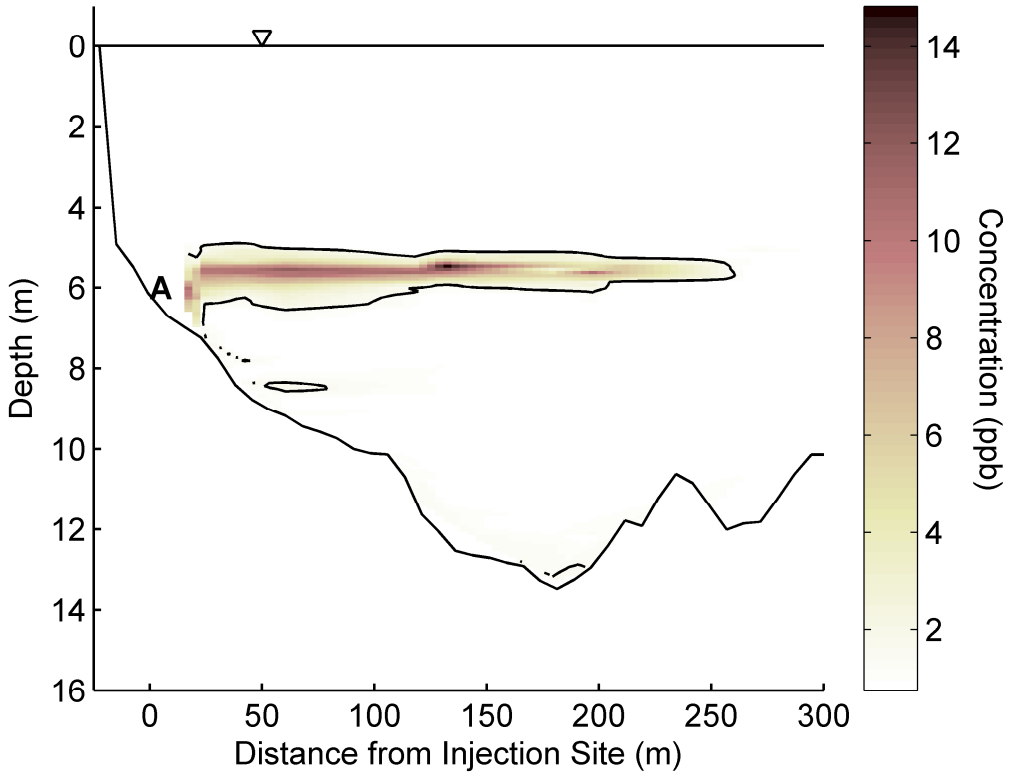

Figure 7. Longitudinal transect of dye cloud 24 hours after injection. The dye was injected at A. The contour indicates where the concentration drops to 5% of the maximum. The depth-averaged background concentration was subtracted from all the profiles. The concentration profiles were mapped onto the corresponding temperature profile to remove internal wave effects and the mean temperature profile was used to convert the profile to a function of depth.

transport offshore and its importance for water quality in lakes and reservoirs.

Internal waves generated turbulence on the slope. In 2005, there was no thermistor chain in the lake, but the displacement of the dye maxima between successive dye measurements indicates the possibility of seiching motions with an amplitude of at least 0.5 m being present. Unfortunately, without thermistor chain data, we can only make assumptions about the amplitude of the seiche. Given the small size of the lake, we do not expect the seiche amplitude to ever get much larger than 1 m during summer stratification; thermistor chain data from subsequent summers support this assumption. Modal analysis

with the stratification during the experiment yields a V1H1 seiche with a period of 1.3 hours. The time between the wind speed peaks of atmospheric gravity wave passing over the lake was 1.5 hours, which may potentially resonate with the natural frequency of the V1H1 seiche. Although detailed information regarding the internal wave field is not available for this experiment, the microstructure measurements show enhanced turbulence on the slope relative to lake interior. Eddy diffusivities on the order of 10^{-4} m^2/s have been observed on lake slopes [e.g., *MacIntyre et al.*, 1999]; the current observations are lower than that but similar to those from other studies [e.g., *Gloor et al.*, 2000].

In the lake the boundary mixing is likely due to seiching currents rather than breaking internal waves. For the given stratification, the first mode seiche is critical with respect to the slope only in the region of the deepest turbid layer; while higher frequency waves may be critical at the depths of the two uppermost turbid layers, often most of the energy in the internal wave field in a lake is contained at the dominant seiching frequencies [e.g., *Boegman et al*., 2005; *Münnich et al*. 1992]. Laboratory experiments on critical breaking internal waves on a slope [*De Silva et al.*, 1997; *McPhee-Shaw and Kunze*, 2002] suggest that interaction between incident and reflected rays of slightly supercritical waves may also enhance turbulence at the boundary. For the regions of interest on the slope, the ratio between the seiching frequency and the critical frequency is 0.3, which is lower than the parameter range of these lab experiments (which had lower limits of approximately 0.8 and 0.5, respectively), but both studies imply that the turbulence generation caused by critical reflection decreases as the waves become more subcritical. For these reasons, we eliminate breaking internal waves as the mechanism for generating turbulence and attribute the elevated boundary mixing to the seiche-induced currents passing over the boundary, as observed by others [e.g., *Gloor et al*., 2000; *Lorke and Wüest*, 2005].

Turbulence can also be generated by convective mixing caused by the seiching motions as described in *Lorke et al*. [2005] and *Lorke et al*. [2008]. In this process, shear in the bottom boundary layer advects cooler water over warmer water as the seiche moves upslope, weakening the stratification and potentially causing convective motions. As the seiche moves downslope, the stratification strengthens and less turbulence is observed. The amplitudes of the wave motions that created convective mixing in those studies were several

times greater than the amplitudes observed here. However, time series of turbulence quantities in the bottom boundary layer would be required to determine definitely whether convective mixing generates turbulence in Ada Hayden Lake.

The properties of the intrusion will depend on the force balance at the intrusion generation site. To describe an axisymmetric intrusion generated by a bubble plume, *Lemckert and Imberger* [1995] used the turbulent Froude number and the turbulent Reynolds number, defined as $Fr_T = \varepsilon^{1/3} / (NL_C^{2/3})$ and $Re_T = \varepsilon^{1/3} L_C^{4/3} / \nu$ respectively, where ε is the rate of dissipation of turbulent kinetic energy, L_C is the centered displacement scale (similar to the Thorpe scale), and ν is the kinematic viscosity of water. Using measurements on the slope of the bootstrap mean of the dissipation computed from microstructure measurements, the mean buoyancy frequency, and the mean Thorpe scale we estimate Fr_T = 1.4 and Re_T = 20. These values fall within the parameter range expected for boundary mixing processes [*Imberger and Ivey*, 1991]. As Fr_T number drops to 1, buoyancy begins to affect the turbulence; as Re_T drops to 15, the viscosity begins to affect the turbulence [*Ivey and Imberger,* 1991]. Thus for these values of the parameters, the turbulence can best be described by an inertia-buoyancy balance. The balance regime implied by the turbulent Reynolds and Froude numbers does not depend on the process.

Although an intrusion may start with a balance between buoyancy and inertia, it will eventually reach a critical distance where viscous forces will become important. That distance will depend on the geometry of the spreading. If the boundary mixing occurs at a point, the resulting intrusion will spread radially in three dimensions, but if the mixing occurs along the entire width of the slope, the intrusion will spread in two dimensions only. Because the nature of the source is unclear, we use both formulations. It is important to note that the derivations below assume a continuous source of momentum to drive the intrusion. While the winds forcing the internal waves might be impulse events, the resulting seiching motions do not decay immediately, but rather can maintain the bottom boundary layer (e.g., Gloor et al. 2000). During the current study, another wind event occurred between the dye injection and the dye mapping. For these reasons, we continue this analysis with the assumption that the inertia-buoyancy balance held at all time at the intrusion generation site.

Following *Chen* [1980] and scaling the viscous force as $F_v \sim \rho \upsilon QL / h^2$ and the inertial force as $F_i \sim \rho Q^2 / Lh$, where Q is the volumetric flow rate of mixed fluid away from the source, L is the length of the intrusion, and h is the intrusion thickness, *Lemckert and Imberger* [1993] derived an expression for the transition distance for a radially axisymmetric intrusion as

$$L_{tax} = 0.91\left(\frac{Q^3}{N\nu^2} \right)^{1/5} \tag{6}$$

The coefficient was determined with results from a dye injection in a bubble plume intrusion. It is important to note that this expression was derived for an intrusion generated in the center of the lake which spreads symmetrically in all directions and does not interact with the boundary. In the current study, the flow is bounded by the slope, but the pressure gradient still only exists in a radially outward direction. For a two-dimensional intrusion, the transition distance is

$$L_{t2D} = 0.67\left(\frac{q^3}{N\nu^2} \right)^{1/2} \tag{7}$$

where q is the flow per unit width and the constant comes from the theory of *Chen* [1980]. We use N = 0.081 rad/s, the average buoyancy frequency at the depth of the intrusion, and estimate Q = 0.53 m^3/s from the average intrusion thickness, the areal extent of the dye cloud away from the source, and the time between the injection and the dye cloud mapping (1.06 d). Then the transition distance for an axisymmetric intrusion is $L_{tax} \approx$ 260 m, and with an average intrusion width of 170 m, the transition distance for a two-dimensional intrusion is L_{t2D} = 420 m. Both estimates imply that the intrusion was governed by an inertia-buoyancy balance during the experiment. In contrast, the propagation of intrusions in the laboratory experiments of *De Silva et al.* [1997] and the field observations of *Gloor et al*. [2000] were described by a viscous-buoyancy balance.

The force balance allows the intrusion's propagation to be predicted. By equating the inertial force and the buoyancy force, $F_b \sim \rho L h^3 N^2$, *Lemckert and Imberger* [1993] used their results to estimate the intrusion position as a function of time as

$$L_{ax} = 0.4(QN)^{1/3} t^{2/3}, \tag{8}$$

while *Chen*'s [1980] results for a two-dimensional intrusion can be used to obtain

$$L_{2D} = 0.71(qN)^{(1/2)} t. \tag{9}$$

In the current experiment, the theoretical propagation distance under an inertia-buoyancy balance is 280 m for an axisymmetric intrusion and 980 m for a two-dimensional intrusion. The actual propagation distance was 260 m away from the source, implying that the three-dimensional spreading observed here is better approximated by the axisymmetric model than a two-dimensional model. As the transition distance is approached, viscous effects should start to become important and retard the propagation of the intrusion. Also, these estimates treat the flow as steady; in our flow the currents generating the turbulence oscillate. Time series of temperature in the bottom boundary layer would be needed to determine whether the boundary layer properties remain steady.

As discussed in the introduction, several field observations provide evidence of intrusions, but only one other study has directly measured intrusions in a natural environment. *Inall* [2009] injected dye into the stratified water column of a fjord in a manner similar to *Goudsmit et al.* [1997] (as opposed to on the bottom boundary as in the present study). The tracer was then mapped two-dimensionally along the main axis of the fjord, which differs from the three-dimensional spreading observed in Ada Hayden Lake. The tracer was eventually entrained into the bottom boundary layer and swept upslope and downslope by the internal tide, which is presumed to generated turbulence at the rough boundary (although there were no turbulence measurements in the bottom boundary layer). Vertical mapping of the dye cloud showed that the dye swept downslope and intruded into the interior along isopycnals. In our study, most of the dye did not travel far up or down the

slope, most likely because the amplitude of the seiching motions was on the order of 1 m, which is ten times smaller than the displacements in the fjord. However, turbidity measurements before the dye injection show three distinct turbid layers (Figure 3c), indicating that the entire slope might be a site for turbulence generation and a source of suspended sediment. The lack of dye in the epilimnion, the upper 4 m of the water column, shows that the dye did not move upslope.

The vertical scales of the intrusions (the thickness and the vertical separation) can be set by the stratification, the forcing, or the topography. The intrusion thickness of 1 m is 6.3 times the Ozmidov scale of 0.16 m. This result is similar to that for intrusions generated by a horizontally-oscillating vertical grid [*Browand et al*., 1987]. However, *Inall* [2009] found that intrusions generated by the passage of the internal tide over rough topography did not organize according to the Ozmidov scale; the thickness and spacing of the intrusions in his experiments were 20 times the Ozmidov scale or larger. Instead, the spacing and thickness of the intrusions were similar to the dominant wavelength of the bottom topography (determined by spectral analysis of the variation of the bed elevation along the slope to be 10 m). In Ada Hayden Lake, the separation of the turbid layers (Figure 3c) is about 10 times the Ozmidov scale. However, the bed topography is smoother than in the fjord of *Inall* [2009]. If the wavelength of the topography sets the intrusion spacing, then the separation of the turbid layers should be larger than we observed in Ada Hayden Lake. In both the present experiments and those of *Inall* [2009], vertical scales of the intrusions were on the order of the amplitude of the dominant internal waves. The length and depth of the fjord were about ten times those in Ada Hayden Lake and the internal wave amplitudes and intrusion thickness were also ten times greater. The velocity of the intrusion front in the fjord was also about ten times faster than was measured in Ada Hayden Lake. As the bottom topography and Ozmidov scales did not show this same relationship between the two environments, this implies that some of the length scales of the intrusions might be the result of large scale geometric considerations in the lake and fjord.

Intrusions can be an important path for transporting heat and other scalars offshore. The presence of turbid layers offshore indicates that the turbulence at the boundary may be suspending sediments that then are transported into the lake interior. The resuspension of

sediments by internal seiches in lakes has been documented by several researchers [e.g., *Gloor et al*., 1994; *Pierson and Weyhenmeyer*, 1994]. This sediment resuspension has been shown to release dissolved constituents such as methane [*Murase et al*., 2005] and phosphorus [e.g., *Eckert et al*., 2003] from the sediment pore waters. As *Gloor et al*. [2000] noted, intrusions enhance the efficiency of boundary mixing because they move the mixed fluid offshore. In the current study, almost 60% of the mass of the dye injected moved off the slope and into the interior after one day, indicating that a significant portion of substances entrained into the bottom boundary layer may end up in the pelagic zone of the lake. In this manner, localized mixing at the boundaries can be communicated to other parts of the lake. Thus, in a strongly stratified lake, intrusion formation can play a major role in transporting scalars in a lake.

5. Summary

A field experiment with measurements of tracer concentrations and temperature microstructure was conducted to study the consequences of boundary mixing in a small lake. Rhodamine WT was injected along the sediment-water interface to track an intrusion. Along with the observations of *Inall* [2009], this study is one of the first direct measurements of such boundary generated intrusions in the field, and it is the first to map the intrusion in three dimensions. Enhanced mixing indicated by estimates of the vertical eddy diffusivity from temperature microstructure measurements on the slope is attributed to seiching currents interacting with the boundary. Unlike *Inall* [2009], we did not observe upslope transport within the bottom boundary layer. The observed bottom boundary layer collapsed into an intrusion governed by a balance between inertia and buoyancy. The intrusion had an average thickness of 1 m, and it propagated approximately 260 m into the lake interior after one day. The intrusion's behavior matched the propagation characteristics predicted by *Lemckert and Imberger* [1993] for an axisymmetric intrusion generated by a bubble plume. Almost 60% of the mass of dye injected moved off the slope and into the pelagic zone; the intrusion had a volume flow rate of 0.53 m^3/s. These observations, along with the persistent turbid layer at

the depth of the intrusion, suggests that intrusion formation may be an important mechanism for transporting dissolved substances and affecting lake ecology.

Acknowledgments

The authors thank Ryan Jackson and Meredith Carr for help with the experiments and acknowledge support from the National Science Foundation under Grant OCE 06-47253. Any opinions, findings, and conclusions or recommendations expressed in this material are those of the authors and do not necessarily reflect the views of the National Science Foundation.

CHAPTER 4. OBSERVATIONS OF OFFSHORE TRANSPORT BY INTERNAL SEICHES

A paper in preparation for *Limnology and Oceanography*

Danielle Wain and Chris Rehmann

Abstract

A field experiment was conducted to study boundary-interior exchange in a small lake. Tracking of a tracer injected into the metalimnion was combined with wind measurements and measurements of internal waves from two thermistor chains. Horizontal and vertical coherence and phase spectra indicated that V1H1 and V2H1 seiches were initiated after a wind event, after which the tracer was observed to move offshore. Four potential mechanisms for the spreading of the tracer from the boundary to the interior were investigated: intrusions from boundary mixing, advection from the V2H1 seiche, spreading by internal wave strain, and internal wave driven shear dispersion. The interaction between the internal wave strain and shear was determined to be the most likely explanation for the tracer behavior, although the combination of strain and shear dispersion could not completely account for the lateral dispersion of the tracer as determined from a moment analysis. The horizontal variation in the velocity field leads to an increase in the lateral dispersion as tracer moves into the interior. The strain can spread the mixed fluid far enough from the boundary that vertical shear becomes an important dispersion process**.** These findings improve the understanding of the pathway from energy input from the wind to offshore transport.

Understanding the transport of dissolved substances such as oxygen, nutrients, microorganisms, and plankton is essential for managing water quality in lakes and reservoirs. The current paradigm in ocean and lake mixing is that turbulence created at the boundaries by internal waves and currents is responsible for the majority of the mixing that occurs. While much work has been done investigating mixing at boundaries in lakes and the ocean, less attention has been paid to the fate of this mixed fluid. In this study, we investigate mechanisms for boundary-interior communication by the internal wave field, including

intrusions from boundary mixing, advection from the V2H1 seiche, spreading by internal wave strain, and internal wave driven shear dispersion.

Wind acting on the surface of a lake can cause basin-scale standing waves (seiches) to form. For a rectangular basin of constant width, the first horizontal mode seiche has a wavelength that is twice the length of the lake with a single node in the middle; the complex geometry and bathymetry of real lakes change the modal structure (e.g., Fricker and Nepf 2000). Higher modes have more nodes (the second mode has two nodes, etc.). In a two-layer stratification, only the first vertical mode can exist; in lakes with a thermocline of finite thickness, the second vertical mode can dominate the first mode and can cause large isotherm displacements (e.g., Wiegand and Chamberlain 1987, Münnich et al. 1992).

A first vertical mode seiche has peak velocities at the top and bottom of the water column with a minimum in the metalimnion. The compression of the metalimnion that is a signature of the second vertical mode results in a velocity maximum in the metalimnion. Higher vertical modes (which are more rarely observed) have more peaks in the velocity profile (e.g., Antenucci et al. 2000). One consequence of this velocity structure is that the higher shear generated by changes in velocity over shorter vertical length scales means that these higher modes are more dampened (Vidal et al. 2005).

While first vertical modes are most likely to be excited, higher vertical modes can have a large impact on the lake hydrodynamics. In addition to often having larger amplitudes than first vertical mode waves, in larger lakes the period of the higher modes is often long enough to resonate with diurnal wind patterns. Identification of higher mode seiches is typically accomplished with thermistor chains and/or current profilers. Observations of the second vertical mode are relatively common (e.g. Wiegand and Chamberlain 1987, Münnich et al. 1992, Appt et al. 2004, MacIntyre et al. 1999, Saggio and Imberger 1998, Boehrer et al. 2000), but even higher vertical modes have been documented in the field as well, although such observations are rare.

Antenucci et al. (2000) observed the first three vertical modes in Lake Kinneret, but the vertical profile of velocity in the lake was largely attributed to the currents generated by the higher mode seiches when they were excited. For the thermal structure of Lake Kinneret, the second and third vertical mode waves had similar frequencies and thus could not be

isolated from each other by spectral analyses. These higher vertical mode seiches were found to be first horizontal mode seiches. Antenucci et al. (2000) also found that the higher mode seiches were not always generated as a result of the regular wind forcing; residual motions from previous wind events were determined to play a role. Third vertical mode waves have also been observed in the Sau Reservoir (Vidal et al. 2005, Marce et al. 2007). The thick continuously stratified metalimnion and diurnal wind patterns were shown to favor excitation of the third vertical mode. The third vertical mode frequency resonated with the wind patterns and, as a result, dominated the internal wave motion of the reservoir.

While higher vertical modes may exist, these uncommon observations suggest that a combination of environmental conditions is necessary for the higher modes to be excited. Higher horizontal modes are less rare. Lemmin and Mortimer (1986) several studies of lake first vertical mode waves that have up to five horizontal modes. The combination of high vertical mode and high horizontal mode is documented in a few instances for second vertical mode waves (MacIntyre et al. 1999, Munnich et al. 1992), but there does not appear any documented cases of third vertical mode, high horizontal mode seiches.

The interaction between the seiches and lake boundary can generate a turbulent bottom boundary layer that hydrodynamically unstable with respect to the stratified interior. Gravitational adjustment of this mixed fluid leads to collapse into an intrusion that propagates horizontally along an isopycnal (level of constant density) into the interior. These intrusions can transport the mixed fluid from the boundaries into the lake interior (Thorpe 1998).

While intrusions are an outcome of the internal waves interacting with the boundary, the internal waves themselves may drive transport between the boundary and the interior. The mechanisms by which internal waves may contribute to horizontal mixing in a lake are through lateral advection by the mean velocity field of the internal waves in the metalimnion, shear dispersion by the vertical variation of internal wave induced velocities, and strain due to the horizontal variation in the internal wave velocity field, and

In a lake, the first potential mechanism for this offshore transport is the water column currents generated by the internal seiches. Marti and Imberger (2008) observed a well-defined turbid layer in a large lake and used numerical modeling with field measurements of

turbulence and the internal wave field to predict exchange between the boundary and the lake interior. They associated the change in the turbid layer with the changes in the bottom boundary layer as the seiches passed over the slope. Given the basin-scale internal waves in the lake, they concluded that the turbid layer was advected offshore by a jet in the metalimnion that resulted from a second vertical mode wave. Their numerical model showed residual velocities in the metalimnion after such a seiching event and these residual velocities can explain some aspects of the observed distribution of the turbid layer.

Due to the oscillatory nature of seiching motions, significant movement due to mean advection as observed in Marti and Imberger (2008) is expected to be rare as any transport into the interior will be reversed when the seiche moves in the other direction. But the velocities in a lake vary significantly both horizontally and vertically. The vertical variations in velocity can lead to lateral shear dispersion, while the horizontal velocity variations causes straining of the water mass.

Young et al. (1982) studied dispersion in an infinite fluid with an oscillating velocity profile and a horizontal velocity component given by

$$u = U \cos mz \cos \omega t \tag{1}$$

and found

$$K_{eff} = K_x + \frac{1}{4}\frac{U^2}{\omega}\frac{d}{1+d^2}. \tag{2}$$

where $d = K_z m^2 / \omega$, U is the maximum velocity, m is the vertical wavenumber, K_x is the horizontal diffusivity without the presence of internal wave shear, and K_z is the vertical eddy diffusivity. Sundermeyer and Ledwell (2001) used the Young et al. (1982) results with the results of Smith (1982) to estimate this enhanced horizontal diffusivity and compare the estimates to the observed spreading from four dye release experiments in the coastal ocean. They found that this shear dispersion was not sufficient to explain their dye distributions and oftentimes was an order of magnitude too low. There appear to be no similar tracer

experiments in lakes; tracer experiments carried out in the metalimnion of the lake focused on mean shear, not internal wave induced shear (Peeters et al. 1996).

The horizontal variations in velocity can cause the cloud to spread laterally. Unlike shear dispersion, this spreading mechanism is reversible (Sundermeyer and Ledwell 2001). Because there can be no flow into a boundary, the horizontal velocity normal to the wall of the lake must be zero. For basin scale seiches, a first horizontal mode wave has a sinusoidal form with the horizontal velocity maximum in the middle of the lake. Thus all velocity fields induced by seiches have horizontal gradients. While the internal wave strain parameterizations have been used to estimate vertical mixing in lakes (e.g. MacIntyre et al. 2009), internal wave strain as a mechanism for spreading mixed fluid away from the boundaries has not been investigated. As the straining is at a maximum at the boundary for first horizontal modes, this process may be important for moving mixed fluid into the interior where other dispersive forces may act on it.

To investigate offshore transport by basin scale seiches, we used a tracer to lateral dispersion in the metalimnion between the boundary and the interior. We first describe the lake, the measurements, and the analysis. The details of the internal wave field and the results of the dye tracking are then described. Finally, we compare the results with the theoretical spreading due to shear dispersion and straining from seiches.

Field Site

The measurements and dye release experiment were conducted at Ada Hayden Lake in Ames, Iowa (Figure 1) on 6-7 August 2007. Ada Hayden Lake is an abandoned rock quarry that was filled to create a secondary water supply for Ames. It consists of two basins, and the experiments were performed in the larger, deeper south basin, which has a surface area of about 0.3 km^2 and a maximum depth of about 17 m. The lake is strongly stratified in the summer with a well-mixed epilimnion lying over a strongly stratified metalimnion and a weakly stratified hypolimnion (Figure 2). The metalimnion occupies over a third of the water column, a condition which increases the potential for higher vertical mode seiches to be important (Wiegand and Chamberlain 1987, Münnich et al. 1992). Water enters the lake from

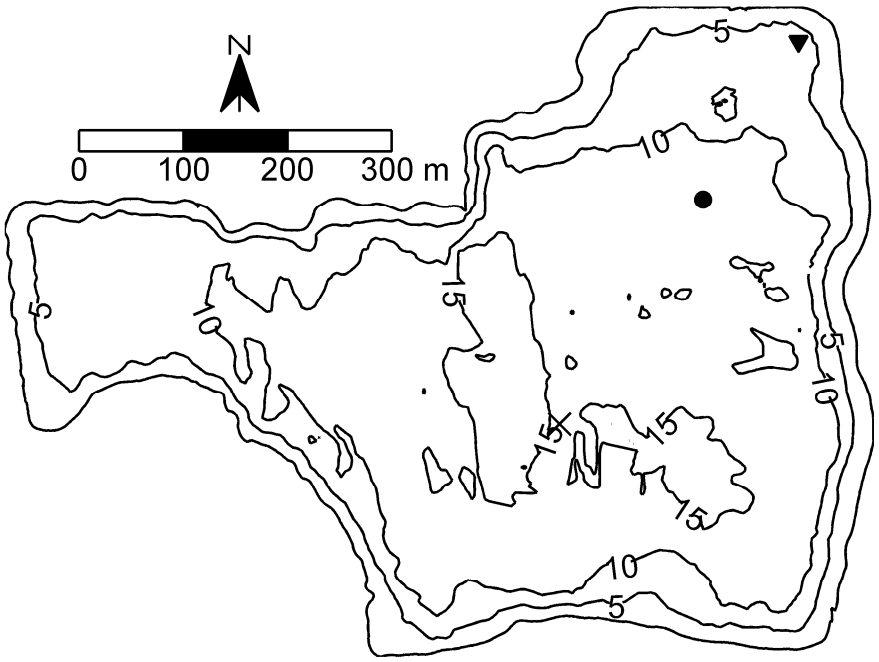

Figure 1. Map of the south basin of Ada Hayden Lake. Depth contours are marked in meters. Shown are the dye injection location (▼),thermistor chain (●), and the LDS (×).

groundwater and surface water runoff, which is filtered through wetlands. The two basins are separated by a 3-m deep sill. Because the sill is shallower than the summer thermocline, exchange between the two basins probably consists only of epilimnetic waters. Stirring from boat traffic is small because motorized boats are prohibited on the lake. The lake has steep sides except for a few areas; the northeast corner, where dye was injected, has a more moderate slope ranging between 5 and 10%. Stirring from boat traffic is small since motorized boats are prohibited on the lake. During the summer, the mean winds at Ada Hayden Lake are 2-3 m/s SSE. Stronger winds (>5 m/s) are typically associated with storms, most often from the south.

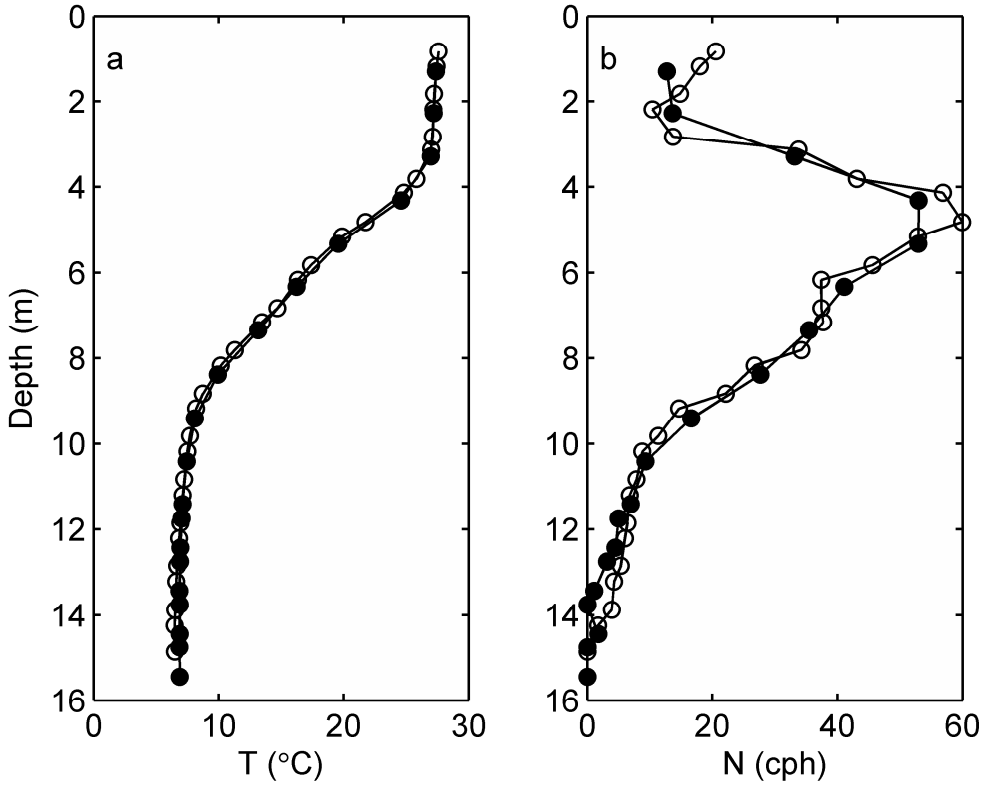

Figure 2. Conditions during the experiment: (a) Average temperature profile and (b) buoyancy frequency N as measured by the LDS (○) and the thermistor chain (●).

Measurements

Meteorological Station - A Lake Diagnostic System (LDS) manufactured by Precision Measurements Engineering was moored in the lake at the position denoted in Fig. 1. The LDS measures wind speed and direction, solar radiation, net radiation, relative humidity, and air temperature. To determine the wind forcing on the lake, the wind speed and direction were measured approximately 2.4 m above the water surface by a propeller anemometer and a wind vane, respectively, both by Met One Instruments, Inc. All the sensors on the LDS are sampled every 15 s.

Thermistor Chains **-** Two thermistor chains manufactured by Precision Measurements Engineering were deployed in the lake. One was attached to the LDS, and another was deployed 215 m from the LDS (Fig. 1). The thermistor chain at the LDS had 29 nodes

starting approximately 1 m below the surface and spaced every 0.5 m thereafter. The other thermistor chain had 19 functioning nodes spaced approximately every 1 m, and the sample interval was 15 s.

Fluorometry - Dye tracking was used to measure the spread of the mixed fluid. Rhodamine WT, a non-toxic tracer designed to track water, was used for the studies. One liter of the dye was injected in a horizontal streak on a target isotherm to focus on spreading of the intrusion away from the boundary. The Rhodamine WT was mixed with surface water of known density (based on temperature measurements) to yield a mixture of the proper density. The dye was injected from a boat; the injection hose was equipped with a diffuser pipe to minimize turbulence generation from the injection. In the experiment, the dye was injected approximately 6 m deep along the slope under calm conditions on 6 August 2007.

Once the dye was injected, it was tracked using a Self-Contained Underwater Fluorescence Apparatus (SCUFA) by Turner Designs. Before use, the SCUFA was calibrated using a 50 ppb Rhodamine WT standard. The range where the relationship between the emissions detected by the receptors and the fluorescence is linear extends to approximately 200 ppb (Turner Designs, pers. comm.). The SCUFA was mounted in a protective cage, along with an SBE 50 Digital Oceanographic Pressure Sensor from Sea-Bird Electronics to measure the depth of the SCUFA. The SCUFA and SBE 50 were sampled simultaneously with position from a global positioning system at 1 Hz through LabVIEW. To capture both the vertical and horizontal extents of the dye cloud, a tow-yo sampling strategy was employed. Measurements along a transect were taken both horizontally and vertically until background fluorescence levels determined by pre-injection surveys were reached to ensure that the entire cloud was captured.

Processing

Temperature and Buoyancy Frequency Profiles-The temperatures recorded by the thermistor chains on 7 August 2007 were averaged to generate a mean temperature profile. The equation of state of Chen and Millero (1977) was used to compute the density profile

from the mean temperature profile. The buoyancy frequency was then computed using a centered difference.

Lake Number - The strength of the wind, which can cause the stable density structure to overturn, was compared to the strength of the stratification, which resists overturning, with the Lake number (Imberger and Patterson 1990):

$$L_N = \frac{gS_t(1 - z_T / z_S)}{\rho_s u_*^2 A_s^{3/2}(1 - z_v / z_s)} \tag{3}$$

where g is the acceleration of gravity, z_T is the center of the metalimnion, z_S is the height of the water surface, ρ_s is the density at the surface, u_* is the shear velocity of the wind, A_s is the area of the surface, z_v is the height of the center of volume, and S_t is the stability of the water body defined as

$$S_t = \int_0^{z_s} (z_v - z)\rho(z)A(z)dz, \tag{4}$$

where $A(z)$ is the surface area as a function of depth. All measurements are with respect to the bottom at $z = 0$. The shear velocity of the wind is defined as

$$u_* = \left(C_{Dw} \frac{\rho_a}{\rho_1} \right)^{1/2} u_w \tag{5}$$

where ρ_a is the air density, C_{Dw} is the wind drag coefficient, and u_w is wind speed, typically taken as the velocity 10 m above the water. The drag coefficient was computed with the formulas from Wüest and Lorke (2003). A Lake number of 1 implies upwelling conditions. Low Lake numbers ($L_N < 10$) indicate that the wind stress is sufficient to generate wind setup throughout the water column (Imberger and Patterson 1990).

A 15-minute moving average of the meteorological and thermistor chain data from the LDS were used to compute the Lake number. The temperature profile was interpolated

onto a 1-m grid to match the hypsograph. The thick metalimnion with a non-constant buoyancy frequency complicated finding the depth of the thermocline to use in computing the Lake number . The region of highest temperature gradient is directly below the well-mixed surface layer; computing the Lake number using this depth will most likely underestimate the Lake number. Instead, the depth of the thermocline was taken as the depth of the maximum isotherm displacement of the first vertical mode seiche.

Seiching modes – To determine the natural seiching frequencies in the lake, the model of Münnich et al. (1992) was used. The temperature data recorded by the freestanding thermistor chain on 7 August 2007 was averaged and then linearly extrapolated onto a 25-cm grid that covered the entire water column. The density and buoyancy frequency profile were computed as described above. The eigenvalue problem was then solved to determine the phase speeds of the first four vertical modes. At the depth of the thermocline, the fetch of the lake is 755 m when the wind comes from the west, as during the period of the study. The theoretical frequencies of these modes were computed with this length.

Internal wave spectra - To investigate the internal wave field, linear interpolation was used for each temperature profile to determine the level of each isotherm to create a time series of isotherm depth versus time. After subtracting the mean isotherm position, Welch's periodogram method was used to create a spectrum of the isotherm displacements in frequency space. Coherence and phase spectra were used to determine the modal nature of the seiching motions. A coherence spectrum measures the similarity between the spectral energy distribution of two signals. At a given frequency, if two signals are perfectly coherent, then the coherence spectrum will have a value of one. For coherent signals, we can compute a phase spectrum to determine the lag between the two signals. For example, two sine waves of the same frequency are both coherent and in phase. A sine wave and a cosine wave of the same frequency are coherent, but 90 degrees out of phase.

Within a single thermistor chain, the coherence and phase spectra were computed between isotherms so the existence of higher vertical mode waves could be confirmed (e.g., Münnich et al. 1992). Between the two thermistor chains, the coherence spectrum for displacements for a given isotherm was calculated to determine whether the internal waves were coherent across the entire basin (e.g., Lemckert et al. 2004). The phase spectrum was

computed to determine the horizontal mode of the seiches. For all spectra, a window of 4096 points (~17 hrs) was advanced by one hour and the eight resulting spectra were averaged.

Dye mapping - All the measurements in a set of transects were combined to yield a map of the dye cloud. Following Ledwell et al. (2004), a column integral of the concentration was computed for each up or down profile measured while tow-yoing. The column integral essentially yields a depth-averaged value; thus, it is insensitive to vertical movement of the dye cloud by the internal waves. Each profile's position was determined by averaging the position reading from the GPS during each profile time. The column integral was calculated for each profile to yield a two-dimensional map of the dye cloud.

To determine the horizontal dispersion coefficient, we used a moment analysis of the dye cloud (e.g. Fischer et al. 1979). Because of the nature of the process being investigated, the typical moment analysis must be adapted. With one mapping, it is common to assume that the initial variance of the dye cloud is zero. In the current study, the dye cloud is subjected to two different forcings and thus a single K_{eff} is not adequate to describe the dye movement. The dye was injected in the northeastern corner of the lake during calm conditions. Fourteen hours later, the westerly wind event generated the seiching movements in the lake. The northern portion of the dye cloud was mapped 12 hours later, followed by the southern portion of the dye cloud (including the portion that moved into the lake interior). This mapping was completed approximately 14 hours after the wind event. To compute the moments in the x-direction (the E-W axis), we divide the dye cloud into this northern and southern portion, with the division at approximately y = 160 m (see Figure 10 below), which is approximately where the lake opens up to a longer westerly fetch. For the northern portion of the cloud, we assume the initial x-variance is zero. Using the horizontal diffusivity for the northern portion, we estimate the x-variance at the time of the wind event and use that value as ths intital variance for computing the horizontal diffusivity in the south portion. We are primarily concerned with the enhanced horizontal diffusivity observed along the x-axis in the southern portion of the cloud relative to the northern portion of the cloud.

Results

In this section, we discuss the conditions during the experiment and describe the theoretical behavior of the first four vertical modes. Using the measurements from the thermistor chains, we evaluate the potential for existence of these modes during the experiment. We then use the dye study results to investigate the implication of the internal wave field in offshore transport in lakes.

Lake Number - At approximately 2 am on 7 August 2007, the wind increased in speed and changed direction to come from the west (Figures 3a-b). The minimum Lake number observed during this event was approximately 11 (Figure 3c). While the Lake number was higher than the threshold of 10 described above, the wind stress was still sufficient to displace isotherms (Figure 3d).

Seiching Modes - The vertical profiles of modal amplitudes are shown in Figure 4. The natural periods for the VxH1 mode for x = 1, 2, 3, and 4 are 1.4 hrs, 4.0 hrs, 6.8 hrs, and 9.3 hrs respectively. The periods of the VxH2-4 modes are half, one-third, and one-quarter of the VxH1 periods, respectively. For a rough approximation to the velocity field, we can assume a simple bathymetry and compute the horizontal velocity profile for a standing wave for each mode.

Internal Wave Spectra – Now that we have theoretical approximations for the first four vertical modes, we can use the coherency and phase spectra to determine if the higher modes exist. First we look for coherent motions within the water column. We use the temperature measurements from the freestanding thermistor chain, as on a westerly fetch it was closer to the lake boundary than the LDS. Consequently the displacement of isotherms due to seiching motions should be clearer at the thermistor chain.

The coherency and phase spectra were computed between all isotherm pairs. In Figure 5, we show phase of each isotherm with respect to the 26°C isotherm (the warmest isotherm) at the frequencies that are closest to the theoretical frequencies of the VxH1 seiches computed above. At the V1H1 frequency, most of the water column moves in phase (Figure 5a), which is the expected response. At the V2H1 frequency (Figure 5b), the upper portion of the water column moves out of phase with the lower portion of the water column,

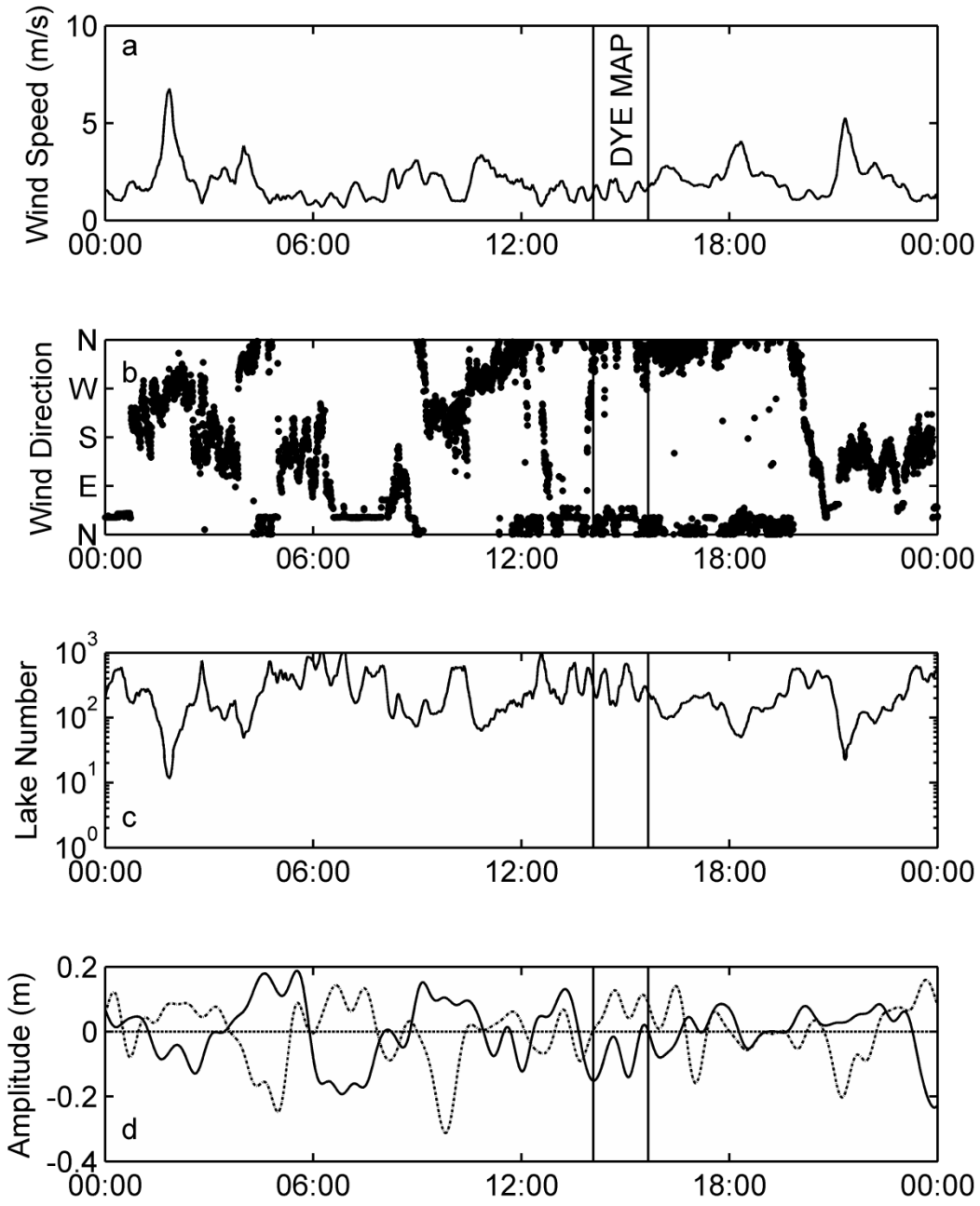

Figure 3. (a) – (c) Wind measured by the LDS on 7 August 2007: (a) Wind speed, (b) wind direction, and (c) Lake number. (d) Displacement of the 19°C (solid line) and 12°C (dashed line) isotherms as measured at the thermistor chain and low pass filtered with a pass frequency of twice the theoretical period of the V1H1 seiche. The time of the dye cloud mapping is also indicated.

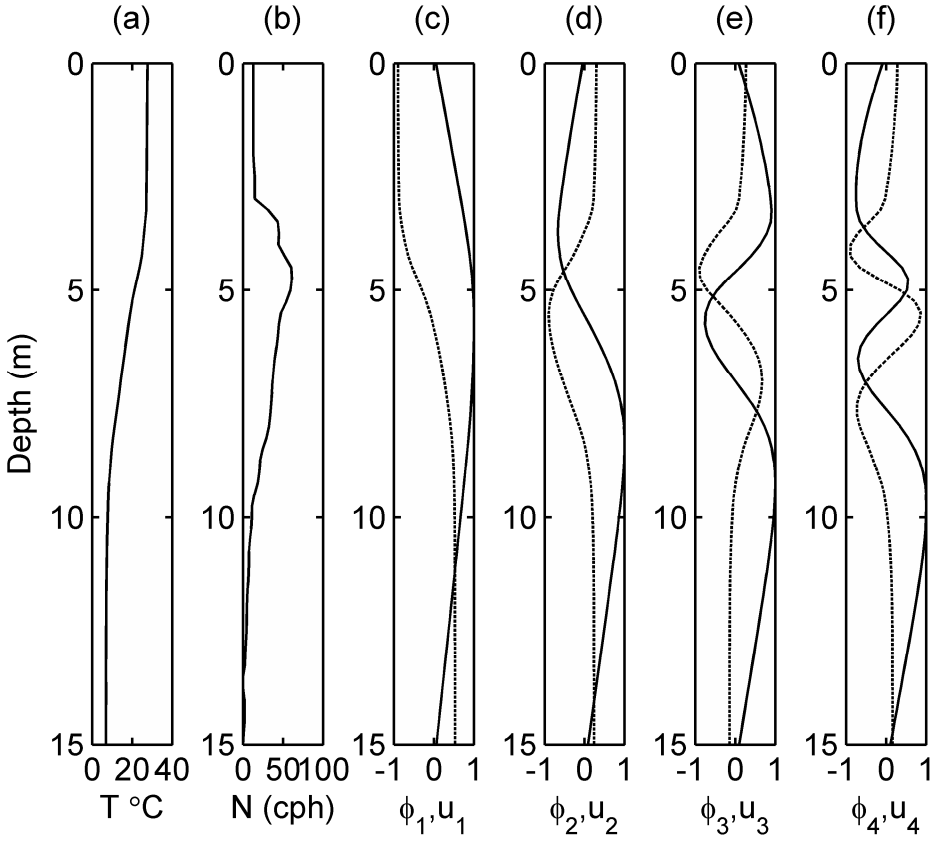

Figure 4. (a) Temperature profile used for computing the vertical modes based on the data from the stand alone thermistor chain. (b) Buoyancy frequency profile associated with (a). (c) - (f). Theoretical modal amplitudes (solid line) and associated horizontal velocities (dashed line) for the first four vertical modes (arbitrary units).

consistent with a second vertical mode. The solid circles indicate the depth of the peaks in the theoretical modal amplitudes; each peak is necessarily 180 degrees out of phase with the ones above and below it. At the V2H1 frequency, the computed phases match the theoretical phases at these depths well. Because of the record length, the frequency resolution is such that the closest resolved frequency to the V3H1 and V4H1 is the same. The phase profile atthis frequency was compared to the theoretical phases for these two modes (Figures 5c,d). The V3H1 structure fits the measured profiles better than the V4H1 structure. This does not eliminate the possibility that a V4H1 seiche may exist, but our sample length precludes isolating the signal. As the thermistor chain recorded for several months during summer 2007, it is possible to extend the sample length from 17 hours (2^{12} data points) to 34 hours

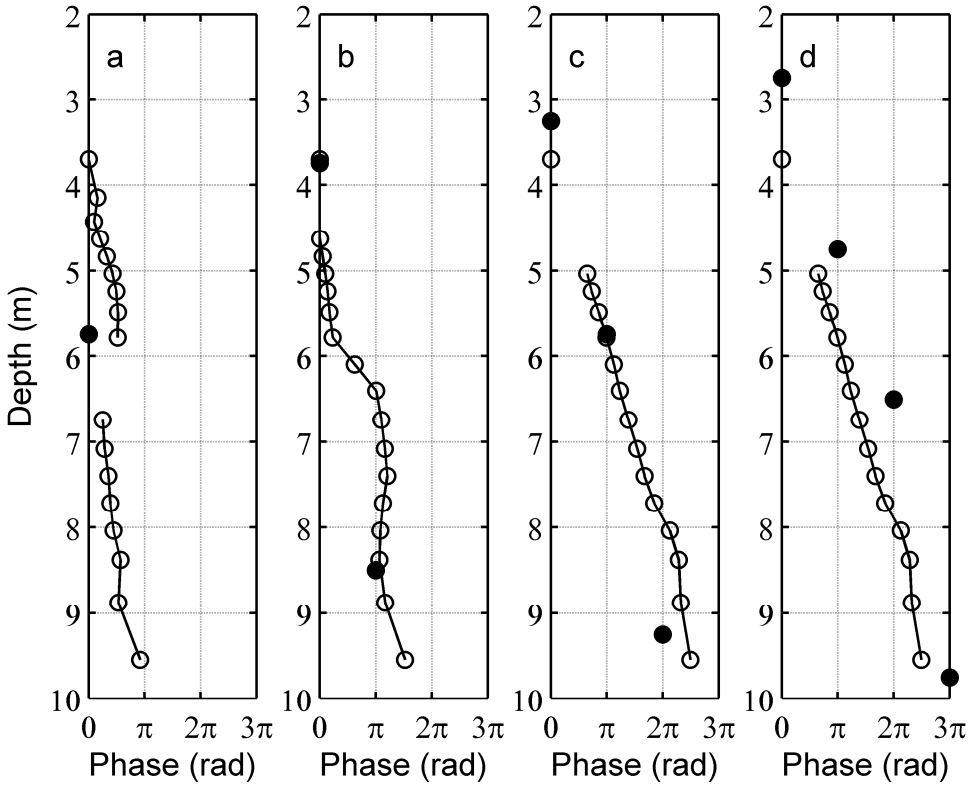

Figure 5. Phases of the 25°C – 8°C isotherms with respect to the 26°C isotherm (○) at the frequencies approximating the theoretical frequencies of the first four modes: (a) f = 0.70 cph (2.0×10^{-4} Hz), (b) f = 0.23 cph (6.5×10^{-5} Hz), (c) f = 0.12 cph (3.3×10^{-5} Hz), and (d) f = 0.12 cph (3.3×10^{-5} Hz). Only isotherms with coherence with the 26°C isotherm of greater than 0.5 are shown. The closed circles (●) indicate the depths of the peaks in the theoretical modal amplitudes for each mode.

(2^{13} data points), but as the wave life is shorter than this, a longer sampling window does not seem reasonable.

The phase profiles described above indicate that there is potential for V1H1, V2H1, and V3H1 seiches in the lake. In the following we use the results from two isotherms (19°C and 12°C) in the lower and upper portions of the metalimnion to determine if higher horizontal harmonics may exist. These isotherms were chosen because the maximum displacements in the water column interior (i.e., not on the bottom or top of the water column) were observed at these isotherms. These isotherms will be in phase for the V1H1

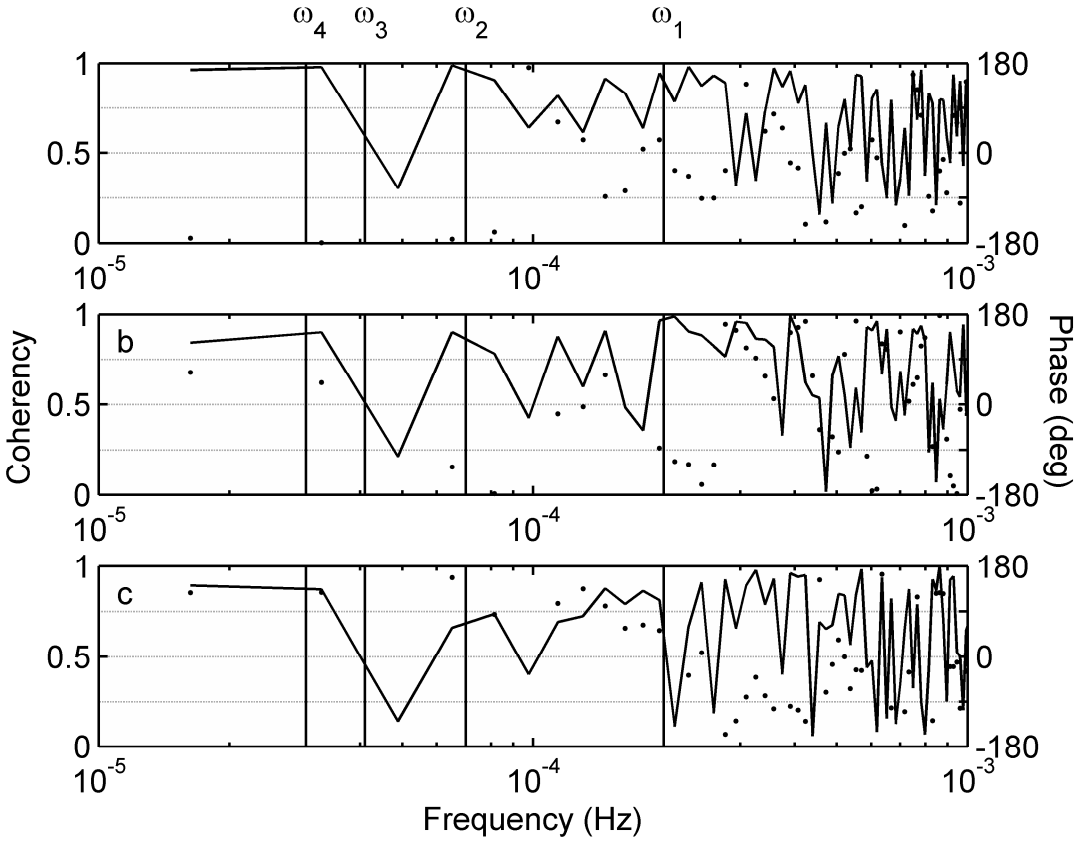

Figure 6. Coherency (solid line) and phase (•) spectra at the VxH1 frequencies: (a) between the 19°C and 12°C isotherms as measured by the stand alone thermistor chain, (b) between the stand alone thermistor chain and the LDS thermistor chain for the 19°C isotherm, and (c) between the stand alone thermistor chain and the LDS thermistor chain for the 12C isotherm. The phase is only indicated when the coherency is greater than 0.5. The theoretical frequencies of the first four vertical modes are indicated.

seiche and all of its associated higher harmonics and out of phase for the V2H1, V3H1, and V4H1 seiches and their higher harmonics. The coherency and phase spectra between the 19°C and 12°C isotherms are shown in Figures 6a, 7a, 8a, and 9a for the VxH1-VxH4 modes respectively. At the VxH1 seiching frequencies (Figure 6a), the two isotherms move coherently for all four vertical modes. The isotherms are out of phase at the frequencies closest to vertical mode 2-4 frequencies and in phase at the vertical mode 1 frequency, implying that all four vertical modes may exist in the lake. The isotherms are also coherent at all the VxH2 frequencies (Figure 7a). The isotherms are in phase at the VIH2 and V2H2

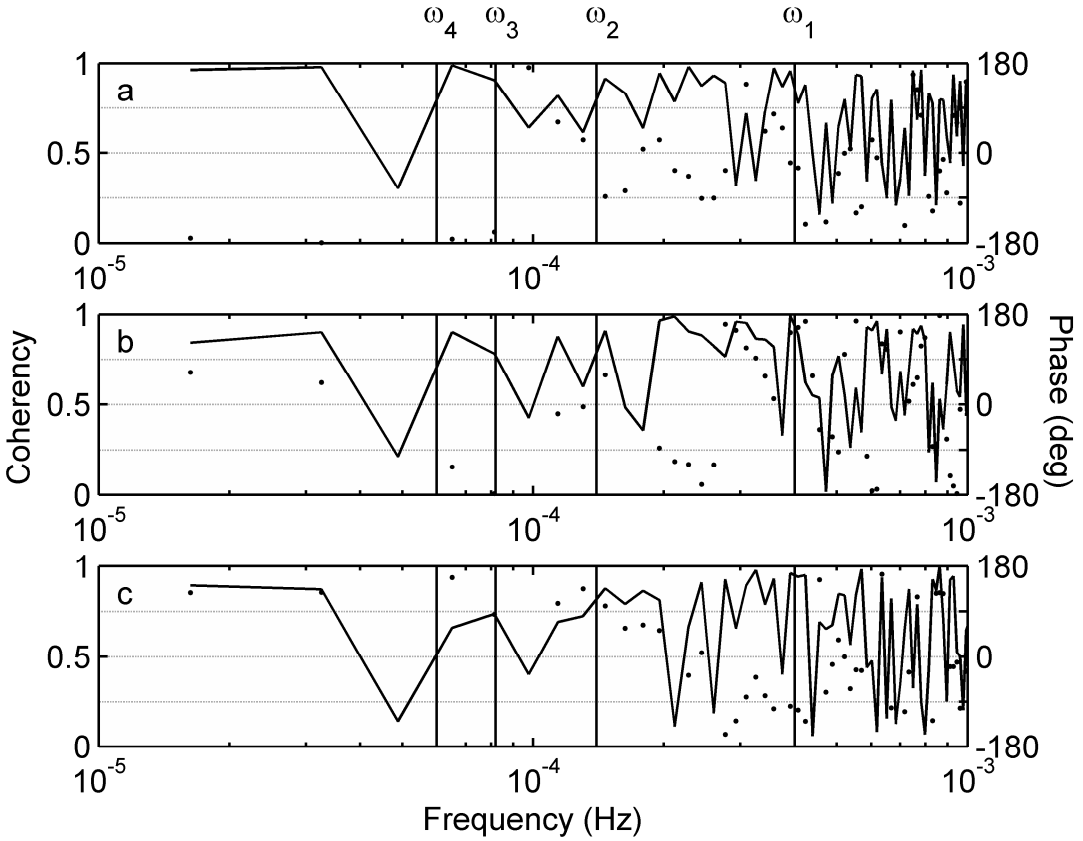

Figure 7. Same as Figure 6 for the VxH2 seiche frequencies.

frequencies and out of phase at the V3H2 and V3H2 frequencies. This evidence indicates the possible existence of the V1H2, V3H2, and V4H2 modes but is contrary to the existence of a V2H2 mode (as such a mode should have the isotherms out of phase). At the VxH3 frequencies (Figure 8a), the isotherms also move coherently. At the V4H3 frequency, they are out of phase, but they are in phase at the V3H3, V2H3, and V1H3 frequencies; thus, the phases indicate that potentially the V4H3 and V1H3 seiches may exist. Finally, the isotherms are coherent at the V4H4, V3H4, and V2H4 seiching frequencies (but not at V1H4), but are in phase, which is not consistent with the existence of the higher vertical mode seiches (Figure 9a).

To determine if the seiches are horizontally coherent, we computed the coherency and phase spectra for the 19°C and 12°C isotherms between the freestanding thermistor chain and the LDS. In an idealized lake, given the position of the thermistor chain and the LDS along the fetch, we would expect that for the VxH1 and VxH4 modes the isotherm displacements

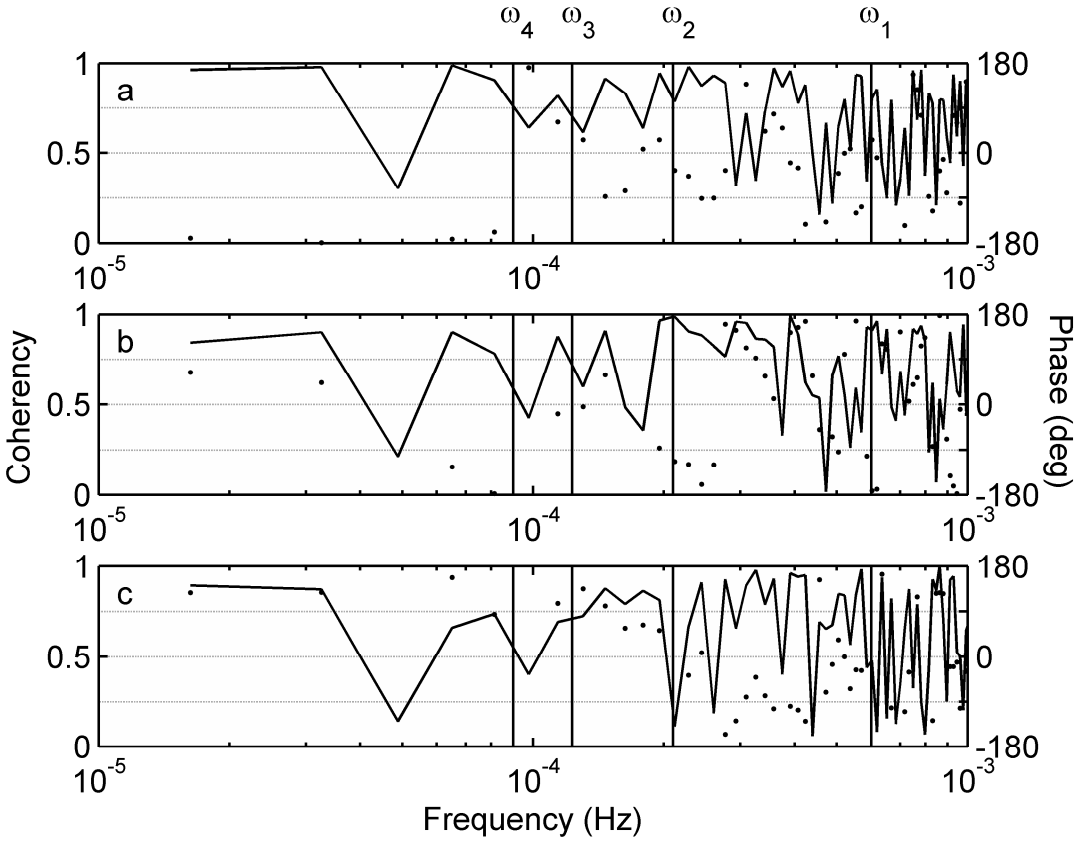

Figure 8. Same as Figure 6 for the VxH3 seiche frequencies.

will be in phase, and that for the VxH2 and VxH3 modes the isotherm displacements will be out of phase. At the VxH1 frequencies (Figure 7b,c,d), both the isotherm movements are coherent between the thermistor chain and the LDS at the V4H1, V2H1, and V1H1 frequencies but not at the V3H1 frequency. At the V4H1 frequency, the signal is in phase for the 19°C isotherm and out of phase for the 12°C isotherm, implying that the motions at this frequency are not due to a V4H1 seiche. At the V2H1 frequency, both signals are out of phase and at the V1H1 frequency they are in phase; these observations are consistent with the existence of these two modes. At the VxH2 frequencies (Figure 8b,c,d), there are coherent motions for all modes for both isotherms. With the exception of the 19°C isotherm signal at the V3H2 frequency, all of the coherent motions are not of the correct phase to be VxH2 seiches. As the upper and lower portions of the water column are horizontally of different phase, we expect that the motions at this frequency are not due to a V3H2 mode. At the VxH3 frequencies, both the isotherm movements are coherent between the thermistor chain

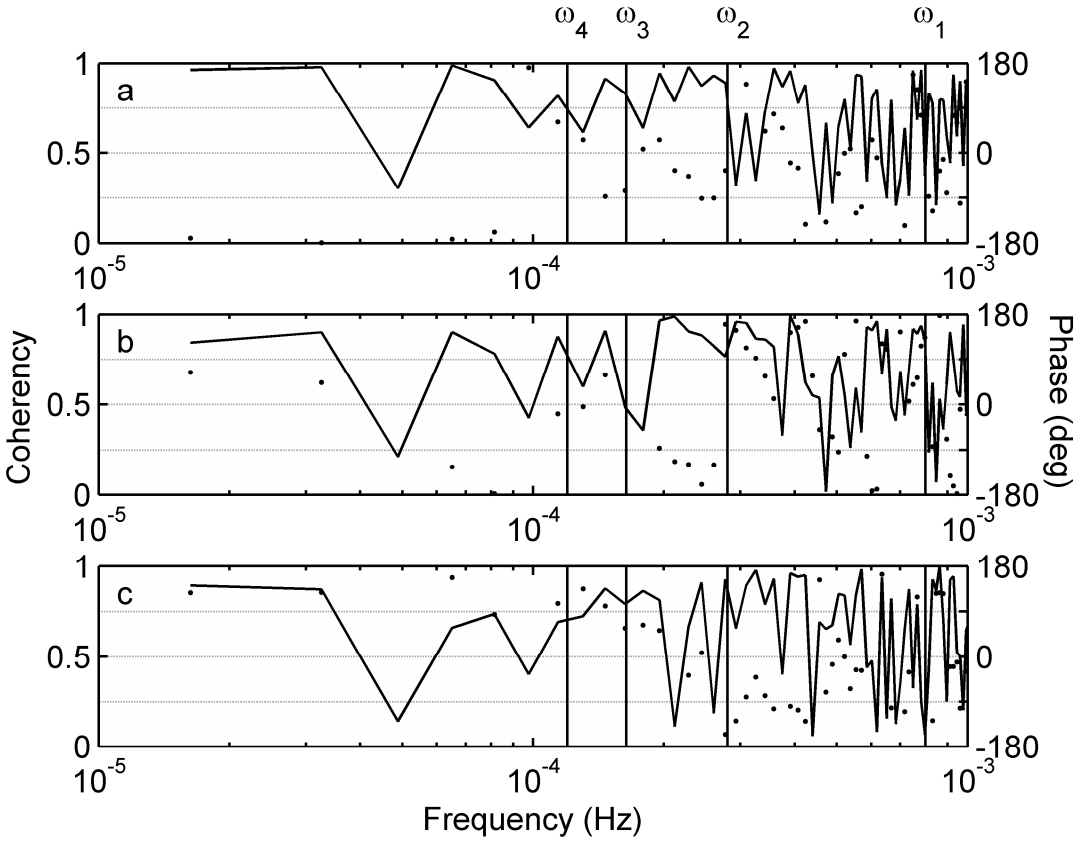

Figure 9. Same as Figure 6 for the VxH4 seiche frequencies.

Table 1. Summary of evidence from coherency and phase spectra for the seiching modes. At the frequency of each mode, if the isotherms are coherent and of the proper phase shift for the mode, then there is potential for that mode to exist according to that isotherm pair. The 19°C-12°C pair pertains to vertical coherence; the other two pertain to horizontal coherence.

Isotherms	V1H1	V2H1	V3H1	V4H1	V1H2	V2H2	V3H2	V4H2
19°C-12°C	x	x	x	x	x		x	x
19°C-19°C	x	x		x			x	
12°C-12°C	x	x				x		
	V1H3	V2H3	V3H3	V4H3	V1H4	V2H4	V3H4	V4H4
19°C-12°C	x			x				
19°C-19°C		x				x		x
12°C-12°C			x	x		x		

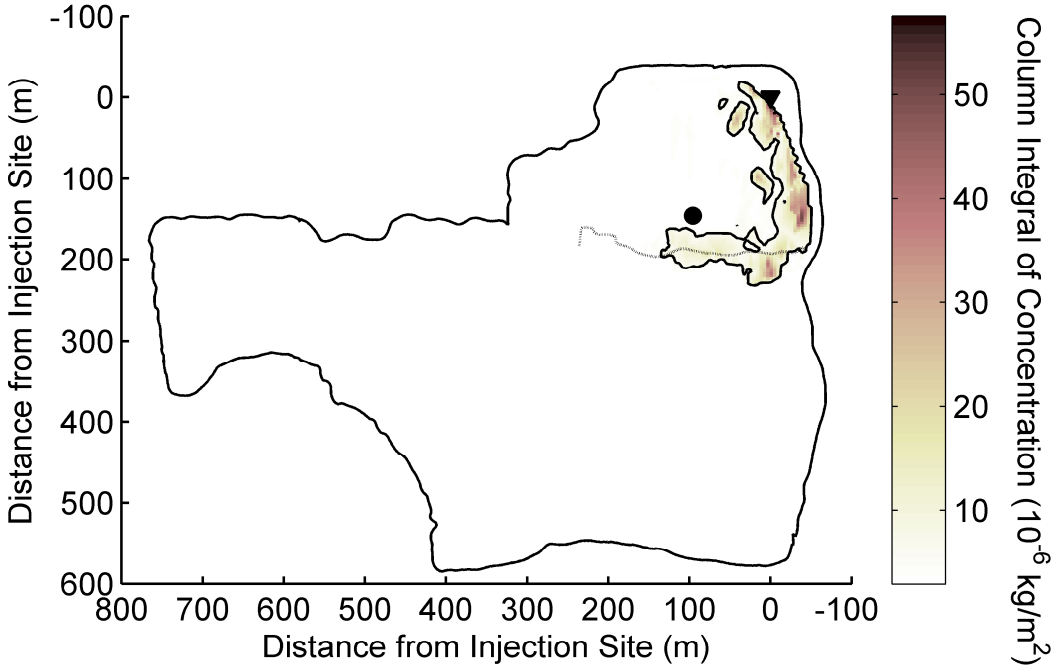

Figure 10. Spread of the dye cloud approximately 24 hours after injection. The contour indicates where the column integral is below 5% of the maximum. The dye injection location (▼) and the freestanding thermistor chain (●) are indicated. The dotted line marks the transect shown in Figure 11.

and the LDS at the V4H3 and V3H3 frequencies but not at the V2H3 and V3H3 frequencies. At both the V4H3 and V3H3 frequencies, the upper and lower portions of the water column are again not of the same horizontal phase shift, so these motions are most likely not V4H3 and V3H3 seiches. At the VxH4 frequencies (Figure 9b,c,d), both the isotherms are horizontally coherent for the V4H4 and V2H4 frequencies, but not the V3H4 and V1H4 frequencies. Both isotherms are correctly out of phase for the V2H4 seiche, but of different phase shifts at the V4H4 frequencies, implying the former may exist, while the latter should not.

Table 1 summarizes which modes may possibly exist according to the coherency and phase spectra presented in Figures 6-9. While an individual spectrum may show evidence for

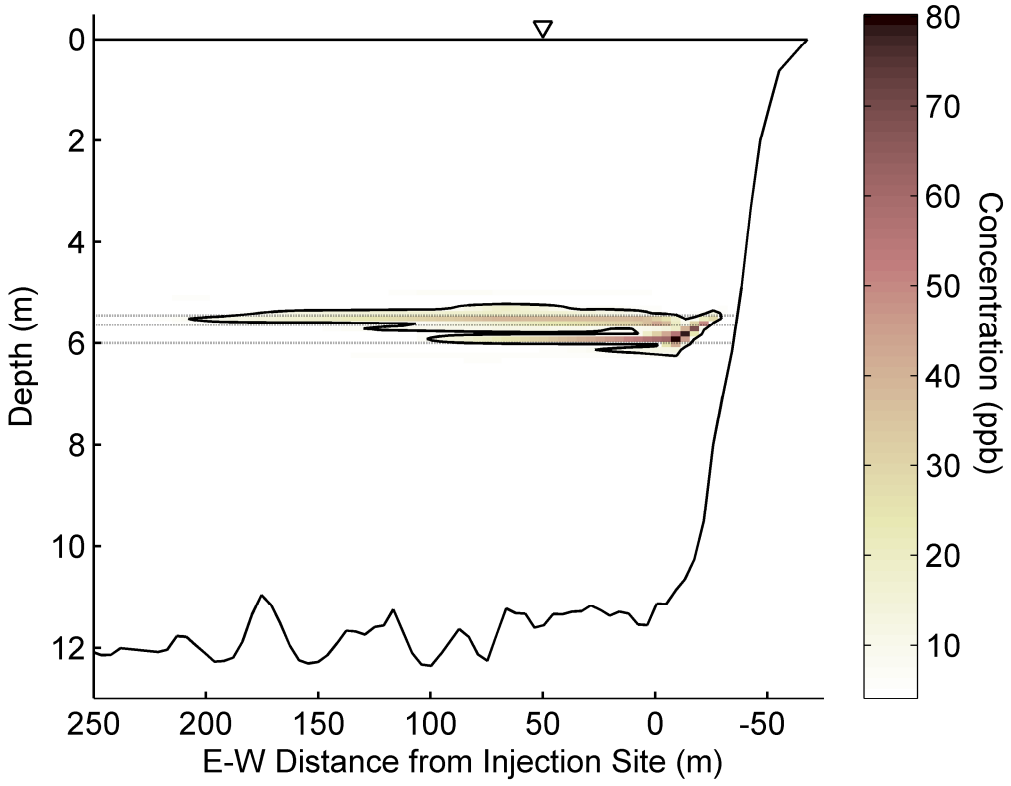

Figure 11. Longitudinal transect of dye cloud approximately 24 hours after injection. The contour indicates where the concentration drops to 5% of the maximum. The dotted lines indicate the mean depth of the 20°C, 19°C, and 18°C isotherms.

the existence of a particular mode, if the same evidence is not present in the other spectra, there is no compelling reason to believe that such seiching motions are controlling the isotherm movements. As is apparent in Table 1, the only seiching modes that are coherent and in proper phase in all three spectra are the V1H1 and V2H1 seiches.

Dye Mapping- Because the stronger winds at the lake typically come from the south, we chose the north slope for the dye injection. After the injection, the winds were atypically very calm until the wind event at 2 am. The dye mapping (Figures 10 and 11) occurred approximately 12-14 hours after this wind event. Between the injection and the mapping, the dye stayed close to the eastern shore of the lake until it reached the portion of the lake exposed to the longest westerly fetch. The dye then spread over 200 meters into the interior

of the lake at a rate of approximately 0.4 cm/s, although the concentration maximum remained near the shoreline.

Following the procedure of Sundermeyer and Ledwell (2001), we first compute the moments of the distribution of the column integral $\widetilde{C}(x,y,t)$ of dye in Figure 10. To determine the relative importance of internal wave generated shear and strain, we first estimated the effective horizontal diffusivity assuming no straining by internal waves. For the northern half of the cloud, we assume that the initial variance is zero and using the time of completion of that mapping, we estimate K_x = 0.008 m^2/s. This can be considered the background horizontal diffusivity. Estimating the enhanced effective horizontal diffusivity is more complicated. Based on the diffusivity in the *y*-direction, we expect that the dye had reached the open region of the lake before the wind event. Using K_x, we can estimate the *x*-variance of the dye cloud at the time of the wind event. With this estimate of initial variance, we computed K_{eff} = 0.017 m^2/s (see Equation 20 in the appendix), or approximately twice the diffusivity in the northern portion of the lake.

Discussion

We consider four potential mechanisms for the spreading of the dye into the interior due to the internal waves: an intrusion generated by internal waves interacting with the slope advection due to the velocity field generated by the V2H1 seiche, internal wave strain, and shear dispersion from the internal wave field.

Intrusion Caused by Internal Wave Interactions with the Slope – Intrusions can be generated as the result of breaking internal waves or the generation of a frictional boundary layer from the seiching currents. Breaking of critical internal waves probably did not contribute to the transport. The eastern slope of the lake is approximately 30%, which is relatively steep in comparison to slopes in other field studies of intrusions generated by boundary mixing (e.g Inall 2009). At the depth of the dye, critical internal waves in the lake have a frequency of 0.004 Hz, which is over an order of magnitude higher than the V1H1 seiche frequency. The energy in the internal wave field contained at this frequency is more than two orders of magnitudes smaller than the energy contained in the range of the seiching

frequencies. Thus, it is not expected that this mechanism played a role in the dye propagation. While the seiching currents may have possibly generated a turbulent bottom boundary layer, the steep slope angle is not conducive to that process as the boundary layer thickness is inversely proportional to the slope (Gloor et al. 2000, Hondzo and Haider 2004).

Advection by Seiching Velocities - Next we look at the advection generated by the internal wave field. . Direct velocity measurements were not available, but if V1H1 and V2H2 seiches drive the dominant motions in the lake, the horizontal velocity field can be computed from the isotherm displacements measured at the freestanding thermistor chain. To remove the high frequency motions, we first filtered the isotherm displacements with a low pass filter with a pass band of $f < 2\omega_1$--that is, twice the frequency of the V1H1 seiche. The profile of the vertical velocity w was then computed as

$$w_{TC}(z,t) = \frac{\partial \zeta}{\partial t} \tag{6}$$

where ζ is the isotherm displacement. If we model the basin as two-dimensional in the x-z plane, then continuity,

$$\frac{\partial u}{\partial x} + \frac{\partial w}{\partial z} = 0 \tag{7}$$

where u is the horizontal velocity, holds at any position in the plane. For a first horizontal mode seiche, the horizontal and vertical velocities can be expressed as

$$u(x,z,t) = u_0(z,t)\sin\left(\frac{\pi x}{L}\right) \tag{8}$$

$$w(x,z,t) = w_0(z,t)\cos\left(\frac{\pi x}{L}\right) \tag{9}$$

where L is the length of the lake at the depth of the thermocline. The velocity u_0 can be found by substituting (8) and (9) into (7):

$$u_0(z,t) = -\frac{L}{\pi}\frac{\partial w_0}{\partial z}. \qquad (10)$$

Because w is known at the thermistor chain, we can compute w_0 using (9), u_0 using (10) and finally u using (8).

If we place particles at x = 0 m (in Figure 11), we can observe the transport by the advective field from the seiches. Most of the dye sits between the 20°C and 18°C isotherms. Due to the sinusoidal form of the horizontal velocity, as the particle moves into the interior it accelerates and as it moves towards the shore it decelerates. The velocity right at the lake boundary is necessarily zero, because there can be no flow into the wall. As noted above, the 19°C isotherm displacement is a relative maximum in the water column. This implies that there is a zero velocity crossing at this depth (see Figure 4). If we place particles at the depth of the 18°C and 20°C isotherms, advection from the seiching motions is in opposite directions (Figure 12). While these particles experience velocities between ±1.25 cm/s, because of the oscillatory nature of the flow, there is no significant net advection that can explain the propagation of the dye into the interior.

Marti and Imberger (2008) attributed the net advection into the interior in the metalimnion to residual currents from internal wave rectification. They computed the magnitude of the residual currents by averaging the velocity field from a numerical model of the lake over a six day period. Averaging the velocities over the time period above yields very small currents (< 0.02 cm/s) that are too small to cause the observed dye propagation.

Internal Wave Strain – The horizontal variation in u can lead to internal wave driven straining of the dye cloud. Next we include the strain in the moment analysis to determine the lateral dispersion coefficient (see Appendix A for details). Because of the zero velocity crossing at the 19°C isotherm, we cannot average the velocity over the depth of the dye cloud to compute the strain, as the depth averaged velocity of the cloud is close to zero due to velocity reversal at the zero crossing. Using the strain measured at the 20°C, 19°C, and 18°C isotherms respectively, K_{eff} is estimated to be 0.011 m^2/s, 0.013 m^2/s and 0.017 m^2/s respectively. In essence, the straining reduces the dispersion required to explain the dye

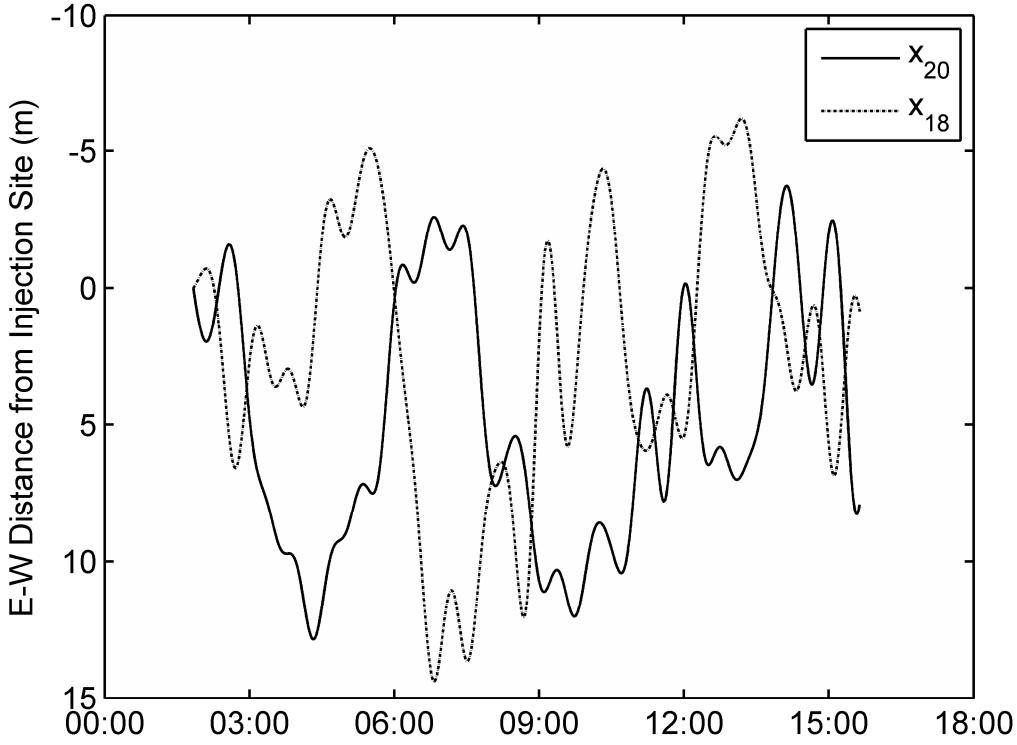

Figure 12. Track of particles placed at $x = 0$ at the depth of the 20°C isotherm (solid line) and the 18°C isotherm (dashed line). The particle tracks begin at the time of the low Lake number event on 7 August 2007 and end at the completion of the dye mapping.

spreading. This implies that in the upper portion of the dye cloud, the strain can account for some of the spreading of the dye cloud, thus reducing the effective horizontal diffusivity needed to produce the observed variance, but in the lower portion of the cloud the straining has no effect. This is consistent with the vertical structure of the dye cloud observed in Figure 11.

Shear Dispersion from Internal Waves - Even when the background diffusivity is included, there was still a "missing" diffusivity between 0.003 m^2/s and 0.009 m^2/s. We next computed the effective diffusivity from the vertical internal wave shear to determine if this process could account for the missing mixing. Sundermeyer and Ledwell (2001) use a modified form of the relationship between the variance and the shear dispersion which allows for an arbitrary time dependence of the vertical shear

$$\frac{1}{2}\frac{\partial \sigma_x^2}{\partial t} = K_{eff} = K_x + K_z G^2(t) \tag{11}$$

where G is a distortion factor given by

$$G = \frac{1}{(t-\tilde{t})}\int_0^t (t'-\tilde{t})\alpha(t')dt' \tag{12}$$

where α is the vertical shear and $\tilde{t} = -\sigma_{z0}^2 / 2K_z$. Equation (11) is equivalent to the $m = 0$ case presented by Young et al. (1982) and consequently is an upper bound on the effective diffusivity. The variance is then

$$\sigma_x^2(t) = \sigma_{x0}^2 + 2K_x t + 2K_z \int_0^t G^2(t)dt \tag{13}$$

where K_z was determined to be 1.2 x 10^{-6} m^2/s using microstructure measurements and the Osborn-Cox model (e.g. Wain and Rehmann 2005). The dye cloud was approximately 1 m thick. We approximated the thickness of the cloud by $4\sigma_z$ (Fischer et al. 1979), but a range between 0.25 m and 1 m was tested; the results differed by only 4% and thus are very insensitive to this choice. Using the estimates of the shear at the x-position of the center of mass of the southern portion of the dye cloud, we estimate the shear dispersion due to the internal waves to be approximately 0.001 m^2/s, which is not sufficient to account for the missing mixing.

Sundermeyer and Ledwell (2001) also found that this form of shear dispersion was not sufficient to explain their dye distributions and oftentimes was an order of magnitude too low. They attributed the remaining missing mixing to lateral intrusions from interleaving of adjacent water parcels and from the collapse of mixed patches. Lakes typically have a more quiescent interior than the ocean. During the the experiment, the strong stratification

prevented the Richardson number from dropping below 0.25; thus vertical mixing from the vertical shear is unlikely.

Combined effects of internal wave driven shear and strain - One of the key assumptions of the moment analysis is that the horizontal eddy diffusivity does not change in space. For all horizontal modes and all bathymetries, both the horizontal strain $\partial u/\partial x$ and the vertical shear $\partial u/\partial z$ change with x. Closer to the edge of the basin for the first horizontal mode, the horizontal strain is the largest, and it decreases to zero in the middle of the lake. Conversely, the vertical shear is necessarily zero at the wall (since u is zero everywhere), and it reaches a maximum in the middle of the lake where u reaches a maximum. While the spreading of the cloud by straining is not a dispersion process, in trying to evaluate the observed spreading, we can represent the contribution by the strain to the variance as a "diffusivity." For example as noted above, the strain stretches the cloud so that less lateral dispersion is required to explain the dye distribution. The strain reduced the effective horizontal diffusivity to 0.011–0.017 m^2/s dependent upon the depth. Without strain, the required effective horizontal diffusivity is 0.017 m^2/s. Thus the strain contributes a "diffusivity" of 0.006 – 0 m^2/s, depending on the depth. The contribution of the strain and the shear to the observed diffusivity as a function of x is shown in Figure 13. In the analysis above, both K_{sh} and K_{st} were computed at the location of the center of mass of the dye cloud, which was approximately $x/L = 0.9$. As the dye cloud spreads into the interior, parts of the cloud are exposed to higher total diffusivities, which could possibly explain the missing mixing.

The patterns observed in Figure 13 will be true of any lake with a dominant first horizontal mode velocity field; this has implications for exchange between the pelagic and interior regions of the lake. If fluid is mixed at the boundary, but the boundary layer is not thick enough to cause lateral intrusions to form (Gloor et al. 2000), then that fluid and its constituents (e.g., nutrients, suspended sediments) will have no means of spreading into the interior of the lake. The $u = 0$ boundary condition implies that fluid right along the boundary is subject to very little advection by the internal wave field. Because of this, shear dispersion will also be low (Figure 13). But at the boundary, the horizontal velocity gradient is the greatest. So conceivably the two processes can work in conjunction to cause spreading of

mixed fluid into the interior. After the fluid is mixed, it is subjected to high strains, which may cause the cloud to grow large enough that regions of the cloud are then subject to appreciable effective horizontal diffusivities from shear dispersion.

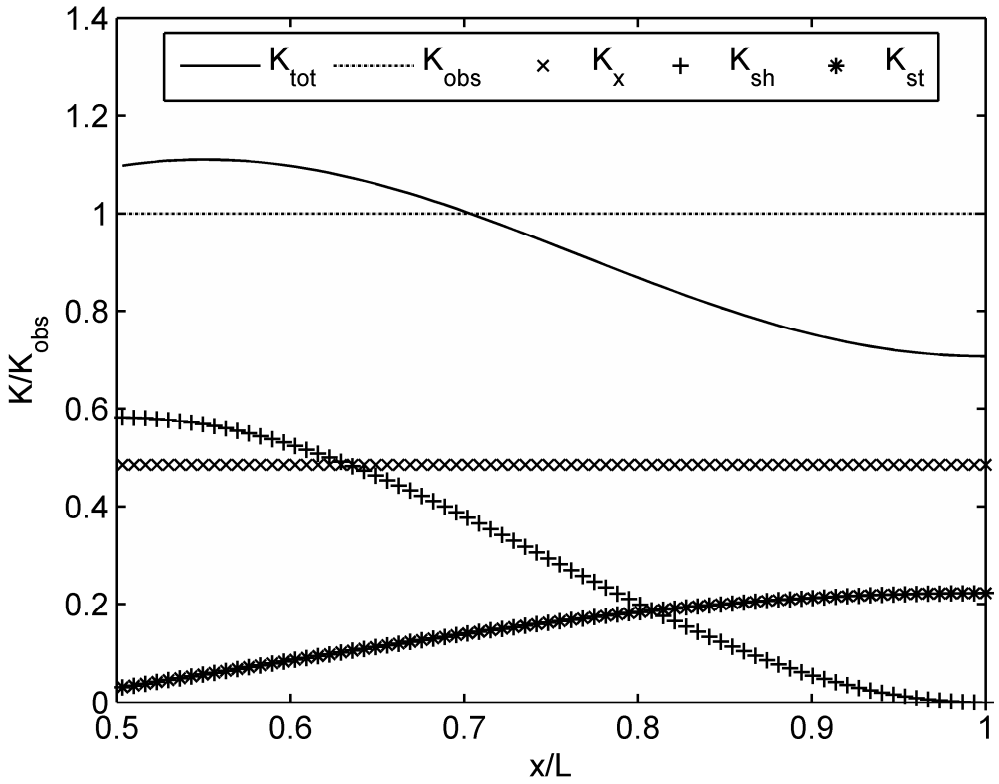

Figure 13. Patterns of diffusivity as a function of x. $K_{tot} = K_{sh} + K_{st} + K_{x.}$ K_{sh} is depth averaged over the vertical extent of the dye cloud.

Summary

A field experiment with measurements of tracer concentrations, meteorological conditions, and internal wave response was conducted to study boundary-interior exchange in a small lake. Rhodamine WT was injected into the metaliminion near the shoreline and tracked as it spread into the interior after a westerly wind event that generated basin scale seiches. Coherence and phase spectra between the 19°C and 12°C isotherms, which were in the upper and lower portions of the metalimnion, and between the same isotherms at two

thermistor chains indicate the existence of V1H1 and V2H1 seiches in the lake. The spreading of the dye cloud in the E-W direction changed dramatically once the cloud reached the open portion of the lake with the longest westerly fetch, where the dye spread over 200 meters at into the interior. The enhanced spreading could not be attributed to either advection from the internal wave field, despite the presence of a second vertical mode wave, or to residual currents from the internal wave field. The observed diffusivity in this portion of the lake calculated with a strain-free model after the westerly wind event was K_{obs} = 0.017 m^2/s. The background horizontal diffusivity measured in the sheltered part of the lake was K_x = 0.008 m^2/s, less than half that observed in the open part. We use the internal wave field at the location of the center of mass of the dye cloud and determine the contribution of the strain to the diffusivity was estimated to be K_{st} = 0-0.006 m^2/s, depending on the depth, and the effective horizontal diffusivity due to the vertical shear was estimated to be K_{sh} = 0.001 m^2/s. The gap between the observed spreading of the dye and the theoretical spreading due to internal wave shear and strain may be due to the horizontal variation in K. As the dye cloud spreads into the interior, K increases, accelerating the spreading process. This horizontal variation may also enhance the importance of internal wave shear and strain to boundary-interior exchange, as the strain can spread the mixed fluid far enough from the boundary that vertical shear becomes an important for dispersion.

Acknowledgments

The authors thank Mike Kohn, Josh Scanlon, Adam Wright, and Emily Libbey for help with the experiments and acknowledge support from the National Science Foundation under Grant OCE 06-47253. Any opinions, findings, and conclusions or recommendations expressed in this material are those of the authors and do not necessarily reflect the views of the National Science Foundation.

Appendix A: Moment Analysis with Unsteady Strain

The moments are defined as

$$M_{pq} = \int_{-\infty}^{\infty} x^p y^q \widetilde{C} dx dy \tag{14}$$

The zeroth moment M_{00} is related to the mass. The first moments, M_{10} and M_{01}, are related to the position of the center of mass (μ_x,μ_y) by $\mu_x = M_{10}/M_{00}$ and $\mu_y = M_{01}/M_{00}$. The second moments are related to the variances of the dye cloud by

$$\sigma_x^2 = \frac{M_{20}}{M_{00}} - \mu_x^2 \tag{15}$$

$$\sigma_y^2 = \frac{M_{02}}{M_{00}} - \mu_y^2 \tag{16}$$

The moments computed above are computed directly from the dye distribution. We can manipulate the advection-diffusion equation to yield the theoretical properties of these moments, in particular the variance in the *x* direction. Following Sundermeyer and Ledwell (2001), we assume that the growth of horizontal variance of the dye cloud is the result of an effective horizontal diffusivity and a large scale horizontal strain $\gamma = \partial u/\partial x$. They treated γ as a constant; Equation (8) shows that γ depends on *x, z,* and *t* for basin scale seiches. Including the *x* dependence in γ in the advection-diffusion equation yields an expression for the growth of the horizontal variance that cannot be solved analytically. Thus here we retain the time dependence of γ but compute $\partial u/\partial x$ at the location of the center of mass of the dye cloud denoted by μ_x.

We multiply the advection-diffusion equation by x^2 and integrate between -∞ and ∞:

$$\int_{-\infty}^{\infty} x^2 \left[\frac{\partial \tilde{C}}{\partial t} + \gamma(t) x \frac{\partial \tilde{C}}{\partial x} \right] dx = \int_{-\infty}^{\infty} x^2 \left[K_{eff} \frac{\partial^2 \tilde{C}}{\partial x^2} + K_y \frac{\partial^2 \tilde{C}}{\partial y^2} \right] dx \tag{17}$$

The moment definition in (14) is then used to yield an expression for the growth of the horizontal variance:

$$\frac{\partial \sigma_x^2}{\partial t} - 2\gamma(t)\sigma_x^2 = 2K_e ff \tag{18}$$

which is identical to Equation (5) from Sundermeyer and Ledwell (2001), as the time dependence of γ does not play a role until we integrate the above equation with respect to time to determine the behavior of the variance with time. Doing so yields the expression

$$\sigma_x^2(t) = \sigma_{x0}^2 exp\left[\int_0^t 2\gamma(t)\,dt\right] + 2K_{eff} exp\left[\int_0^t 2\gamma(t)\,dt\right]\int_0^t exp\left[-\int_0^t 2\gamma(t)\,dt\right]dt \tag{19}$$

which reduces to Equation (7) in Sundermeyer and Ledwell (2001) when γ is constant and the more common

$$\sigma_x^2(t) = \sigma_{x0}{}^2 + 2K_{eff}t \tag{20}$$

when γ is zero. Moving from Equation (17) to Equation (18) requires the standard moment analysis assumption that there is no interaction with the boundary. The dye mapping in Figure 11 does not show the dye cloud impinging on the boundary, but this could be sampling error.

CHAPTER 5. CONCLUSIONS

1. Summary

Boundary mixing in lakes and oceans plays an important role in governing budgets of heat, salt, and other dissolved constituents. Many studies have shown elevated mixing at the side of the basin or at underwater topography as compared to the interior of the lake or ocean, but because the mixing occurs over such a small portion of the basin, it is critical to understand if, when, and how such mixing affects the entire water body. Without understanding the fate of fluid mixed at the boundary, basin scale effects can be incorporated into global heat transport models in the ocean or water quality models in lakes and reservoirs. To address this issue, the objectives of present work were to

1. Predict the occurrence and strength of turbulent mixing in terms of meteorological forcing and stratification by investigating the dependence of internal waves and turbulence on the slope on the Lake number, which compares the stabilizing tendency of stratification to the destabilizing tendency of the wind.
2. Investigate the fate of mixed fluid in a lake by using a tracer to track an intrusion generated at the boundary and conducting simultaneous turbulence measurements.
3. Evaluate offshore transport by basin scale seiches by tracking tracer as it spreads from the boundary region into the interior

To address objective 1, three field campaigns with measurements of meteorological conditions, internal wave response, and dissipation of turbulent kinetic energy were conducted to study generation of turbulence on the sloping boundary of a small lake. To evaluate the Lake number conditions under which turbulence will be generated at the slopes, histograms of $\varepsilon/\nu N^2$ were analyzed for all the data and for five different Lake number regimes. While the spread of the measurements was restrictively large for determining a quantitative relationship between the Lake number and the turbulence intensity, some relationships between the Lake number and $\varepsilon/\nu N^2$ for different Lake number regimes could

be observed. In general, the typical value of $\varepsilon/\nu N^2$ increased as the Lake number decreased below 30. A larger jump within the energetic regime was observed when the Lake number dropped below 1. Further work to understand the spread of $\varepsilon/\nu N^2$ in each Lake number regime would assist in helping to define a functional relationship between Lake number and mixing that could be used by those responsible for lake and reservoir management.

To address objective 2, a field experiment with measurements of tracer concentrations and temperature microstructure was conducted to study the consequences of boundary mixing in a small lake. Along with the observations of Inall (2009) this study is one of the first direct measurements of such boundary generated intrusions in the field, and it is the first to map the intrusion in three dimensions. The observed bottom boundary layer collapsed into an intrusion governed by a balance between inertia and buoyancy. The intrusion's behavior matched the propagation characteristics predicted by Lemckert and Imberger (2003) for an axisymmetric intrusion generated by a bubble plume. Almost 60% of the mass of dye injected moved off the slope and into the pelagic zone. These observations, along with the persistent turbid layer at the depth of the intrusion, suggests that intrusion formation may be an important mechanism for transporting dissolved substances and affecting lake ecology.

To address objective 3, a field experiment with measurements of tracer concentrations, meteorological conditions, and internal wave response was conducted to study boundary-interior exchange in a small lake. Coherence and phase spectra between the 19°C and 12°C isotherms (located in the upper and lower portions of the metalimnion) and between the same isotherms at two thermistor chains suggest the existence of V1H1 and V2H1 seiches in the lake. The spreading of the dye cloud in the E-W direction changed dramatically once the cloud reached the open portion of the lake with the longest westerly fetch, where the dye spread over 200 meters into the interior. The enhanced spreading could not be attributed to either advection from the internal wave field (despite the presence of a second vertical mode wave) or to residual currents from the internal wave field. The observed diffusivity in this portion of the lake based on a strain-free model after the westerly wind event was twice the background horizontal diffusivity measured in the sheltered part of the lake. Using the internal wave field at the location of the center of mass of the dye cloud, the contribution of the strain to the diffusivity was determined to be significant, while the

contribution from the vertical shear was estimated to be very small. The gap between the observed spreading of the dye and the theoretical spreading due to internal wave shear and strain may be due to the horizontal variation in K. As the dye cloud spreads into the interior, K increases, accelerating the spreading process.

The three key findings from these experiments are

1. While the Lake number was not derived to estimate mixing, there is potential for relating the Lake number to turbulence on the slope of a lake.
2. The mass transport offshore from intrusions may be an important mechanism for transporting dissolved substances and affecting lake ecology.
3. The horizontal variation in internal wave shear and strain can increase the lateral dispersion between the boundary and the interior; the strain can spread the mixed fluid far enough from the boundary that the magnitude of shear induced dispersion is significant when compared to other dispersion mechanisms.

These findings contribute to our better understanding of the pathway from energy input from the wind to offshore transport.

2. Future Work

Further research can be divided into three categories related to the objectives. For the first objective, a better parameterization of the internal wave energy should be developed so that the pathway between wind and slope turbulence is better defined. Displacement of a single isotherm is not a useful parameter as different modes of waves will create oscillations in different isotherms. As the obvious next step is constructing an energy budget relating the wind energy input to the energy in the internal wave field to the energy dissipated on the slope, a single isotherm is useless. Also, the three thermistor chains provide spatial information regarding the internal wave field; this information could be better integrated to determine if spatial heterogeneity may play a role in turbulence prediction on the slope.

An important element of the first objective is evaluating the universality of the results between lakes. Aquadopp data collected in summer 2009 at West Okoboji Lake, a much larger and deeper lake, can be evaluated to see if the Lake number and turbulence intensity are related in the same manner as at Ada Hayden Lake. A key part of this question is the role of the slope angle in determining if a bottom boundary layer will form. The role of the lag between the wind event and the turbulence has also not been fully investigated; adjusting the lag might reduce the spread of the measurements. Whether the lag is different between the lakes of different sizes and strong pulse-like events and longer more steady events should also be addressed. From the data presented here, there seems to be some indication that the time integrated wind energy input might be a more relevant forcing parameter than the instantaneous wind input as parameterized by the Lake number; this would explain the similar turbulence levels measured during the strong pulses and the long steady events. A comparison of this behavior in the two lakes should also be done. Finally, the alternative methods of calculating the dissipation from the Aquadopp data should be re-visited and evaluated to determine if lower values of the turbulence intensity can be determined, thus covering the entire range of turbulence intensity typically found in lakes.

For the second objective, successful tracking of more than one intrusion that was generated under different conditions would also aid in extrapolating results to other lakes. A particular point of interest is if inertia-buoyancy balances are always the driving force behind intrusion propagation or, if under some conditions, intrusions form and propagate under a viscous-buoyancy balance in the field. Another unanswered question is whether intrusions will always form when a boundary layer is created from mixing on the slope or if in some cases the boundary layer simply restratifies before becoming unstable enough to generate an intrusion.

For the third objective, a series of tracer studies that focus on the horizontal variation in internal wave strain and shear would help confirm the theoretical variability in lateral dispersion due to internal waves, especially if the tracer release is combined with full water column velocity measurements with an acoustic Doppler current profiler. If dye were to be injected at several positions between the lake boundary and the lake interior, the variation in horizontal spreading could be evaluated. Ideally the dye would be injected in calm

conditions, mapped some hours later to estimate the background horizontal diffusivity, and then mapped again after a wind event generated internal waves. There do not appear to be any field measurements that confirm that the Young et al. (1982) estimate of shear dispersion due to oscillating vertical shear can explain horizontal mixing of tracer, so these dye studies help in determining if this process could be important in certain regions of a lake.

REFERENCES

Antenucci, J.P., Imberger, J., Saggio, A.,2000. Seasonal evolution of the basin-scale internal wave field in a large stratified lake. *Limnol. Oceanogr*. 45, 1621 – 1638.

Appt, J., Imberger, J., Kobus, H., 2004. Basin-scale motion in stratified upper Lake Constance. Limnol. Oceanogr. 49, 919 – 933.

Barry, M.E, Ivey, G.N., Winters, K.B., Imberger, J., 2001. Measurements of diapycnal diffusivities in stratified fluids. *J. Fluid Mech.* 442, 267 – 291.

Boegman, L., Ivey, G.N., Imberger, J., 2005. The degeneration of internal waves in lakes with sloping topography. *Limnol. Oceanogr.* 50, 1620 – 1637.

Boehrer, B., Ilmberger, J., and Münnich K., 2001. Vertical structure of currents in western Lake Constance, *J. Geophys. Res.* 105(C12), 28823-28835.

Browand, F.K., Guyomar, D., Yoon, S.C. 1987. The behavior of a turbulent front in a stratified fluid: Experiments with an oscillating grid. *J. Geophys. Res.* 92, 5329 – 5341.

Cacchione, D., Wunsch, C., 1974. Experimental study of internal waves over a slope, *J. Fluid Mech*. 66, 223 – 239.

Caldwell, D.R., Burbaker, J.M., Neal, V.T., 1978. Thermal microstructure on a lake slope. *Limnol. Oceanogr.* 23, 372 – 374.

Chen, C.-T., Millero, F.J., 1977. The use and misuse of pure water PVT properties for lake waters. *Nature* 266, 707 – 708.

Chen, J.-C., 1980. Studies on gravitational spreading currents, Ph.D. thesis, California Institute of Technology.

Dauxois, T., Young, W.R., 1999. Near-critical reflection of internal waves. *J. Fluid Mech.* 390, 271 – 295.

De Silva, I.P.D, Imberger, J., Ivey, G.N., 1997. Localized mixing due to a breaking internal wake ray at a sloping bed. *J. Fluid Mech.* 350, 1 – 27.

Dickson, R.R., McCave, I.N. 1986. Nepheloid layers on the continental slope west of Porcupine Bank. *Deep Sea Res.* 33, 791 – 818.

Eckert, W., Didenko, J., Uri, E., Eldar, D., 2003. Spatial and temporal variability of particulate phosphorus fractions in seston and sediments of Lake Kinneret under changing loading scenarios, *Hydrobiol.* 494, 223 – 229.

Eriksen, C.C., 1985. Implications of ocean bottom reflection for internal wave spectra and mixing. J. Phys. Oceanogr. 15, 1145 – 1156.

Eriksen, C.C., 1998. Internal wave reflection and mixing at Fieberling Guyot. *J. Geophys. Res.* 103, 2977 – 2994.

Ficher, H.B., List, E.J., Koh, R.C.Y., Imberger J., Brooks, N.H. 1979. *Mixing in Inland and Coastal Waters.* Academic Press, San Diego, 483 pp.

Fricker, P.D., Nepf, H.M., 2000. Bathymetry, stratification, and internal seiche structure. *J. Geophys. Res.-Oceans* 105, 14,237 – 14,251.

Garrett, C., 1979. Comment on 'Some Evidence for Boundary Mixing in the Deep Ocean' by Laurence Armi. *J. Geophys. Res*., 84, 5095 – 5095.

Garrett, C., Munk, W., 1979. Internal waves in the ocean. *Annu. Rev. Fluid Mech.* 11, 339 – 369.

Gilbert, D., Garrett, C., 1989. Implications for ocean mixing of internal wave scattering off irregular topography. *J. Phys. Oceanogr.* 19, 1716 – 1729.

Gloor, M., Wüest, A., Munnich, M., 1994. Benthic boundary mixing and resuspension induced by internal seiches. *Hydrobiologia* 284, 59-68.

Gloor, M., Wüest, A., Imboden, D.M., 2000. Dynamics of mixed bottom boundary layers and its implications for diapycnal transport in a stratified natural water basin. *J. Geophys. Res.* 105, 3629 – 8646.

Gordon, L., Lorhmann, A., Jonas, T., 1998. Internal wave generation in lakes with very slow flows. *Proc. Sixth Working Conf. on Current Measurement*, San Diego CA, IEEE, 212 – 215.

Goudsmit, G.-H., Peeters F., Gloor, M., Wüest, A., 1997, Boundary versus internal diapycnal mixing in stratified natural waters. *J. Geophys. Res.* 102, 27,903 – 27,914.

Gregg, M.C.,1998. Estimation and geography of diapycnal mixing in the stratified ocean. In *Physical Processes in Lakes and Oceans*. Coastal and Estuarine Studies, J. Imberger (ed.), 305 – 338.

Gregg, M. C., 1999. Uncertainties and limitations in measuring ε and χ_T. *J. Atmos. Oceanic Technol. 16*, 1483 – 1490.

Hondzo, M., Haider, Z., 2004. Boundary mixing in a small stratified lake. *Water Resour. Res.* 40, W03101, doi:10.1029/2002WR001851.

Hopfinger, E.J., 1987. Turbulence in stratified fluids: A review. *J. Geophys. Res.* 92, 5287 – 5303.

Horn, D.A., Imberger, J., Ivey, G.N., 2001. The degeneration fo large-scale internal gravity waves in lakes. *J. Fluid Mech.* 434, 181 – 207.

Imberger, J., Ivey, G.N., 1991. On the nature of turbulence in a stratified fluid. Part II: Application to Lakes. *J. Phys. Oceanogr.* 21, 659 – 680.

Imberger, J., Patterson, J.C., 1990. Physical Limnology. *Adv. Appl. Mech.* 27, 303 – 455.

Inall, M. E., 2009. Internal wave induced dispersion and mixing on a sloping boundary, *Geophys. Res. Lett.* 36, L05604, doi:10.1029/2008GL036849.

Itsweire, E.C., Helland, K.N., Van Atta, C.W., 1986. The evolution of grid-generated turbulence in a stably stratified fluid. *J. Fluid Mech.* 162, 299 – 338.

Ivey, G.N., Corcos, G.M., 1982. Boundary mixing in a stratified fluid. *J. Fluid Mech.* 121, 1 – 26.

Ivey, G.N., Imberger, J. 1991. On the nature of turbulence in a stratified fluid. Part I: The energetics of mixing. *J. Phys. Oceanogr.* 21, 650 – 658.

Ivey, G.N. Nokes, R., 1989. Vertical mixing due to the breaking of critical internal waves on sloping boundaries. *J. Fluid Mech.* 204, 479 – 500.

Ivey, G.N., Winters, K.B., Koseff, J.R., 2008. Density stratification, turbulence, but how much mixing? *Annu. Rev. Fluid Mech.* 40, 169 – 184.

Ledwell, J.R., Montgomery, E.T., Polzin, K.L., St. Laurent, L.C., Schmitt, R.W., Toole, J.M., 2000. Evidence for enhanced mixing over rough topography in the abyssal ocean. *Nature* 403, 179 – 182.

Ledwell, J.R., Duda, T.F., Sundermeyer, M.A., Seim, H.E., 2004. Mixing in a coastal environment: 1. A view from dye disperson. *J. Geophys. Res. – Oceans* 109, C10013, 10.1029/2003JC002194.

Lemckert, C., Antenucci, J., Saggio, A., Imberger, J., 2004. Physical properties of turbulent benthic boundary layers generated by internal waves. *J. Hydr. Eng.* 130, 58 – 69.

Lemckert, C. J., Imberger, J., 1993. Axisymmetrical intrusive gravity currents in linearly stratified fluids. *J. Hydraul. Eng. 119*, 662 – 679.

Lemckert, C. J., Imberger, J., 1995. Turbulence within inertia-buoyancy balanced axisymmetric intrusions. *J. Geophys. Res. 100*, 22,649 – 22,666.

Lemmin, U., Mortimer, C.H., 1986. Tests of an extension to internal seiches of D'Efants procedure for determination of surface seiche characteristics in real lakes. Limnol. Oceanogr. 31, 1207 – 1231.

Lorke, A., 2007. Boundary mixing in the thermocline of a large lake. *J. Geophys. Res.-Oceans* 112, C09019, doi:10.1029/2006JC004008.

Lorke, A., Peeters, F., Wüest, A., 2005. Shear-induced convective mixing in bottom boundary layers on slopes. *Limnol. Oceanogr.* 50, 1612 – 1619.

Lorke, A., Umlauf, L., Mohrholz, V., 2008. Stratification and mixing on sloping boundaries. *Geophys. Res. Lett.* 35, L14610, doi:10.1029/2008GL034607.

Lorke, A., Wüest, A., 2005. Application of coherent ADCP for turbulence measurements in the bottom boundary layer. *J. Atmos. Oceanic Technol.* 22, 1821 – 1828.

Lowe, R.J., Linden, P.F., Rottman, J.W., 2002. A laboratory study of the velocity structure in an intrusive gravity current. *J. Fluid Mech.* 456, 33 – 48.

MacIntyre, S., Clark, J.F., Jellison, R. Fram, J.P., 2009. Turbulent mixing induced by nonlinear internal waves in Mono Lake, California. Limnol. Oceanogr. 54. 2255 – 2272.

MacIntyre, S., Flynn, K.M., Jellison, R., Romero, J.R., 1999. Boundary mixing and nutrient fluxes in Mono Lake, California. *Limnol. Oceanogr.* 44, 512 – 529.

Marce, R., Feijoo, C., Navarro, E, 2007.. Interaction between wind-induced seiches and convective cooling governs algal distribution in a canyon-shaped reservoir. Freshwater Biol. 52, 1336 – 1352.

Marti, C.L., Imberger, J., 2008. Exchange between littoral and pelagic waters in a stratified lake due to wind-induced motions: Lake Kinneret, Israel. *Hydrobiologia*, doi: 10.1007/s10750-007-9243-6.

McPhee-Shaw, E.E., Kunze, E., 2002. Boundary layer intrusions from a sloping bottom: A mechanism for generating intermediate nepheloid layers. *J. Geophys. Res.-Oceans* 107, 3050, 10.1029/2001JC000801.

Morillo, S., Imberger, J., Antenucci J.P., Woods, P.F. (2008). Influence of wind and lake morphometry on the interaction between two rivers entering a stratified lake. *J. Hydraul. Eng,* 134, 1579 – 1589.

Munk, W.H., 1966. Abyssal recipes. *Deep-Sea Res*. 13, 707 – 730.

Münnich M., Wüest A., Imboden D.M., 1992. Observations of the 2nd vertical-mode of the internal seiche in an alpine lake. *Limnol. Oceanogr.* 37, 1705 – 1719.

Murase, J.,Sakai, Y., Kametani, A., Sugimoto, A., 2005. Dynamics of methane in mesotrophic Lake Biwa, Japan. *Ecol. Res.* 20, 377–385.

Nash, J.D, Kunze, E., Toole, J.M., Schmitt, R.W., 2004. Internal tide reflection and turbulent mixing on the continental slope. *J. Phys. Oceanogr.* 34, 1117 – 1134.

Osborn, T.R., 1980. Estimates of the local rate of vertical diffusion from dissipation measurements. *J. Phys. Oceanogr.* 10, 83 – 89.

Osborn, T.R., Cox, C.S., 1972. Oceanic fine structure. *Geophysical Fluid Dynamics* 3, 321 – 345.

Patterson, J.C., Hamblin, P.F., Imberger, J., 1984. Classification and dynamic simulation of the vertical density structure of lakes. *Limnol. Oceanogr.* 29, 845 – 861.

Peeters, F., Wuest A., Piepke, G., 1996. Horizontal mixing in lakes. J. Geophys. Res. 101 – 18361 – 18375.

Pierson, D., Weyhenmeyer, G.A., 1994. High-resolution measurements of sediment resuspension above an accumulation bottom in a stratified lake. *Hydrobiol.* 284, 43 – 57.

Phillips, O.M., Shyu, J.H., Salmun, H., 1986. An experiment on boundary mixing: mean circulation and transport rates. *J. Fluid Mech*. 173, 473 – 499.

Polzin, K.L., Toole, J.M., Ledwell, J.R., Schmitt, R.W., 1997. Spatial variability of turbulent mixing in the abyssal ocean. Science, 276, 93 – 96.

Rao, Y. R., Hawley, N., Charlton, M.N., Schertzer, W.M. 2008,, Physical processes and hypoxia in the central basin of Lake Erie. *Limnol. Oceanogr.* 53, 2007 – 2020.

Rehmann, C.R., Koseff, J.R., 2004. Mean potential energy change in stratified grid turbulence. *Dyn. Atmos. Oceans* 37, 271 - 294.

Romero, J.R., Jellison, R., Melack, J.M., 1998 Stratification, vertical mixing and upward ammonium flux in hypersaline Mono Lake, California. *Archiv Hydrobiol*. 142, 283 – 315.

Ruddick, B., Walsh, D., Oakey, N., 1997. Variations in apparent mixing efficiency in the North Atlantic Central Waters. *J. Phys. Oceanogr.* 27, 2589 – 2605.

Rudnick, D.L., Boyd, T.J., Brainard, R.E., Carter, G.S., Egbert, G.D., Gregg, M.C., Holloway, P.E., Klymak, J.M., Kunze, E., Lee, C.M., Levine, M.D., Luther, D.S., Martin, J.P., Merrifield, M.A., Moum, J.N., Nash, J.D., Pinkel, R., Rainville, L., Sanfrod, T.B., 2003. From tides to mixing along the Hawaiin Ridge. *Science* 301, 355 – 357.

Saggio, A., Imberger, J., 1998. Internal wave weather in a stratified lake. *Limnol. Oceanogr.* 43, 1780 – 1795.

Shih, L.H., Koseff, J.R., Ivey, G.N., Ferziger, J.H., 2005. Parameterization of turbulent fluxes and scales using homogeneous sheared stably stratified turbulence simulations. *J. Fluid Mech.* 525, 193 – 214.

Slinn, D.N., Riley, J.J., 1996. Turbulent mixing in the oceanic boundary layer caused by internal wave reflection from sloping terrain. *Dyn. Atmos. Oceans* 24, 51 – 62.

Smith, R., 1982. Dispersion of tracers in the deep ocean. *J. Fluid Mech.* 123, 131 -142.

Soga, C.L.M., Rehmann, C.R., 2004. Dissipation of turbulent kinetic energy near a bubble plume. *J. Hydraul. Eng.* 130 (5), 441 – 449.

Stevens, C.L., Lawrence, G.A., 1997. Estimation of wind-forced internal seiche amplitudes in lakes and reservoirs, with data from British Columbia, Canada. *Aquatic Sci.* 59, 115 – 134.

Stevens, C., Lawrence, G., Hamblin, P., Carmack, E., 1996. Wind forcing of internal waves in a long narrow stratified lake. *Dyn. Atmos. Oceans* 24, 41 – 50.

Sundermeyer, M., Ledwell, J., 2001. Lateral dispersion over the continental shelf: Analysis of dye release experiments. *J. Geophys. Res.* 106, 9603 – 9621.

Sutherland, B.R., Kyba, P.J., Flynn, M.R., 2004. Interfacial gravity currents in two-layer fluids. *J. Fluid Mech.* 514, 327 – 353.

Thorpe, S.A., 1982. On the layers produced by rapidly oscillating a vertical grid in a uniformly stratified fluid. *J. Fluid Mech.* 124, 391 – 409.

Thorpe, S.A., White, M., 1988. A deep intermediate nepheloid layer. *Deep-Sea Res.* 35, 1665 – 1671.

Thorpe, S.A., 1998. Some dynamical effects of internal waves and the sloping sides of boundaries. In *Physical Processes in Lakes and Oceans*. Coastal and Estuarine Studies, J. Imberger (ed.), 441-460.

Turner, J.S., 1973. *Buoyancy Effects in Fluids.* Cambridge University Press, Cambridge, 368 pp.

Vidal. J., Casamitjana, X., Colomer, J., Serra, T., 2005. The internal wave field in Sau reservoir: Observations and modeling of a third vertical mode. *Limnol. Oceanogr.* 50, 1326 – 1333.

Wain, D. J., Rehmann, C.R., 2005, Eddy diffusivity near bubble plumes, *Water Resour. Res.* 41, W09409, doi:10.1029/2004WR003896.

Wells, J.R., Helfrich, K.R., 2004. A laboratory study of localized boundary mixing in a rotating stratified fluid. *J. Fluid Mech.* 516, 83 – 113.

Wiegand, R.C., Chamberlain, V., 1987. Internal waves of the second vertical mode in a stratified lake. *Limnol. Oceanogr.* 32, 29 – 42.

Wiles, P.J., Rippeth, T.P., Simpson, J.H., Hendricks, P.J., 2006. A novel technique for measuring the rate of turbulent dissipation in the marine environment. Geophys. Res. Lett. L21608, doi:10.1029/2006GL027050.

Wüest, A., Lorke, A., 2003. Small-scale hydrodynamics in lakes, *Annu. Rev. Fluid Mech.* 35, 373 – 412.

Wunsch, C., Ferrari, R., 2004. Vertical mixing, energy, and the general circulation of the oceans. *Annu. Rev. Fluid Mech.* 35, 373 – 412.

Young, W.R., Rhines, P.B., Garrett, C.J.R., 1982. Shear-flow dispersion, internal waves and horizontal mixing in the ocean. *J. Phys. Oceanogr.* 12, 515 – 527.